Doklady Physics, Vol. 48, No. 7, 2003, pp. 325–327. Translated from Doklady Akademii Nauk, Vol. 391, No. 1, 2003, pp. 32–34.

PHYSICS

Hamilton–Jacobi Equation for Fermions Interacting Nonminimally with Electromagnetic Field

V. I. Denisov*, I. P. Denisova*, and I. V. Krivchenkov**

Presented by Academician V.V. Kozlov March 18, 2003

Received March 18, 2003

As was shown in recent experiments carried out at the Stanford electron accelerator [1], vacuum electrodynamics is a nonlinear theory. Therefore, a number of electromagnetic effects must manifest themselves while electromagnetic signals propagate in exterior intense electromagnetic fields. We imply, e.g., curving of light beams, which depends on the polarization of the relevant electromagnetic wave [2], delay of an electromagnetic signal transferred on one normal mode with respect to a signal transferred on another normal mode [3], and generation of the second harmonic [4].

These effects attain measurable values provided that the magnetic fields of such astrophysical objects as pulsars and magnetars are used as exterior fields. In addition, as is shown in [5], the effects of nonlinear vacuum electrodynamics may be observed in experiments with modern precision ring lasers.

Thus, the nonlinear electrodynamic action of exterior electromagnetic fields on the motion of photons will be able to be comprehensively studied in experiments of the near future.

In this connection, a question arises as to whether there exists the nonlinear electrodynamic action of exterior electromagnetic fields on motion of massive particles.

As is well known, in describing the motion of charged particles, modern classical mechanics and electrodynamics employ equations linear in exterior electromagnetic fields, which correspond well to available data of laboratory experiments. However, owing to the fact that electromagnetic fields ($B \le 10^6$ G) generated in laboratory conditions are considerably weaker than fields corresponding to the characteristic quantum-electrodynamic value $B_q = 4.41 \times 10^{13}$ G, the magnitude of the expected effects turns out to be extremely low.

Recently, a possibility stipulated by the progress in development of femtosecond lasers has appeared to subject charged particles to the action of superintense electromagnetic fields. We imply that the intensity of such fields is close to the characteristic electrodynamic value B_q. This fact makes it possible to begin experimentally studying effects of nonlinear electrodynamic action of exterior fields on laws governing the motion of charged particles and on their dynamic characteristics.

From the theoretical standpoint, there are few unambiguous methods for deriving equations of motion for massive particles, which nonlinearly depend on the intensity of an exterior electromagnetic field. The simplest of these methods is to pass in the Dirac equation to the variant of nonminimal coupling [6]. In this case, we may write out the post-Maxwellian Lagrangian of the interacting spinor field and the electromagnetic field in the form

$$L = \frac{i\hbar c}{2}\left\{\bar{\psi}\gamma^n\frac{\partial\psi}{\partial x^n} - \frac{\partial\bar{\psi}}{\partial x^n}\gamma^n\psi\right\}$$
$$- m_0c^2\bar{\psi}\psi - q\bar{\psi}\gamma^n\psi A_n + \mu\eta_3\bar{\psi}\sigma^{nk}\psi F_{nk}$$
$$+ \frac{1}{32\pi}\{2J_2 + \xi[(\eta_1 - 2\eta_2)J_2^2 + 4\eta_2 J_4]\} + O(\xi^2\mathbf{B}^6). \quad (1)$$

Here, $\hbar$ is Planck's constant; m_0 and q are the mass of a particle and its charge; ψ is the spinor field; γ^n are the Dirac gamma matrices; A_n is the four-potential of the electromagnetic field; F_{nk} is the tensor of this field; $J_2 = F_{ik}F^{ki}$ and $J_4 = F_{ik}F^{km}F_{ml}F^{li}$ are independent invariants of the electromagnetic-field tensor F_{ik}, $\xi = \frac{1}{B_q^2}$, η_1, η_2,

* *Moscow State University, Vorob'evy gory, Moscow, 119899 Russia*
e-mail: denisov@srd.sinp.msu.ru

** *Tsiolkovsky Russian State Technological University (MATI), ul. Petrovka 27, Moscow, 103787 Russia*

1028-3358/03/4807-0325$24.00 © 2003 MAIK "Nauka/Interperiodica"

and η_3 are dimensionless parameters,; and $\mu = \dfrac{m_0c^2}{2B_q}$ is the Bohr magneton.

The parameter η_3 entering into Lagrangian (1) describes the contribution of the nonminimal interaction of fermions with an electromagnetic field. The values of dimensionless post-Maxwellian parameters η_1 and η_2 depend on the choice of the nonlinear vacuum electrodynamics. For example, in Heisenberg–Euler nonlinear electrodynamics, these parameters acquire quite particular values $\eta_1 = \dfrac{\alpha}{45\pi} = 5.1 \times 10^{-5}$ and $\eta_2 = \dfrac{7\alpha}{180\pi} = 9.0 \times 10^{-5}$ [7]. At the same time, in the Born–Infeld theory, η_1 and η_2 are expressed in terms of a certain unknown constant a^2, namely, $\eta_1 = \eta_2 = \dfrac{1}{4}a^2B_q^2$.

Equations for spinor and electromagnetic fields, which are found from Lagrangian (1), have the form

$$i\hbar c\gamma^n\frac{\partial\psi}{\partial x^n} - m_0c^2\psi - q\gamma^n\psi A_n + \mu\eta_3\sigma^{nk}\psi F_{nk} = 0,$$

$$\frac{\partial}{\partial x^n}\{[1 + \xi(\eta_1 - 2\eta_2)J_2]F^{mn} + 4\xi\eta_2F^{ml}F_{lk}F^{kn} + O(\xi^2\mathbf{B}^6)\} = -\frac{4\pi}{c}\left\{q\bar{\psi}\gamma^m\psi + 2\mu\eta_3\frac{\partial\bar{\psi}\sigma^{nm}\psi}{\partial x^n}\right\}. \quad (2)$$

Using the first of these equations, we can obtain the Hamilton–Jacobi equation for a particle interacting with an exterior electromagnetic field in a nonminimal manner. To do this, we represent the spinor field in the form $\psi = \Psi\exp\dfrac{iS}{\hbar}$, where S is a certain function of coordinates and time, which changes rapidly compared to the spinor amplitude Ψ. We substitute this expression into the first equation of the set of equations (2) and then reduce it to the form

$$\hat{\Lambda}\psi = \left[\left(\frac{\partial S}{\partial x^n} + \frac{q}{c}A_n\right)\gamma^n + m_0cI - \frac{\mu\eta_3}{c}\sigma^{nk}F_{nk}\right]\psi = 0. \quad (3)$$

In order to have nontrivial solutions of the set of equations (3), we must, as is well known, satisfy the condition $\det\|\hat{\Lambda}\| = 0$. To find the determinant of the 4×4 matrix $\hat{\Lambda}$ in the covariant form, it is convenient to apply the formula

$$24\det\|\hat{\Lambda}\| = [\mathrm{Tr}(\hat{\Lambda})]^4 + 3[\mathrm{Tr}(\hat{\Lambda}^2)]^2 - 6\mathrm{Tr}(\hat{\Lambda}^4) - 6[\mathrm{Tr}(\hat{\Lambda})]^2\mathrm{Tr}(\hat{\Lambda}^2) + 8\mathrm{Tr}(\hat{\Lambda}^3)\mathrm{Tr}(\hat{\Lambda}),$$

which follows from the theorem of [8] on degrees of a second-rank tensor.

As a result, we arrive at the following Hamilton–Jacobi equation:

$$\left[\left(\frac{\partial S}{\partial x^0} + \frac{q}{c}\varphi\right)^2 - \left(\nabla S - \frac{q}{c}\mathbf{A}\right)^2 - m_0^2c^2 + \frac{2\mu^2\eta_3^2}{c^2}J_2\right]^2 + 8m_0^2\mu^2\eta_3^2J_2 + \frac{8\mu^4\eta_3^4}{c^2}(2J_4 - J_2^2) - \frac{16\mu^2\eta_3^2}{c^2}\left(\frac{\partial S}{\partial x^n} + \frac{q}{c}A_n\right)\left(\frac{\partial S}{\partial x^k} + \frac{q}{c}A_k\right)F_{(2)}^{nk} = 0, \quad (4)$$

where $F_{(2)}^{nk} = F^{np}F_{p\cdot}^{\cdot k}$.

Using the last equation, we can analyze the motion of fermions in the field of an intense plane electromagnetic wave. With the goal of attaining the highest degree of generality, we write out the vector potential in the form

$$\mathbf{A} = A_1\mathbf{e}_x + A_2\mathbf{e}_y, \quad \varphi = 0,$$

where $A_1 = A_1\left(t - \dfrac{z}{x}\right)$ and $A_2 = A_2\left(t - \dfrac{z}{x}\right)$.

Denoting by dot the differentiation of $A_1 = A_1\left(t - \dfrac{z}{x}\right)$ and $A_2 = A_2\left(t - \dfrac{z}{x}\right)$ with respect to the argument $t - \dfrac{z}{c}$, we have

$$\mathbf{E} = -\frac{1}{c}[\dot{A}_1\mathbf{e}_x + \dot{A}_2\mathbf{e}_y], \quad \mathbf{H} = \frac{1}{c}[\dot{A}_2\mathbf{e}_x - \dot{A}_1\mathbf{e}_y].$$

Substituting these expressions into Eq. (4), we arrive at the equation

$$\left[\frac{4}{c^2}\left(\frac{\partial S}{\partial u}\right)\left(\frac{\partial S}{\partial v}\right) - \left(\frac{\partial S}{\partial x} - \frac{q}{c}A_1(u)\right)^2 - \left(\frac{\partial S}{\partial y} - \frac{q}{c}A_2(u)\right)^2 - m_0^2c^2\right]^2 - \frac{64\mu^4\eta_3^4}{c^6}[\dot{A}_1^2(u) + \dot{A}_2^2(u)]\left(\frac{\partial S}{\partial v}\right)^2 = 0$$

in the variables x, y, $u = t - z/c$, and $v = t + z/c$. Solving this equation by separation of variables, we have

$$S = -\alpha_0 v + \alpha_1 x + \alpha_2 y + \int du \left\{ \pm \frac{2\mu\eta}{c} \sqrt{\dot{A}_1^2(u) + \dot{A}_2^2(u)} - \frac{c^2}{4\alpha_0} \left[\left(\alpha_1 - \frac{q}{c} A_1(u) \right)^2 + \left(\alpha_2 - \frac{q}{c} A_2(u) \right)^2 + m_0^2 c^2 \right] \right\}, \quad (5)$$

where α_0, α_1, and α_2 are constants, and the sign $\pm$ corresponds to two spin states of a fermion.

Thus, the allowance for nonminimal interaction of a fermion with the field of an intense plane electromagnetic wave ($\eta_3 \neq 0$) results in the appearance of an additional term in the action function S.

It is easy to find the law of motion for a fermion in the field of a plane electromagnetic wave:

$$x = x_0 + \frac{c^2}{2\alpha_0} \int du \left[\alpha_1 - \frac{q}{c} A_1(u) \right],$$

$$y = y_0 + \frac{c^2}{2\alpha_0} \int du \left[\alpha_2 - \frac{q}{c} A_2(u) \right],$$

$$v = v_0 + \frac{c^2}{4\alpha_0^2} \int du \left\{ \left[\alpha_1 - \frac{q}{c} \dot{A}_1(u) \right]^2 + \left[\alpha_2 - \frac{q}{c} \dot{A}_2(u) \right]^2 + m_0^2 c^2 \right\}.$$

In the case of the minimal interaction, these relationships coincide (to an accuracy of denoting the integration constants) with the well known laws of motion for a fermion in the field of an intense plane electromagnetic wave. Analyzing expression (5), we can verify that, in the case of fermion motion in the field of an intense plane electromagnetic wave, there is only one distinction of the nonminimal interaction from the minimal one. This distinction is the dependence of the energy E and the momentum component P_z on η_3:

$$E = -\left(\frac{\partial S}{\partial v} + \frac{\partial S}{\partial u} \right) = \alpha_0 \mp \frac{2\mu\eta_3}{c} \sqrt{\dot{A}_1^2(u) + \dot{A}_2^2(u)} + \frac{c^2}{4\alpha_0} \left[\left(\alpha_1 - \frac{q}{c} A_1(u) \right)^2 + \left(\alpha_2 - \frac{q}{c} A_2(u) \right)^2 + m_0^2 c^2 \right],$$

$$P_z = \frac{1}{c} \left(\frac{\partial S}{\partial v} - \frac{\partial S}{\partial u} \right) = \frac{\alpha_0}{c} \pm \frac{2\mu\eta_3}{c^2} \sqrt{\dot{A}_1^2(u) + \dot{A}_2^2(u)} - \frac{c}{4\alpha_0} \left[\left(\alpha_1 - \frac{q}{c} A_1(u) \right)^2 + \left(\alpha_2 - \frac{q}{c} A_2(u) \right)^2 + m_0^2 c^2 \right],$$

where $u = t - \frac{z}{c}$.

Therefore, measuring the energy–momentum characteristics of fermions under the action of powerful femtosecond laser pulses, it is possible to determine the phenomenological parameter η_3 and thereby experimentally clarify the measure of the nonminimal (nonlinear) action of electromagnetic fields on fermion motion.

ACKNOWLEDGMENTS

The work was supported by the Russian Foundation for Basic Research, project no. 02-02-16598.

REFERENCES

1. D. L. Burke, R. C. Field, G. Horton-Smith, *et al.*, Phys. Rev. Lett. **79**, 1626 (1997).
2. V. I. Denisov, Teor. Mat. Fiz. **132** (2), 211 (2002).
3. V. I. Denisov, I. P. Denisova, and I. V. Krivchenkov, Zh. Éksp. Teor. Fiz. **122**, 227 (2002).
4. P. A. Vshivtseva, V. I. Denisov, and I. P. Denisova, Dokl. Akad. Nauk **387**, 178 (2002) [Dokl. Phys. **47**, 798 (2002)].
5. V. I. Denisov, Phys. Rev. D **61**, 036004 (2000).
6. N. F. Nelipa, *Physics of Elementary Particles* (Vysshaya Shkola, Moscow, 1977), p. 120.
7. V. R. Khalilov, *Electrons in a Strong Magnetic Field* (Énergoatomizdat, Moscow, 1988).
8. I. P. Denisova and B. V. Mehta, Gen. Relativ. Gravit. **29**, 583 (1997).

Translated by G. Merzon

Doklady Physics, Vol. 48, No. 7, 2003, pp. 328–332. Translated from Doklady Akademii Nauk, Vol. 391, No. 1, 2003, pp. 35–39.

PHYSICS

Equilibrium Statistical Physics in Fractal Media with Constant and Variable Memory

L. Ya. Kobelev, Ya. L. Kobelev*, and Yu. L. Klimontovich†*****

Presented by Academician V.P. Skripov November 11, 2002

Received February 3, 2003

Physical phenomena that can be understood only with the inclusion of fractal properties were recently found in large systems (for which the statistical description is applicable [1]). Anomalous diffusion, i.e., diffusion for which the mean squared displacement of a particle is proportional to a fractional power of time ($q\langle x^2\rangle q \sim t^{\beta}$, where β is a fractional number), is among these phenomena and has been actively studied in recent years. It is observed in aerosols, gels, spin glasses, certain disordered systems, aperiodic crystals, electron–ion plasma, in systems described by the statistical physics of open systems [2], etc. Anomalous diffusion (or fractal relaxation) was described theoretically by using fractal geometry [3] in numerous works (see [4]). Many properties of solids (strength, brittleness, etc.) are also well described in the fractal approximation. In view of this circumstance, a new direction, fractal materials science, arose [5]. The fractal properties of large systems are mathematically described by equations with Riemann–Liouville fractional derivatives with constant memory [4, 6, 7] and constant diffusion coefficient. Experiments [8, 9] show that the fractal dimension depends on physical parameters (time and pressure); i.e., it is a variable quantity depending on physical parameters such as time, coordinates, and pressure. For this reason, the mathematical technique of fractional derivatives must be changed so that it includes the dynamics of the fractal (multifractal) dimension.

Current statistical physics is insufficient to describe the statistical properties of large systems with fractal structures. It must be supplemented and extended to the fractal and multifractal sets of physical objects. The question arises: How can we formulate a statistical model including the fractal and multifractal properties of large systems and what new properties does it introduce to the statistical description of equilibrium statistical systems?

In this work, we formulate statistical physics based on fractional derivatives (integrals) of a variable fractional order with respect to time and coordinates. We will develop the theory following classical works by Bogolyubov, Kirkwood, Green, and Yvon [1] (see also [2]).

Thus, to extend equilibrium statistical physics to fractal and multifractal sets, ordinary derivatives and integrals in the basic equations based on the Gibbs canonical distribution must be replaced by the respective fractional derivatives and integrals describing processes with constant or variable memory. Contrary to memory previously taken into account for nonfractal media in both thermodynamics and statistical physics [10], this memory is introduced immediately through fractional derivatives. Memory in nonfractal media is beyond the scope of this study. The basic equations of the Bogolyubov–Kirkwood–Green–Yvon theory for s-particle distribution functions $F_s(\mathbf{q}_1, \ldots, \mathbf{q}_s, \theta)$ ($\theta = kT$, $s = 1, 2, \ldots$) are based on the Gibbs canonical distribution

$$D_N(\mathbf{q}_1, \ldots, \mathbf{q}_N, \theta) = Q_N^{-1} \exp\left(-\frac{U_N}{\theta}\right).$$

Here, D_N is the probability distribution function for the positions of all objects of the system (for simplicity, we will call them particles or molecules), U_N is the potential energy of the system, $U_N = \sum_{1 \le i < j \le N} \Phi(|q_i - q_j|)$, Q is the configuration integral, and $Q_N = \int_V \ldots \int_V e^{-\frac{U_N}{\theta}} d\mathbf{q}_1 \ldots d\mathbf{q}_N$. These equations have the form

$$\frac{\partial}{\partial \mathbf{q}_1} F_s + \frac{1}{\theta} \frac{\partial U_s}{\partial \mathbf{q}_1} F_s + \frac{1}{v\theta} \int \frac{\partial \Phi(|\mathbf{q}_1 - \mathbf{q}_{s+1}|)}{\partial \mathbf{q}_1} F_{s+1} d\mathbf{q}_{s+1}, \quad (1)$$

† Deceased.

* *Institute of Metal Physics, Ural Division, Russian Academy of Sciences, ul. S. Kovalevskoĭ 18, Yekaterinburg, 620219 Russia*
e-mail: yakov@imp.uran.ru
** *Ural State University, pr. Lenina 51, Yekaterinburg, 620083 Russia*
e-mail: leonid.kobelev@usu.ru
*** *Moscow State University, Vorob'evy gory, Moscow, 119899 Russia*

1028-3358/03/4807-0328$24.00

$$F_s(\mathbf{q}_1, \ldots, \mathbf{q}_s)$$

$$= V^s \int_V \ldots \int_V D_N(\mathbf{q}_1, \ldots, \mathbf{q}_N) d\mathbf{q}_{s+1} \ldots d\mathbf{q}_N, \quad (2)$$

$$\frac{\partial}{\partial \mathbf{q}_1} D_N + \frac{1}{\theta} \frac{\partial U_N}{\partial \mathbf{q}_1} D_N = 0, \quad (3)$$

where $\alpha = 1, 2$, and 3 and $v = NV^{-1}$.

The chain of the distribution functions F_s, $s = 1, 2, \ldots, N$ ($F_N = D_N$) completely describes the equilibrium statistical system and was proposed in this form in [1]. The fractal and multifractal properties of the equilibrium statistical system can be simply taken into account by assuming that Eq. (3) is valid for very small distances (much smaller than the fractal clusters of particles forming the fractal structure of the system) and small variations in the coordinates of particles of the system. In other words, it is assumed that the effect of fractal structures can be ignored for mathematically small variations in the positions of particles of the system. Physically small variations already involve the effect of constant or variable memory, although such variations can be described by means of derivatives but fractional rather than ordinary. Therefore, all derivatives and integrals in Eqs. (1)–(3) must be replaced by fractional derivatives and integrals including memory. In this case, the fractal and multifractal characteristics of the system are taken into account for physically small variations both in functions as physical quantities treated as points and in the characteristics of the state of the system. Depending on the form of used fractional derivatives and integrals (Riemann–Liouville, Marchaud, Ritz, etc.), the system under consideration, where the fractal (multifractal) properties of equilibrium statistical systems is included, either transforms to an open system (Riemann–Liouville, Ritz, etc., fractional derivatives) or conserves its close character (Marchaud, Caputo fractional derivatives). The choice of the type of fractional derivative is determined by the properties of the statistical systems under consideration. In this work, we consider only equilibrium statistical systems, where the presence of fractal characteristics gives rise to energy dissipation and, therefore, transforms these systems to open statistical systems. Examples of such systems were given at the beginning of this paper. In what follows, Riemann–Liouville fractional derivatives and their generalization applicable to multifractal systems (systems where the fractal dimension depends functionally on physical parameters) will be used.

FRACTIONAL DERIVATIVES AND INTEGRALS OF A VARIABLE ORDER

To describe non-Markovian equilibrium statistical systems with constant memory (fractional derivatives and integrals have a constant fractional order), it is sufficient to use the well-known Riemann–Liouville fractional derivatives and integrals [11, 12]. To develop statistical physics for a medium with a multifractal dimension depending on coordinates and time (or in physical systems with such fractal properties), the generalized Riemann–Liouville fractional derivatives, which were introduced by one of us (L.Ya.K.) and used in a number of works (see, e.g., [13]), must be used. These derivatives are defined as (for left-side derivatives; for more detail, see [13])

$$\frac{\partial^{1+\varepsilon_t}}{\partial t^{1+\varepsilon_t}} f \equiv D_{a,t}^{d_t} f(t)$$

$$= \frac{d^n}{dt^n} \int_a^t dt' \frac{f(t')}{\Gamma(n - d_t(t'))(t - t')^{d_t(t') - n + 1}},$$

$$\frac{\partial^{1+\varepsilon_\mathbf{q}}}{\partial \mathbf{q}^{1+\varepsilon_\mathbf{q}}} f \equiv D_{a,\mathbf{q}}^{d_\mathbf{q}} f(\mathbf{q}) \quad (4)$$

$$= \frac{d^n}{d\mathbf{q}^n} \int_a^\mathbf{q} d\mathbf{q}' \frac{f(\mathbf{q}')}{\Gamma(n - d_\mathbf{q}(\mathbf{q}'))(\mathbf{q} - \mathbf{q}')^{d_\mathbf{q}(\mathbf{q}') - n + 1}}.$$

Here, Γ is the Euler gamma function; $n = \{d\} + 1$, where $\{d\}$ is the integer part of d for $d \geq 0$ (i.e., $(n-1) \leq d < n$) and $n = 0$ for $d < 0$; $d_t = 1 + \varepsilon(t)$; and $d_\mathbf{q} = 1 + \varepsilon(\mathbf{q})$. Generalized fractional integrals are written for individual $\mathbf{q}$ components. The integral operators defined above for fractional orders d_t and $d_\mathbf{q}$ depending on coordinates and time can be expressed in terms of ordinary derivatives and integrals [13, 14] for $|\varepsilon| \ll 1$. In this case, generalized Riemann–Liouville fractional derivatives satisfy the approximate relations (we present here only relations for derivatives)

$$D_{a,t}^{1+\varepsilon_t} f(\mathbf{q}, t) = (1 + \varepsilon_t) \frac{\partial}{\partial t} f(\mathbf{q}, t) + \frac{\partial \varepsilon_t}{\partial t} f(\mathbf{q}, t),$$

$$D_{a,\mathbf{q}}^{1+\varepsilon_\mathbf{q}} f(\mathbf{q}, t) = (1 + \varepsilon_\mathbf{q}) \frac{\partial}{\partial \mathbf{q}} f(\mathbf{q}, t) + \frac{\partial \varepsilon_\mathbf{q}}{\partial \mathbf{q}} f(\mathbf{q}, t). \quad (5)$$

These relations make it possible to describe the dynamics of a system including the effect of changes in the fractal dimension (if they are much smaller than unity) on the behavior of the physical system by means of ordinary differential and integral equations [13].

CONFIGURATION INTEGRAL AND DISTRIBUTION FUNCTIONS IN FRACTAL SPACES

We consider changes in Eqs. (1)–(3) both for a medium with varying fractal dimensions $d_t(t, \mathbf{q})$ and $d_\mathbf{q}(t, \mathbf{q})$ characterizing non-Markovian processes with variable memory and for a particular case of a medium with constant memory (constant fractal dimensions). In this case, both time and spatial (about passed trajecto-

ries) memories are taken into account. Thus, equilibrium statistical physics of homogeneous statistical media is replaced by nonequilibrium statistical physics of systems with time and spatial memory. In this case, nonequilibrium means that the total energy of the system is not conserved, which follows from the mathematical technique in use. Nonequilibrium in these systems is a consequence of the fractal properties of the medium under consideration, because fractal properties give rise to energy dissipation in the model in use. To take variable memory into account, derivatives with respect to time and coordinates and integrals with respect to coordinates in both Eq. (1) and the definition of *s*-particle distribution functions (4) must be replaced by generalized fractional derivatives defined by formulas (4). This equation has the form (in the absence of external forces)

$$\frac{\partial^{d_{\mathbf{q}_1}}}{\partial \mathbf{q}_1^{d_{\mathbf{q}_1}}} F_s + \frac{1}{\theta}\frac{\partial^{d_{\mathbf{q}_1}} U_s}{\partial \mathbf{q}_1^{d_{\mathbf{q}_1}}} F_s + \frac{1}{v\theta}\int\limits_{V(\mathbf{q})} \frac{\partial^{d_{\mathbf{q}_1}} \Phi(|q_1 - q_{s+1}|)}{\partial \mathbf{q}_1^{d_{\mathbf{q}_1}}} \times \frac{F_{s+1}(\mathbf{q}_1, \ldots, \mathbf{q}_{s+1})}{\Gamma(d_{\mathbf{q}_{s+1}})(\mathbf{q} - \mathbf{q}_{s+1})^{1-d_{\mathbf{q}_{s+1}}}} d\mathbf{q}_{s+1}. \quad (6)$$

After integration with respect to coordinates and momenta in Eq. (6) (and in below formulas), the integration phase-space volume $V(\mathbf{q})$ and $\mathbf{q}$ are set to infinity. Equation (6) is one of the equations of the chain for the distribution function F_s defined in terms of the distribution function F_{s+1} as

$$F_s(\mathbf{q}_1, \ldots, \mathbf{q}_s) = \int\limits_{V(\mathbf{q})} \frac{F_{s+1}(\mathbf{q}_1, \ldots, \mathbf{q}_{s+1})}{\Gamma(d_{\mathbf{q}_{s+1}})(\mathbf{q} - \mathbf{q}_{s+1})^{1-d_{\mathbf{q}_{s+1}}}} d\mathbf{q}_{s+1} \quad (7)$$

for a non-Markovian system with variable memory. In this case, we assume that the system density ($NV^{-1} = v$) is constant and the passage to the limit $n \longrightarrow \infty$ and $V \longrightarrow \infty$ is carried out. Integrals are calculated between infinite limits and we set $a = -\infty$ and $q = \infty$ after their calculation. For variable density, v must be introduced to the fractional integral and its dependence on the multifractal dimension $d_{\mathbf{q}}$ must be taken into account. The configuration integral is also defined in terms of fractional integrals of a variable order as

$$Q = \int\limits_{V(\mathbf{q})} \frac{d\mathbf{q}_1}{\Gamma(d_{\mathbf{q}_1})(\mathbf{q} - \mathbf{q}_1)^{1-d_{\mathbf{q}_1}}} \ldots \int\limits_{V(q)} \frac{d\mathbf{q}_N}{\Gamma(d_{\mathbf{q}_N})(\mathbf{q} - \mathbf{q}_N)^{1-d_{\mathbf{q}_N}}} D(\mathbf{q}_1 \ldots \mathbf{q}_N). \quad (8)$$

Equations (6)–(8) are the basic equations of the statistical physics of fractal media with constant and variable memory. For nonfractal media, i.e., $d_{\mathbf{q}} = 1$, the equations transform to the well-known equations of the Bogolyubov chain of distribution functions for equilibrium statistical physics [1]. These equations can be approximately solved by the method of expansions in the inverse density (or in density). For the fractal dimension close to unity ($|\varepsilon| \ll 1$), corrections to known results are small. The equation relating the single-particle distribution function F_1 to the two-particle function F_2 has the form

$$\frac{\partial^{d_{\mathbf{q}_1}}}{\partial \mathbf{q}_1^{d_{\mathbf{q}_1}}} F_1 + \frac{1}{\theta}\frac{\partial^{d_{\mathbf{q}_1}} U_1}{\partial \mathbf{q}_1^{d_{\mathbf{q}_1}}} F_1 + \frac{1}{v\theta}\int\limits_V \frac{\partial^{d_{\mathbf{q}_1}} \Phi(|q_1 - q_2|)}{\partial \mathbf{q}_1^{d_{\mathbf{q}_1}}} \times \frac{F_2(\mathbf{q}_1, \mathbf{q}_2)}{\Gamma(d_{\mathbf{q}_2})(\mathbf{q} - \mathbf{q}_2)^{1-d_{\mathbf{q}_2}}} d\mathbf{q}_2 = 0. \quad (9)$$

For the approximate representation $F_2(\mathbf{q}_1, \mathbf{q}_2) \simeq F_1(\mathbf{q}_1)F_1(\mathbf{q}_2)$ of the two-particle distribution function, Eq. (9) takes the form

$$\frac{\partial^{d_{\mathbf{q}_1}}}{\partial \mathbf{q}_1^{d_{\mathbf{q}_1}}} F_1(\mathbf{q}_1) + \frac{1}{\theta}\frac{\partial^{d_{\mathbf{q}_1}} U_1}{\partial \mathbf{q}_1^{d_{\mathbf{q}_1}}} F_1(\mathbf{q}_1) + \frac{1}{v\theta}\int\limits_{V(\mathbf{q})} \frac{\partial^{d_{\mathbf{q}_1}} \Phi(|q_1 - q_2|)}{\partial \mathbf{q}_1^{d_{\mathbf{q}_1}}} \times \frac{F_1(\mathbf{q}_2)}{\Gamma(d_{\mathbf{q}_2})(\mathbf{q} - \mathbf{q}_2)^{1-d_{\mathbf{q}_2}}} d\mathbf{q}_2 F_1(\mathbf{q}_1) = 0. \quad (10)$$

This equation differs from the corresponding equations presented in [1] only by the replacement of ordinary derivatives by fractional derivatives and integrals with a variable order $d(\mathbf{q}, \theta)$. The form of the fractal dimension is determined by the corresponding equations (see [13]).

CASE OF CONSTANT MEMORY

As is known, Eq. (10) for a nonfractal medium ($\alpha = 1$) can be represented in the form

$$F_1(\mathbf{q}_1) = F_1^0(\mathbf{q}_1) \times \exp\left[-\frac{1}{v\theta}\int\limits_{V(\mathbf{q})} \frac{\partial \Phi(|q_1 - q_2|)}{\partial \mathbf{q}_1} F_1(\mathbf{q}_2) d\mathbf{q}_2\right]. \quad (11)$$

This form allows one to successfully apply the iteration method to approximately solve Eq. (10), because Eq. (11) is the Gibbs distribution for an arbitrary particle in the mean-field potential. How does distribu-

tion (11) change in the presence of constant memory in the system? Equation (10) takes the form

$$\frac{\partial^\alpha}{\partial \mathbf{q}_1^\alpha} F_1(\mathbf{q}_1) + \frac{1}{\theta}\frac{\partial^\alpha U_1}{\partial \mathbf{q}_1^\alpha} F_1(\mathbf{q}_1) + \frac{1}{v\theta\Gamma(\alpha)}$$

$$\times \int\limits_{V(\mathbf{q})} \frac{\partial^\alpha \Phi(|q_1 - q_2|)}{\partial \mathbf{q}_1^\alpha} \frac{F_1(\mathbf{q}_2)}{(\mathbf{q} - \mathbf{q}_2)^{1-\alpha}} d\mathbf{q}_2 F_1(\mathbf{q}_1) = 0. \quad (12)$$

Introducing the notation

$$K(\mathbf{q}_1|, F_1) = \frac{1}{\theta}\frac{\partial^\alpha U_1}{\partial \mathbf{q}_1^\alpha} + \frac{1}{v\theta\Gamma(\alpha)}$$

$$\times \int\limits_{V(\mathbf{q})} \frac{\partial^\alpha \Phi(|q_1 - q_2|)}{\partial \mathbf{q}_1^\alpha} \frac{F_1(\mathbf{q}_2)}{(\mathbf{q} - \mathbf{q}_2)^{1-\alpha}} d\mathbf{q}_2, \quad (13)$$

we write Eq. (12) in the form

$$\frac{\partial^\alpha}{\partial \mathbf{q}_1^\alpha} F_1(\mathbf{q}_1) + K(\mathbf{q}_1|, F_1) F_1(\mathbf{q}_1) = 0. \quad (14)$$

If $K(\mathbf{q})$ is treated as a known quantity [by approximately specifying F_1 in $K(\mathbf{q})$], Eq. (12) is a linear equation with fractional derivatives and the variable coefficient $K(\mathbf{q})$. Let $K(\mathbf{q})$ depend only slightly on $\mathbf{q}$ and admit expansion in this variable. We take only the first (constant) term of the expansion and, for simplicity, consider the equation for one of the coordinates (solutions for different coordinate projections coincide with each other in the approximation in use). In this case, Eq. (14) transforms to a relaxation-type equation with the relaxation time $\tau^\alpha = K^{-1}$. The exact solution of this equation with the initial condition $F_1(\mathbf{q} = 0) = F_0$ has the form (see [6])

$$F_1(\mathbf{q}) = \frac{F_0}{\alpha} H_{1,2}^{1,1}\left(\begin{array}{c|c} \mathbf{q} & \left(0, \frac{1}{\alpha}\right) \\ \tau & \left(0, \frac{1}{\alpha}\right), (0, 1) \end{array} \right), \quad (15)$$

where $H_{1,2}^{1,1}$ is the Fox function. The expansion of function (15) in $\frac{\mathbf{q}}{\tau}$ has the form

$$F_1(\mathbf{q}) = F_0 \sum_{k=0}^{\infty} \frac{(-1)^k}{\Gamma(1 + \alpha k)} \left(\frac{\mathbf{q}}{\tau}\right)^{\alpha k}, \quad (16)$$

where $\Gamma(1 + \alpha k)$ is the Mittag-Leffler function. As $\mathbf{q}\tau^{-1}$ increases and α decreases, a decrease in $F_1(\mathbf{q}\tau^{-1})$ becomes slower than the exponential decrease for $\alpha = 1$, as could be expected for Levi distributions.

APPROXIMATION OF WEAK VARIABLE MEMORY

For weak variable memory ($|\varepsilon| \ll 1$), fractional derivatives and integrals can be expressed in terms of ordinary derivatives and integrals and Eq. (10) takes the form

$$(1 + \varepsilon(\mathbf{q}))\frac{\partial}{\partial \mathbf{q}} F_1(\mathbf{q}) + \left[\frac{\partial \varepsilon(\mathbf{q})}{\partial \mathbf{q}} + \frac{1}{\theta}\frac{\partial^\alpha U_1}{\partial \mathbf{q}^\alpha}\right] F_1(\mathbf{q})$$

$$+ \frac{1}{v\theta}\int_V \frac{\partial \Phi(|\mathbf{q} - \mathbf{q}_1|)}{\partial \mathbf{q}} [1 + \varepsilon(\mathbf{q}_1)] F_1(\mathbf{q}_1) d\mathbf{q}_1 F_1(\mathbf{q}) = 0. \quad (17)$$

In this case, ε can be determined from the approximate equation [13] $\frac{\partial}{\partial \theta^{-1}} d = -L(\mathbf{q})d$, which provides the solution

$$d = 1 + \varepsilon = \exp\left[\frac{-L(\mathbf{q})}{\theta}\right] \simeq 1 - \frac{L(\mathbf{q})}{\theta}.$$

In the last equations, the Lagrangian density function $L(\mathbf{q})$ is determined by the type of the fractal (or multifractal) structure of the physical system under consideration. Additional terms in Eq. (16), which are absent for nonfractal media, arise due to the multifractal dimension ε of the medium. New forces (fractal additions to forces existing in nonfractal media) depending on ε appear due to the structure of the fractal medium, which involves particles into additional motion (see [15], where similar forces were obtained).

CONCLUSIONS

Equations for multiparticle distribution functions of equilibrium statistical physics for systems with constant and variable fractal memory were derived. It was shown that, for constant-memory systems (systems with a constant fractal dimension), the Gibbs distribution for the single-particle distribution function in the mean field of remaining particles of the system for high temperatures transforms to a Levi-type distribution. An equilibrium statistical system with weak variable memory was considered. A new force proportional to the gradient of the fractal dimension was found. It does not vanish in the absence of external forces and vanishes for constant memory.

ACKNOWLEDGMENTS

This work was supported in part by INTAS (grant no. 00-0847), the Russian Foundation for Basic Research (project no. 00-02-16285), and the U.S. Civilian Research and Development Foundation for the Independent States of the Former Soviet Union (grant no. REC-005).

REFERENCES

1. N. N. Bogolyubov, *Problems of Dynamic Theory in Statistical Physics* (Gostekhizdat, Moscow, 1946). English translation: N. N. Bogolyubov, in *Studies in Statistical Mechanics*, Ed. by J. de Boer and G. E. Uhlenbeck (Wiley, New York, 1961), p. 5.
2. Yu. L. Klimontovich, *Statistical Theory of Open Systems* (Yanus, Moscow, 1995; Kluwer, Dordrecht, 1995), Vol. 1.
3. B. B. Mandelbrot, *Fractal Geometry of Nature* (Freeman, New York, 1982).
4. A. V. Chechkin, R. Gorenflo, and I. M. Sokolov, Phys. Rev. E **66** (4), 046129 (2002).
5. V. S. Ivanova, A. S. Balankin, I. Zh. Bunin, and A. A. Oksogoev, *Synergetics and Fractals in Materials Science* (Nauka, Moscow, 1994).
6. W. G. Gloecke and T. F. Nonnenmacher, J. Stat. Phys. **71** (34), 741 (1993).
7. V. L. Kobelev, E. P. Romanov, L. Ya. Kobelev, and Ya. L. Kobelev, Dokl. Akad. Nauk **361**, 755 (1998) [Dokl. Phys. **43**, 487 (1998)].
8. V. Ya. Shur, S. A. Negashev, E. L. Rumyantsev, *et al.*, Ferroelectrics **169**, 63 (1995).
9. P. V. Korolev and S. N. Kul'kov, Perspekt. Mater., No. 3, 21 (1997).
10. U. F. Day, *Thermodynamics of Simple Materials with Fading Memory* (Springer-Verlag, Berlin, 1972; Mir, Moscow, 1974).
11. S. G. Samko, A. A. Kilbas, and O. I. Marichev, *Fractional Integrals and Derivatives, Theory and Applications* (Nauka i Tekhnika, Minsk, 1987; Gordon and Breach, Amsterdam, 1993).
12. I. M. Gelfand and G. E. Shilov, *Generalized Functions* (Academic, New York, 1964).
13. L. Ya. Kobelev, *Fractal Theory of Space and Time*, Available from VINITI, No. 2677-B99 (Moscow, 1999).
14. L. Ya. Kobelev, in *Proceedings of 24th International Workshop on High Energy Physics and Field Theory, Protvino, 2001*, p. 126; http://dbserv.ihep.su/~pubs.
15. Ya. L. Kobelev, L. Ya. Kobelev, and Yu. L. Klimontovich, Dokl. Akad. Nauk **390** (6) (2003) (in press).

Translated by R. Tyapaev

Doklady Physics, Vol. 48, No. 7, 2003, pp. 333–336. Translated from Doklady Akademii Nauk, Vol. 391, No. 1, 2003, pp. 40–43.

PHYSICS

Magnetohydrodynamic Analogue and the Seismoelectric Effect

V. L. Natyaganov

Presented by Academician E.I. Shemyakin January 25, 2003

Received February 5, 2003

Lomonosov, in his works *Tale of the Birth of Metals Due to Shaking of the Earth* and *On Terrestrial Layers* [1], wrote about acoustic, hydrologic, and light precursors to earthquakes, referring to the testimony of eyewitnesses and to works of other authors even of ancient times.

Theoretical models of the development of earthquakes are based on solid mechanics and the physics of rock fracture. The three most known models concern elastoplastic deformation, avalanche-unstable crack formation, and dilatant diffusion processes. Unfortunately, while adequately describing the development of earthquakes, these models do not provide indications predicting their onset time.

The methodology of a long-term (years to decades) seismic prediction was developed by Academician S.A. Fedotov. The situation with short-term (weeks to months) and particularly with operative predictions of earthquakes is much worse, although numerous observational data make it possible to identify various types of precursors, from acoustic to electromagnetic, of strong earthquakes.

Electromagnetic precursors to earthquakes are associated with the anomalous behavior of the atmospheric electric field (AEF). In his famous *Tale of Atmospheric Phenomena Caused by the Electric Force* [1], published 250 years ago, Lomonosov stated that this field existed even in clear, cloudless weather. Only two centuries later did G. Simpson make considerably advances in instrumental investigation of variations in the AEF under thunderclouds [2] by using measuring instruments available in the mid-20th century.

During recent decades, the attention of many scientists in various countries has been focused on a new atmospheric-electricity mystery—seismoelectromagnetic phenomena (SEMP)—whose particular case is the seismoelectric effect. The determination of their mechanism and the development of adequate physical–mathematical models of these phenomena will provide a reliable criterion for operative prediction of strong earthquakes. The growth of the technosphere in the Earth increases the risk that natural catastrophes, whose number and intensity have recently been rising, can be accompanied by induced technogenic catastrophes [3], which can significantly increase the possible damage. Therefore, the reliable operative prediction of earthquakes is much more important at present.

Systematic investigation of SEMP was begun in the 1970s by A.A. Vorob'ev and now represents a separate direction of geophysics, where a wealth of data have been accumulated [4–7]. This investigation was stimulated by the observation of the anomalous increase in the AEF before the Kurshabsk (1924), Chatkalsk (1946), and Khait (1949) earthquakes [5]. Analysis shows that the detected types of AEF anomalies do not fit into a simple scheme. However, the following four basic types of their manifestation in time before strong earthquakes are distinguished [7].

(i) Disturbance of the characteristic form of a precursor signal, which successively passes through the stages of growth, quasisaturation, and sharp drop to the undisturbed level at the time of the earthquake.

(ii) Disturbance with a "fading phase" (even the AEF direction can be reversed), which approaches the background level immediately before an earthquake or after a sharp burst.

(iii) Bell-shaped Gaussian-type disturbance, which approaches the background level (a plunge is sometimes possible) before the earthquake onset.

(iv) Bell-shaped disturbance without plunge; in this case, the time of the earthquake is not identified in the signal record.

Other types of AEF disturbances for individual earthquakes are obtained by the simple superposition of these basic types. Disturbance types can be complicated under foreshock or aftershock activity.

Faculty of Mechanics and Mathematics, Moscow State University, Vorob'evy gory, Moscow, 119899 Russia
e-mail: tenzor@mail.lib.msu.su

1028-3358/03/4807-0333$24.00

Despite three decades of investigations, there is no commonly accepted physical explanation of various types of SEMP, and even the common origin of the four basic types of the seismoelectric effect is in doubt [5–7]. For this reason, the method of mathematical analogues with well-studied phenomena and processes is substantial for the simulation of these types of the seismoelectric effect [3, 8].

In this work, to describe the seismoelectric effect, I propose the aircraft model [9], according to which the fields of velocity **v** and turbulence **ω** of an incompressible ideal fluid passing over the airfoil of an aircraft are magnetohydrodynamically similar to the geomagnetic field **H** and corresponding electric current **j**. The role of the airfoil profile of varying geometry (due to slats and flaps) in this analogue is the development of the main crack in the lithosphere until its collapse, inducing an earthquake. The hydrodynamic analogue of the seismoelectric effect is based on airfoil theory that was developed by the well-known Soviet scientists Chaplygin, Golubev, Kochin, and Sedov [10] and date from Zhukovsky's ideas of the attached eddies of the airfoil.

The magnetohydrodynamic analogue follows from the simple comparison of the kinematic boundary value problems [9]

$$\begin{cases} \operatorname{div}\mathbf{v} = 0 \\ \begin{cases} \operatorname{curl}\mathbf{v} = 0 \ \text{ outside } G \\ \operatorname{curl}\mathbf{v} = 2\boldsymbol{\omega} \ \text{ inside } G, \end{cases} \\ \{v_n\}\big|_G = 0, \quad r \to \infty: \ \mathbf{v} \to \mathbf{v}_0, \end{cases} \quad (1) \quad \Leftrightarrow \quad \begin{cases} \operatorname{div}\mathbf{H} = 0 \\ \begin{cases} \operatorname{curl}\mathbf{H} = 0 \ \text{ outside } G \\ \operatorname{curl}\mathbf{H} = \mathbf{j} \ \text{ inside } G, \end{cases} \\ \{H_n\}\big|_G = 0, \quad r \to \infty: \ \mathbf{H} \to \mathbf{H}_0, \end{cases} \quad (2)$$

for the airfoil flow and seismoelectric effect, respectively. The braces mean the jump of the corresponding quantity and subscript "n" denotes the normal component to the contour G of the airfoil profile or the corresponding crack in the aircraft model of the seismoelectric effect.

We do not present assumptions accepted in airfoil theory and mention only several fundamental points.

(i) The flow beyond the airfoil is potential. However, if the airfoil is replaced by attached Zhukovsky eddies of the airfoil and the flow is continued onto the entire plane, the flow inside the airfoil is turbulent [10].

(ii) The transition from the boundary condition $v_n = 0$ to $\{v_n\} = 0$ on the contour G corresponds to the forward movement of slats and flaps, which changes the character of the flow (including **ω** and the integral circulation around the airfoil). In the seismoelectric effect, this phenomenon corresponds to the pushing of field lines of **H** by the differential rotation of the medium [11] inside the growing main crack and the formation of current layers along its contour G. The difference is in the characteristic times: the rearrangement of the flow around the cut airfoil takes 10 s, whereas the seismoelectric effect continues 10 h or even several days.

(iii) When the contour G is given, boundary value problems (1) and (2) are standard but require, as a rule, numerical solution. When the contour G is deformable, problem (1) reduces to a complex problem of matching of potential and turbulent flows at an *a priori* unknown boundary with an additional dynamic condition on pressure. In problem (2), the contour G, as well as an additional condition on it, is unknown in principle. However, the results obtained from mathematical analogues between physical processes of different origins are frequently more general if they follow from minimal restrictions (e.g., kinematically possible flows) than those derived from a hypothetical dynamic model [3, 8, 11].

(iv) It is important that the equations of sets (1) and (2) are invariant under the Galilean transformations. This means that the problem of airfoil flow is equivalent to the problem of airfoil motion with respect to the unmovable medium, where vortices leaving the airfoil remain at the place where they originate. According to the magnetohydrodynamic analogue for the seismoelectric effect, this circumstance makes it possible to pass from the space coordinate to the time pattern of AEF variation, which is detected by instruments before earthquakes.

The problem of the stationary flow of the airfoil profile (for simplicity, G is taken as the interval xOy: $0 \le x \le b$, $y = 0$ of the x axis) reduces to the following singular integral equation with the Cauchy kernel for the vorticity intensity $\gamma(x)$:

$$v_y(x) = \frac{1}{2\pi}\int_0^b \frac{\gamma(s)ds}{x-s}, \quad x \in [0; b]. \quad (3)$$

When $v_y(x) = f(x)$ is a certain given function, Eq. (3) can have three different types of solutions [9, 12]:

$$\gamma_{10}(x) = \frac{2}{\pi}\sqrt{\frac{x}{b-x}}\int_0^b \sqrt{\frac{b-s}{s}}\frac{f(s)}{s-x}ds,$$

$$\gamma_{1b}(x) = \frac{2}{\pi}\sqrt{\frac{b-x}{x}}\int_0^b \sqrt{\frac{s}{b-s}}\frac{f(s)}{s-x}ds,$$

$$\gamma_2(x) = \frac{2}{\pi\sqrt{x(b-x)}}\left[\int_0^b \frac{f(s)\sqrt{s(b-s)}}{s-x}ds + \text{const}\right], \quad (4)$$

$$\gamma_3(x) = \frac{2}{\pi}\sqrt{x(b-x)}\int_0^b \frac{f(s)ds}{\sqrt{s(b-s)}(s-x)}$$

$$\text{for } \int_0^b \frac{f(s)ds}{\sqrt{s(b-s)}} 0,$$

which are, respectively, unlimited at one end of the interval and limited at the other end (where Chaplygin–Zhukovsky condition is satisfied), unlimited, and limited at both ends of the interval $0 \le x \le b$.

Singular integrals (4) are considered in the principal-value sense. To calculate them, it is convenient to make the change

$$s = \frac{b}{2}(1 + \cos\theta), \quad x = \frac{b}{2}(1 + \cos\mu),$$

where $\theta, \mu \in [0, \pi]$. If $f(x)$ is specified as an expansion in $\cos n\theta$ or Chebyshev polynomials, the calculation reduces to a combination of known integrals [10]. For the simplest case $f(x) = 1$,

$$\gamma_{10}(x) = 2\sqrt{\frac{x}{b-x}}, \quad \gamma_{1b}(x) = 2\sqrt{\frac{b-x}{x}}, \quad \gamma_2(x) = \frac{2(2x-b)}{\sqrt{x(b-x)}}, \quad (5)$$

where γ_{10}, and γ_{1b} are limited for $x \longrightarrow 0$ and $x \longrightarrow b$, respectively, and satisfy the Chaplygin–Zhukovsky condition, whereas γ_2 does not satisfy this condition. For $f(x) = \pm\left(1 - \frac{2x}{b}\right)$, we obtain

$$\gamma_3^-(x) = -4\sqrt{\frac{x}{b}\left(1-\frac{x}{b}\right)} \text{ and } \gamma_3^+(x) = 4\sqrt{\frac{x}{b}\left(1-\frac{x}{b}\right)} \quad (6)$$

for the upper and lower signs, respectively.

Analysis reveals the clear similarity between the shapes of the precursor signals of the AEF [7] and the superposition of the corresponding plots of γ_{1b}, γ_{10}, and γ_2 [Eqs. (5), (6)] without tails going to $\pm\infty$ for $x \longrightarrow 0$ or $x \longrightarrow b$. This similarity follows from the Galilean invariance of systems (1) and (2) in combination with the magnetohydrodynamic analogue.

Existing seismically active zones are usually attributed to the tectonics of lithospheric plates. According to this concept, thermal convection in the Earth's mantle [3, 13] in combination with the dynamic effects of complex Il'yushin loading due to the proper rotation of the Earth and gravitational interaction with other bodies of the solar system [14] is responsible for the motion of lithospheric plates. High mechanical stresses arise at the boundaries of plates. These stresses induce breakages in the lithosphere and the formation of cracks and their collapse, which are responsible for earthquakes. The development of earthquakes in the lithosphere is accompanied by various SEMP in the atmosphere. In particular, the seismoelectric effect anomalously increases the natural AEF from 120–140 V/m to an atmospheric prebreakdown voltage of almost several kilovolts per centimeter.

Such voltages arise only under strong thunderclouds [2], which can be accompanied by strong disturbances of the atmospheric air under the pendulum-like transfer of electric energy to the kinetic energy of the hydrodynamic motion of a dielectric continuous medium [15]. However, this phenomenon, as well as the electric-field breakdown, which accompanies the seismoelectric effect and passes from the lithosphere to the atmosphere through sediment and soil layers, is beyond the scope of this work.

REFERENCES

1. M. V. Lomonosov, *Selected Papers*, Vol. 1: *Natural Sciences and Philosophy* (Nauka, Moscow, 1986).
2. Ya. I. Frenkel', *Theory of Atmospheric Electricity Phenomena* (GITTL, Moscow, 1949).
3. *Cosmic Earth Science: Dialogs of Nature and Society. The Stable Development*, Ed. by V. A. Sadovnichiĭ (Mosk. Gos. Univ., Moscow, 2000).
4. A. A. Vorob'ev, *Equilibrium and Transformation of Energy Types Inside the Earth* (Tomsk Univ., Tomsk, 1980).
5. *Electric and Magnetic Precursors of Earthquakes*, Ed. by V. P. Golovkov (Phys. Inst., Tashkent, 1983).
6. M. B. Gokhberg, V. A. Morgunov, and O. A. Pokhotelov, *Seismoelectromagnetic Phenomena* (Nauka, Moscow, 1988).
7. *Methods of Analysis of Seismoelectromagnetic Processes*, Ed. by O. M. Barsukov (Inst. Fiz. Zemli, Moscow, 1991).

8. A. A. Samarskiĭ and A. P. Mikhaĭlov, *Mathematical Simulation: Ideas, Methods, Examples* (Fizmatlit, Moscow, 2001).
9. V. L. Natyaganov, in *Books of Abstracts of 5th International Congress of Mathematical Modeling* (Yanus-K, Moscow, 2002), Vol. 1, p. 33.
10. A. I. Nekrasov, *Theory of Airfoil in a Nonstationary Flow* (Akad. Nauk SSSR, Moscow, 1947).
11. H. K. Moffatt, *Magnetic Field Generation in Electrically Conduction Fluids* (Cambridge Univ. Press, Cambridge, 1978).
12. F. D. Gakhov, *Boundary Value Problems* (Addison-Wesley, Reading, Mass., 1966; Nauka, Moscow, 1977).
13. V. P. Myasnikov and V. E. Fadeev, *Models of the Evolution of the Earth and Earth-Group Planets* (VINITI, Moscow, 1980).
14. E. I. Shemyakin, Vestn. Mosk. Univ., Ser. 1: Mat., Mekh., No. 3, 63 (1993).
15. V. A. Dubrovskiĭ and N. N. Rusakov, Dokl. Akad. Nauk SSSR **306**, 64 (1989).

Translated by R. Tyapaev

Doklady Physics, Vol. 48, No. 7, 2003, pp. 337–339. Translated from Doklady Akademii Nauk, Vol. 391, No. 3, 2003, pp. 324–326.

PHYSICS

Contribution of Octupole Transitions to the Angular Distribution of Photoelectrons Emitted in Photoionization

Corresponding Member of the RAS V. I. Nefedov*, V. G. Yarzhemsky*, I. S. Nefedova*, M. B. Trzhaskovskaya, and R. Szargan*****

Received March 25, 2003

We recently showed [1–12] that, contrary to widespread opinion, nondipole transitions, including dipole–quadrupole and quadrupole, make a noticeable contribution to the intensity and angular distribution of electrons emitted in photoionization even for comparatively low energies 0.5–1 keV of photoelectrons. We know of only one work [7] where it was shown that the effect of even octupole transitions in the photoionization of the Ne 2*p* shell on the determination of the parameters of dipole–quadrupole transitions could be revealed for photoelectrons with energies below 1 keV under special experimental conditions. The experiment reported in [7] was carried out with linearly polarized radiation.

In this work, we determine the effect of octupole transitions on the angular distribution of photoelectrons in a solid with allowance for the elastic scattering of photoelectrons when unpolarized exciting radiation is used. The solution of this problem is important both from the theoretical viewpoint and for practical application of the X-ray–electron quantitative analysis of the surface of solids to determine the sensitivity factors and, with high-energy photoelectrons, to determine the thicknesses of thin films.

When electron spectra are excited by unpolarized radiation, the angular distribution of photoelectrons, which is obtained with the inclusion of $O(k^1, r^1)$ terms, where k is the photon energy and r is the radius of the ionized atomic electron shell, has the form [6]

$$\frac{d\sigma_i}{d\Omega} = \frac{\sigma_i}{4\pi}[1 - 0.5\beta_i P_2(\cos\theta) + (\delta_i + 0.5\gamma_i \sin^2\theta)\cos\theta]. \quad (1)$$

Here, σ_i is the cross section for the photoionization of the ith atomic shell, $P_2(\cos\theta) = \frac{1}{2}(3\cos^2\theta - 1)$ is the Legendre polynomial, θ is the angle between the photon momentum and the direction of the photoelectron emission. The parameter β describes the angular distribution of photoelectrons in the dipole approximation. Parameters γ and δ describe the $E1$–$E2$ and $E1$–$M1$ interactions, where E and M mean the electric and magnetic interactions, respectively, and the number after these letters means the multipole order. In particular, $E1$–$E2$ means the electric dipole–quadrupole interaction making the dominant contribution to the parameters γ and δ.

The expression for the angular distribution of photoelectrons in the octupole approximation for linearly polarized excitation was presented in [7] and for excitation by unpolarized radiation was first obtained in [12]:

$$\frac{d\sigma_i}{d\Omega} = \frac{\sigma_i}{4\pi}[1 - 0.5(\beta + \Delta\beta_{\text{unpol}})P_2(\cos\theta) + (\delta_i + 0.5\gamma_i \sin^2\theta)\cos\theta + \xi P_4(\cos\theta)], \quad (2)$$

where $P_4(\cos\theta) = \frac{1}{8}(35\cos^4\theta - 30\cos^2\theta + 3)$. Here, two additional parameters, $\Delta\beta_{\text{unpol}}$ and ξ, appear compared to Eq. (1). The notation of parameters corresponds to the notation for linearly polarized excitation [7]. The notation for angles is shown in Fig. 1.

The parameter $\Delta\beta_{\text{unpol}}$ includes the terms $M1$–$M1$, $E1$–$M2$, $M1$–$E2$, $E2$–$E2$, and $E1$–$E3$ and the $(kr)^2$-order

* *Kurnakov Institute of General and Inorganic Chemistry, Russian Academy of Sciences, Leninskiĭ pr. 31, Moscow, 117907 Russia*
e-mail: vgyar@igic.ras.ru
** *Petersburg Nuclear Physics Institute, Russian Academy of Sciences, Gatchina, St. Petersburg, 188350 Russia*
*** *Leipzig Universität, Leipzig, Germany*

1028-3358/03/4807-0337$24.00 © 2003 MAIK "Nauka/Interperiodica"

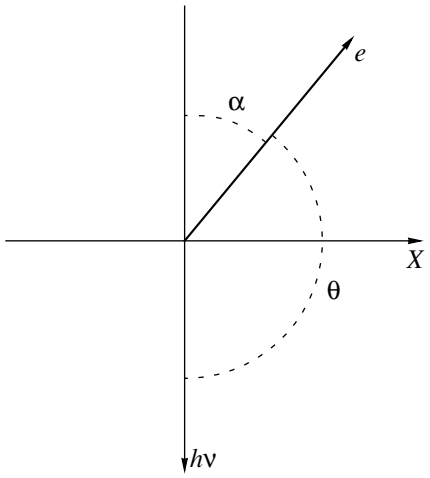

Fig. 1. Notation of angles.

correction to the $E1$–$E1$ term. The parameter ξ is associated with the $E2$–$E2$ and $E1$–$E3$ interactions.

For linearly polarized excitation, there are four additional parameters—$\Delta\beta_{pol}$, η, μ, and ξ—to formula (1) [7]. Interactions corresponding to these parameters were presented in [7]. For polarized and unpolarized excitation of spectra, the parameters $\Delta\beta_{unpol}$ and $\Delta\beta_{pol}$ are different, whereas the parameter ξ is the same.

TRANSPORT THEORY

We will determine the angular distribution of photoelectrons in a solid with allowance for octupole parameters, elastic and inelastic scattering for the Al 2*s* line excited by unpolarized 1253.6-eV Mg MgK_α radiation by two independent methods. The first method is associated with transport theory [13]. The second method is the Monte Carlo simulation of the paths of photoelectrons in the solid. According to Eq. (2), the contribution of the octupole transitions to the intensity of a line excited by unpolarized radiation for free atoms has the form

$$F = \frac{\sigma_i}{4\pi} f, \tag{3}$$

where $f = -0.5\Delta\beta_{unpol}P_2(\cos\theta) + \xi P_4(\cos\theta)$.

We consider experimental conditions of practical interest (see Fig. 1). Ionizing radiation is perpendicular to the plane of the sample. In this case,

$$\cos\theta = -\cos\alpha. \tag{4}$$

According to transport theory, for a solid with allowance for elastic and inelastic scattering of photoelectrons, the quantity f transforms to

$$\begin{aligned} f_1 &= A + \delta \\ &= a[-0.5\Delta\beta_{unpol}P_2(\cos\theta) + \xi P_4(\cos\theta)] + \delta. \end{aligned} \tag{5}$$

Here,

$$\begin{aligned} \delta = -\frac{\omega a}{16} H(\cos\alpha, \omega) \\ \times \left[\xi \int_0^1 \frac{x^3 H(x, \omega)[35x^5 - 30x^3 + 3x]dx}{\cos\alpha + x} \right. \\ \left. + 2\Delta\beta_{unpol} \int_0^1 \frac{H(x, \omega)[x - 3x^3]}{\cos\alpha + x} \right], \end{aligned} \tag{6}$$

where $H(x, \omega)$ is the Chandrasekhar function, ω is the albedo of single scattering, and $a = 1 - \omega$.

In order to show that δ is usually negligibly small compared to A, we calculate δ for $\omega = 0.1$, 0.25, 0.4 and $\alpha = 0$, 10, 20, …, 90. The quantities $\Delta\beta_{unpol}$ and ξ are taken from relativistic calculations for the 1*s*, 2*s*, and 2*p* levels of atoms from Li to Ne and Al 2*s*, Ar 2*p*, Xe 4*s*, 4*p*, and 4*d* levels for $E_{kin} = 1$ keV. For the data calculated for 640 variants of δ, we can arrive at the following conclusions illustrated by Table 1 for the Al 2*s* line.

(i) δ is always small and is equal to about 1% of A, in addition to the α values, for which A is equal to or close to zero.

(ii) The absolute value of $A + \delta$ is always close to A, although $K = \frac{\delta}{A} + \delta$ can be large for angles α for which A is close to zero.

Table 1. Octupole contribution to the Al 2*s*-line intensity (excitation by the MgK_α line)

α, deg	δ	A	$A + \delta$	K
0	-1.279×10^{-05}	−0.00091	−0.000927	0.013798
10	-1.215×10^{-05}	−0.00064	−0.000649	0.018741
15	-1.220×10^{-05}	−0.00032	−0.000334	0.036496
20	-1.242×10^{-05}	6.02×10^{-5}	4.776×10^{-5}	−0.25999
30	-1.286×10^{-05}	0.000829	0.0008166	−0.01575
40	-1.351×10^{-05}	0.001281	0.0012672	−0.01066
45	-1.365×10^{-05}	0.0013	0.001286	−0.01061
50	-1.435×10^{-05}	0.001165	0.0011507	−0.01247
60	-1.537×10^{-05}	0.000496	0.000481	−0.03195
65	-1.552×10^{-05}	3.32×10^{-5}	1.764×10^{-5}	−0.87948
70	-1.633×10^{-05}	−0.00045	−0.000467	0.035007
80	-1.616×10^{-05}	−0.00126	−0.001279	0.01264
90	-3.379×10^{-06}	−0.00158	−0.001584	0.002133

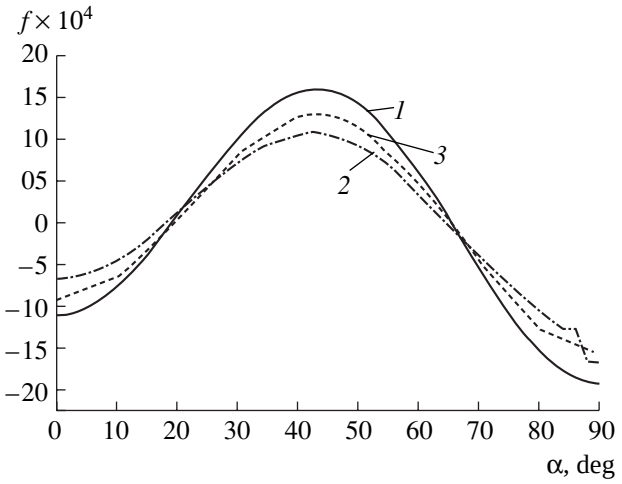

Fig. 2. Octupole corrections to the angular distribution of photoelectrons in the ionization of the Al 2*s* level by unpolarized X rays from the MgK_α line: (*1*) free atom, (*2*) Monte Carlo method, and (*3*) transport theory.

(iii) Since the absolute value of A is usually of interest, δ is negligible.

MONTE CARLO CALCULATIONS

Monte Carlo calculations were carried out according to [4, 13] for the Al 2*s* line excited by unpolarized 1253.6-eV Mg MgK_α radiation for the experimental case described above. The α and azimuth-angle range were divided into 90 and 80 parts, respectively. One thousand trajectories for 16 depths of the sample began from each section. The number of independent trajectories was equal to 1.152×10^8, $\omega = 0.18$ [13], and the elastic and inelastic mean free paths were equal to 14.8 and 21.1 Å, respectively. In this work, we calculated the parameters $\Delta\beta$ and ξ including the quadrupole and octupole interactions $E1$–$E3$, $E1$–$E2$, and $E1$–$M2$ of the $O(k^2\alpha^2)$ order for the Al 2*s* line excited by unpolarized 1253.6-eV MgK_α radiation. As in [1], calculations were made in the relativistic approximation. We used the Dirac–Fock–Slater atomic potential with the coefficient $C = 1$ for the exchange term. The wave functions of bound states were calculated by the method of the self-consistent field for a neutral atom. The continuous-spectrum functions were calculated in the approximation of frozen orbitals with the Dirac–Fock–Slater potential for an ion with a vacancy induced by photoionization. The calculated $\Delta\beta$ and ξ values are equal to –0.00345 and –0.00284.

Figure 2 shows the Monte Carlo calculations in comparison with the transport-theory calculations. In addition, data for the 2*s* line of a free Al atom are shown. As could be expected, the intensity for the solid Al sample for most angles is lower than that for the free atom due to the elastic scattering of photoelectrons in the solid. The Monte Carlo calculations agree well with transport-theory calculations.

ACKNOWLEDGMENTS

This work was supported by the Russian Foundation for Basic Research (project no. 02-03-32693) and by the Division of Chemistry and Material Sciences, Russian Academy of Sciences.

REFERENCES

1. M. B. Trzhaskovskaya, V. I. Nefedov, and V. G. Yarzhemsky, At. Data Nucl. Data Tables **77**, 97 (2001); **82**, 257 (2002).
2. M. B. Trzhaskovskaya, V. K. Nikulin, V. I. Nefedov, and V. G. Yarzhemsky, J. Phys. B **34**, 3221 (2001).
3. V. I. Nefedov, V. G. Yarzhemsky, I. S. Nefedova, *et al.*, J. Electron. Spectrosc. Relat. Phenom. **107**, 123 (2000).
4. V. I. Nefedov and I. S. Nefedova, J. Electron. Spectrosc. Relat. Phenom. **113**, 3 (2000).
5. V. I. Nefedov, V. G. Yarzhemsky, R. Hesse, *et al.*, J. Electron. Spectrosc. Relat. Phenom. **125**, 153 (2002).
6. J. W. Cooper, Phys. Rev. A **47**, 1841 (1993).
7. A. Derevianko, O. Hemmers, S. Oblad, *et al.*, Phys. Rev. Lett. **84**, 2116 (2000).
8. V. I. Nefedov and I. S. Nefedova, Poverkhnost **4**, 50 (2000).
9. V. I. Nefedov, V. G. Yarzhemsky, I. S. Nefedova, *et al.*, Poverkhnost **6**, 10 (2000).
10. V. I. Nefedov, I. S. Nefedova, V. G. Yarzhemsky, *et al.*, Dokl. Akad. Nauk **385**, 515 (2002) [Dokl. Phys. **47**, 583 (2002)].
11. V. I. Nefedov, V. G. Yarzhemsky, I. S. Nefedova, *et al.*, Dokl. Akad. Nauk **367**, 324 (1999) [Dokl. Phys. **44**, 423 (1999)].
12. M. B. Trzhaskovskaya, V. I. Nefedov, V. G. Yarzhemsky, and R. Szargan, Dokl. Akad. Nauk **390** (5) (2003) (in press).
13. V. I. Nefedov and I. S. Fedorova, J. Electron. Spectrosc. Relat. Phenom. **85**, 211 (1997).

Translated by R. Tyapaev

Doklady Physics, Vol. 48, No. 7, 2003, pp. 340–342. Translated from Doklady Akademii Nauk, Vol. 391, No. 1, 2003, pp. 44–46.

TECHNICAL PHYSICS

Improvement of the Properties of Anisotropic Soft Magnetic Materials by Laser Treatment and Monitoring of Its Efficiency

Yu. N. Dragoshanskiĭ*, B. K. Sokolov, V. I. Pudov, Yu. Ya. Reutov, V. F. Tiunov, and V. V. Gubernatorov

Presented by Academician V.P. Skripov January 10, 2003

Received January 21, 2003

The improvement of the properties of magnetic materials is a necessary element in the process of metal and power saving. The formation of sharp crystallographic and magnetic textures in the most widely used materials—anisotropic electrical steels (Fe–Si-based alloys)—increases the magnetic induction. However, large crystallites (up to 50 mm in size), or magnetic domains, are formed in this case. As a result, eddy-current (P_{ec}) magnetic losses increase considerably up to 85% of the total losses. Large domains and high P_{ec} losses are also characteristic for a new class of soft magnetic materials—strips of amorphous, nanocrystalline Fe- and Co-based alloys. Theoretically, P_{ec} losses can be reduced due to a decrease in the rate of domain-wall motion. This can be realized by decreasing the width of strip domains and by bending the planes of domain walls over the section of a ferromagnet [1].

An effective method of narrowing the domains and reducing the magnetic losses P is the formation of structural barriers in the ferromagnet, which are transversely oriented narrow regions whose structure differs from the structure of the basic material [2]. Magnetic charges are concentrated in these regions, thereby limiting the sizes of main domains, and are responsible for the appearance of closure regions—magnetic reversal centers (see the upper panel in Fig. 1). An effective method of producing such barriers is local laser treatment, which deforms the material by rapid heating and cooling. Laser treatment provides both the fragmentation of the domains and the longitudinal extension of the ferromagnet [3]. The effect of local laser treatment was experimentally found to increase from 10–15% to 20–25% after thermomagnetic treatment in an alternating magnetic field [4, 5] due to enhancement of magnetic uniaxiality in triaxial and amorphous ferromagnets. The effect is associated with the induction of uniaxial magnetic short-range order anisotropy, which increases a fraction of the strip domain structure, and with the destabilization of the magnetic-domain walls [6]. A new thermomagnetic-treatment concept including the strain aging of materials makes it possible to predict the efficiency of such an action. For the subsequent local laser treatment, the optimum irradiation energy density (resulting in the minimization of P_{ec}) and its variations along the strip length (~10%) were found to exist due to instabilities in radiation, material properties, and the state of its surface [7].

To optimize the effect of reducing losses in various parts of inhomogeneous anisotropic electrical steel, methods of monitoring the magnetic characteristics, which make it possible to determine the effect of laser

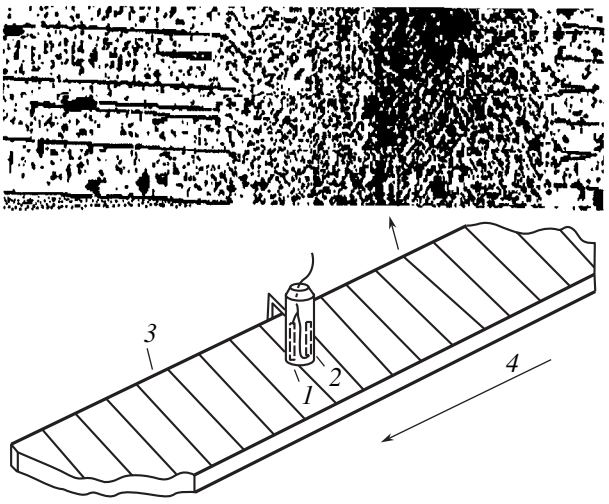

Fig. 1. (Upper panel) Magnified fragment of a region of magnetic domains near the laser-action region; (lower panel) *1* and *2* are the magnetically sensitive elements of the transducer situated over transformer-steel strip *3* continuously moving in direction *4*.

Institute of Metal Physics, Ural Division, Russian Academy of Sciences, ul. S. Kovalevskoĭ 18, Yekaterinburg, 620219 Russia

** e-mail: drago@imp.uran.ru*

1028-3358/03/4807-0340$24.00 © 2003 MAIK “Nauka/Interperiodica”

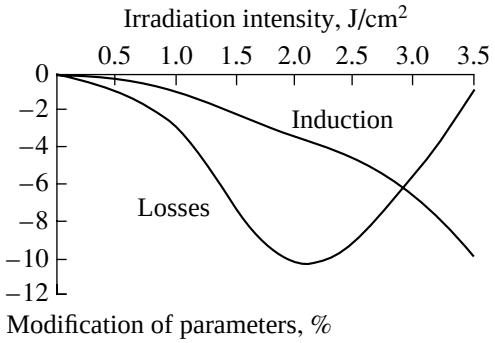

Fig. 2. Magnetic induction B_{100} and magnetic losses $P_{1.7/50}$ vs. the intensity of laser irradiation.

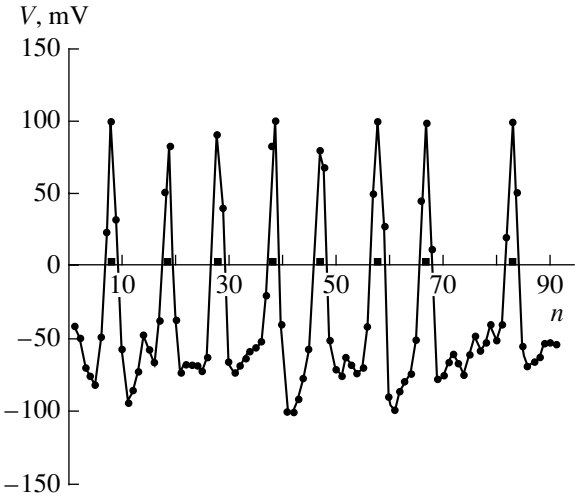

Fig. 3. Amplitude of the ferroprobe transducer signal that corresponds to the regions of laser action (denoted by dark squares along the x axis) and to the irradiation intensity close to optimal (3.3 J/cm^2).

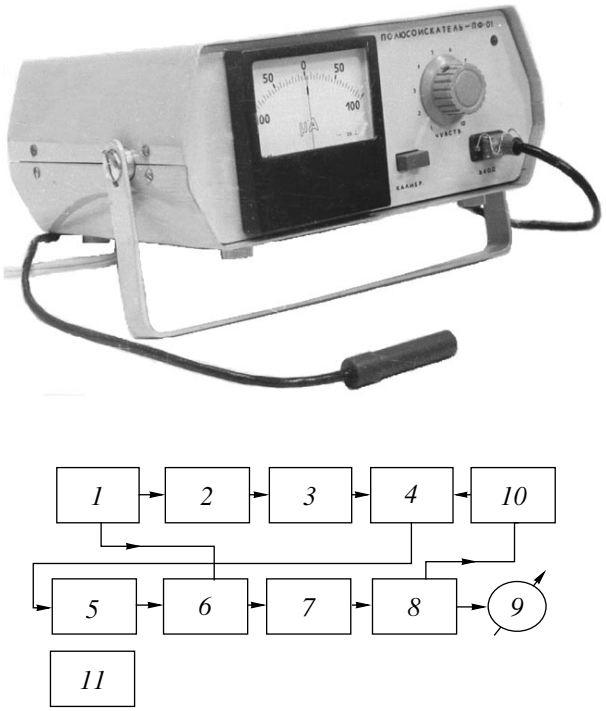

Fig. 4. Ferroprobe instrument for measuring magnetic stray fields over the transformer-steel strip and its block representation: (*1*) square-pulse generator at the frequency 2*f*, (*2*) frequency divider (by 2), (*3*) power amplifier, (*4*) ferroprobe transducer, (*5*) selective amplifier at the frequency 2*f*, (*6*) synchronous detector, (*7*) low-pass filter, (*8*) direct-current amplifier, (*9*) indicator, (*10*) switch of measurement ranges, and (*11*) stabilizing block of secondary electric power supply.

action and to correct the treatment regime, were developed. For nondestructive testing, we used the Barkhausen effect, magnetoelastic acoustic emission, eddy-current method, and electromagnetic induction methods [8, 9]. Among them, two magnetic induction methods, where ferroprobes and attached detectors made of amorphous alloys are used, are best applicable for a moving strip of a material [10, 11]. Ferroprobe monitoring is realizable due to the correlation discovered (Fig. 2) between variations in magnetic losses (for the amplitude $B \sim 1.7$ T and frequency $f \sim 50$ Hz) and a decrease in the magnetic induction B_{100} (the induction in a magnetic field of 100 A/m), which corresponds to an increase in a stray magnetic field H_s in regions subjected to the laser action, when the radiation energy density of a CO_2 laser is controlled.

The minimum magnetic losses in a material correspond to a certain decrease in induction (Fig. 2). Under local laser treatment, the minimum level of energy losses in a moving ferromagnetic strip is provided by maintaining the optimum amplitude of the signal that arises in miniature (0.1×2.5 mm) ferroprobe transducers, when stray fields H_s from the laser-action regions pass near them (Fig. 1). The method of connection of the ferroprobe elements makes it possible to measure the horizontal gradient of the vertical component of the magnetic field H_s, thereby clearly revealing the regions of the action of laser treatment and their intensity (Fig. 3).

Thus, the efficiency of laser treatment was monitored by measuring an indirect characteristic H_s. In addition, we developed a method of direct measurement of magnetic losses in a moving steel strip by an instrument based on an F-530 electronic wattmeter. The basic element of the instrument is an attached inductive detector containing (instead of an ordinary permeameter) a core that is made of ten strips of a $Fe_{80}B_{20}$ amorphous soft magnetic alloy and is bent on a mandrel 25 mm in diameter. Magnetic losses in it are one-tenth losses in the measured region of the material. For $P_{1.5/50}$, we detected small changes in losses in local regions (~25 mm in length) of the steel strip. The measurement error of magnetic losses did not exceed 6–7% [11].

Thus, by investigating the effect of local laser treatment on soft magnetic electrical steels and alloys, we developed representations about the processes of their magnetization reversal and mechanisms of changing the domain structure and magnetic properties. A new thermomagnetic-treatment concept that includes the processes of strain aging under treatment and makes it possible to predict its efficiency was proposed. Two magnetic methods (based on either of two measured parameters H_s and $P_{1,5/50}$) for the continuous nondestructive monitoring of the effect of local laser treatment on moving strips made of soft magnetic steels and alloys in the process of their production were developed. Setups with a ferroprobe and inductive instruments were constructed (Fig. 4).

ACKNOWLEDGMENTS

This work was supported by the Russian Foundation for Basic Research (project nos. 02-02-16443, 03-02-16185).

REFERENCES

1. Yu. N. Dragoshanskiĭ, V. V. Gubernatorov, B. K. Sokolov, and V. V. Ovchinnikov, Dokl. Akad. Nauk **383**, 761 (2002) [Dokl. Phys. **47**, 302 (2002)].
2. Yu. N. Dragoshanskiĭ, Candidate's Dissertation in Physics and Mathematics (Inst. Fiz. Met., Sverdlovsk, 1968).
3. B. K. Sokolov and Yu. N. Dragoshanskiĭ, Fiz. Met. Metalloved. **72** (1), 92 (1991).
4. V. V. Gubernatorov, A. P. Potapov, B. K. Sokolov, *et al.*, Fiz. Met. Metalloved. **91** (3), 40 (2001).
5. V. V. Gubernatorov and T. S. Sycheva, in *Proceedings of 16th Ural School on Problems of Physical Metallurgical Science of Perspective Materials, Ufa, 2002*, p. 163.
6. Yu. N. Dragoshanskiĭ, RF Inventor's Certificate No. 2025504, Byull. Izobret., No. 24, 105 (1994).
7. S. V. Smirnov, A. M. Yudin, B. P. Yatsenko, *et al.*, in *Proceedings of 9th International Conference on Using of Accelerators of Charged Particles in Industry and Medicine* (TsNII Atominform, Moscow, 2002), p. 397.
8. E. S. Gorkunov and Yu. N. Dragoshanskiĭ, Defektoskopiya, No. 12, 3 (2001).
9. E. S. Gorkunov and Yu. N. Dragoshanskiĭ, in *Proceedings of 8th European Conference for Non-Destructive Testing, Barcelona, 2002*, p. MC-75.
10. B. K. Sokolov, Yu. Ya. Reutov, V. I. Pudov, *et al.*, Defektoskopiya, No. 3, 54 (2003).
11. V. F. Tiunov, Defektoskopiya, No. 5, 41 (2003).

Translated by Yu. Vishnyakov

Doklady Physics, Vol. 48, No. 7, 2003, pp. 343–346. Translated from Doklady Akademii Nauk, Vol. 391, No. 1, 2003, pp. 47–50.

TECHNICAL PHYSICS

Low-Temperature Superplasticity of Microcrystalline High-Strength Magnesium Alloys Produced by Equal-Channel Angular Pressing

V. N. Chuvil'deev, V. I. Kopylov, M. Yu. Gryaznov, and A. N. Sysoev

Presented by Academician O.A. Bannykh December 9, 2002

Received January 13, 2003

Magnesium alloys are lighter than other structural metals and have very low plasticity, which hampers their practical use. The elongation to failure of high-strength magnesium alloys to failure is usually less than 12–17% at room temperature and is equal to 25–40% at temperatures 150–300°C. The formation of structures facilitating the superplasticity effect is an efficient method for improving the deformability of alloys. The low-temperature superplasticity of magnesium alloys from room temperature to 300°C is of particular interest for applications. The transition to the superplasticity state can be achieved through the formation of the microcrystalline structure by intense plastic deformation. In this study, the microcrystalline structure in MA14 (Mg–6% Zn–0.6% Zr) and MA2-1 (Mg–4% Al–1% Zn) magnesium alloys was formed by equal-channel angular pressing (ECAP) [1–3], which is a new method for processing metals by pressure and provides an efficient control of the formation of their structure [1]. Multipass ECAP under the optimally chosen temperature–strain-rate conditions provides an efficient grain refinement, formation of large-angle grain boundaries, and a homogeneous nano- and microcrystalline structure in bulk samples [3].

In this study, ECAP was realized in an instrument where the angle between the working and output channels was equal to 90°. The homogeneity of the simple shear strain was controlled at every cycle by observing the fiducial marks scratched on the flow plane of the billet in the direction perpendicular to the working axis. We used an extremely rigid regime of ECAP during which a bar was turned through 90° around its longitudinal axis at every pass. The pressing speed for a $22 \times 22 \times 165$-mm bar was equal to 0.4 mm/s. The cast and extruded magnesium-alloy samples were processed in six ECAP passes at temperatures 200–250°C. As a result of pressing, the alloys had a homogeneous microcrystalline structure with a mean grain size of ~1 μm. For mechanical tests, flat double-blade-shaped samples with the gauge sizes of $2 \times 2 \times 3$ mm were cut from the bars by electric-spark cutting.

Tensile tests with a constant velocity of crosshead displacement and with an initial strain rate from 10^{-4} to 3×10^{-1} s^{-1} were carried out on an INSTRON tensile testing machine in the temperature region 20–430°C (430°C is the maximum test temperature for magnesium alloys in air). The samples were heated to test temperature in four minutes. To establish thermal equilibrium, the samples were kept at working temperature for three minutes.

The results of the tensile tests of MA14 and MA2-1 microcrystalline magnesium alloys at temperatures 200–430°C with a strain rate of 3×10^{-3} s^{-1} are shown in Fig. 1.

Figure 2 displays the elongation δ to failure as a function of deformation temperature. It is seen that the temperature dependence of the quantity δ is nonmonotonic for a constant strain rate. In MA14 alloy, δ increases rapidly from 170 to 810% with an increase in the deformation temperature from 150 to 260°C and decreases abruptly down to 170% at 280°C. With further an increase in the deformation temperature, plasticity increases slowly to 340% at 430°C.

A similar but less pronounced behavior is observed in MA2-1 alloy. The elongation to failure increases rapidly from 175 to 385% with an increase in the deformation temperature from 200 to 250°C (Fig. 2). However, δ decreases near 250°C less than in MA14 alloy, and plasticity attains a maximum of 650% at 430°C.

The decrease in the plasticity of the alloys in the region 260–280°C is caused by the rapid dissolution of the structure-stabilizing Mg_2Zn_3 phase in both alloys at these temperatures. In MA14 alloy, this dissolution is accompanied by an intense growth of grains: at a temperature of 280°C, grain size increases up to 10 μm dur-

Research Physicotechnical Institute, Nizhni Novgorod State University, pr. Gagarina 23, korp. 3, Nizhni Novgorod, 603950 Russia

e-mail: fmv@phys.unn.runnet.ru, chuvildeev@phys.unn.runnet.ru

1028-3358/03/4807-0343$24.00

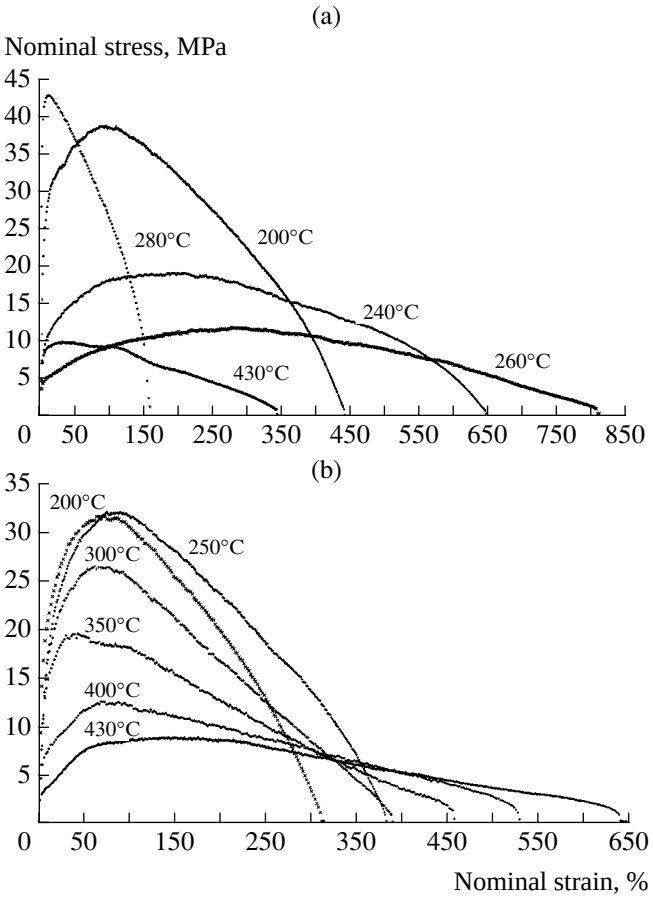

Fig. 1. Stress–strain curves for the tension of (a) MA14 and (b) MA2-1 microcrystalline alloys for a strain rate of 3×10^{-3} s^{-1} and various deformation temperatures.

ing the heating of the sample up to the superplastic-deformation temperature (4 min). In MA2-1 alloy, the dissolution of the Mg_2Zn_3-phase particles also promotes the growth of grains; however, this growth is negligible (up to 2–3 μm), because this alloy includes $Mg_{17}Al_{12}$ particles of the second structure-stabilizing phase.

The elongation to failure as a function of the strain rate $\dot{\varepsilon}$ is shown in Fig. 3 for the optimal superplasticity temperature (260°C for MA14 and 400°C for MA2-1). With a decrease in the strain rate, δ increases to 960 and 720% in MA14 and MA2-1 for $\dot{\varepsilon} = 8 \times 10^{-4}$ and 1.4×10^{-4} s^{-1}, respectively.

The comparison between our results and the results of other authors (Table 1) shows that the plasticity of MA2-1 and MA14 microcrystalline magnesium alloys in the region of low-temperature superplasticity (200–300°C) is higher than that of their analogues by factors of 3 and 2, respectively [4–9].

The effect of an increase in plasticity at room temperature without a significant decrease in strength (Table 2), which was also found for the magnesium alloys under consideration, is very interesting. The elongation to failure in MA2-1 microcrystalline alloy is equal to 65% for room temperature and a strain rate of 3×10^{-3} s^{-1} (in comparison with conventional 12–19% and 46% obtained in [11]). The elongation to failure in MA14 microcrystalline alloy is equal to 45% at room temperature, which is twice as large as the best values for analogues [7, 12].

Large elongations for magnesium alloys at temperatures 200–260°C and for a strain rate of 3×10^{-3} s^{-1} can be explained in terms of the low-temperature superplasticity developing under these conditions [13]. The rheological equation relating the rate of superplastic flow to the flow stress σ and deformation temperature T has the form

$$\dot{\varepsilon} = A\left(\frac{\sigma}{G}\right)^n\left(\frac{b}{d}\right)^p\left(\frac{GD_{b0}\varphi}{kT}\right)\exp\left(-\frac{Q}{RT}\right).$$

Here, b is the Burgers vector, d is the mean grain size, φ is the grain-boundary thickness, D_{b0} is the pre-expo-

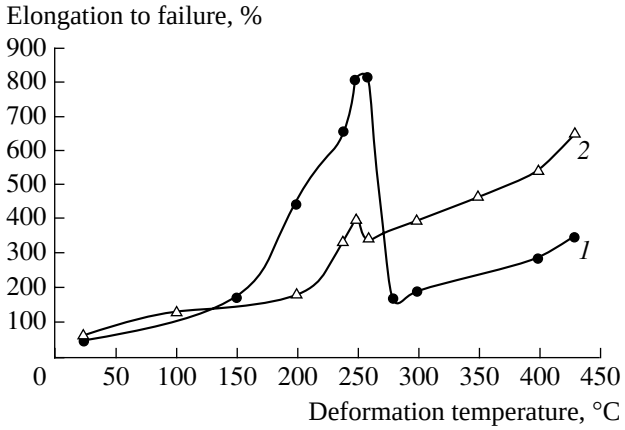

Fig. 2. Elongation to failure as a function of a deformation temperature in (*1*) MA14 and (*2*) MA2-1 microcrystalline alloys for a strain rate of 3×10^{-3} s^{-1}.

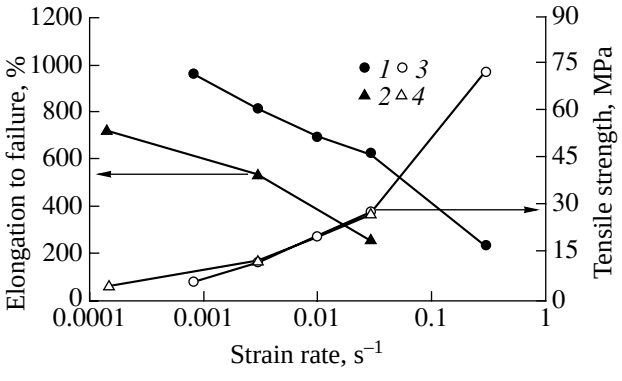

Fig. 3. (*1*, *2*) Elongation to failure and (*3*, *4*) tensile strength as functions of a strain rate for (*1*, *3*) MA14 (at a temperature of 260°C) and (*2*, *4*) MA2-1 (at a temperature of 400°C) microcrystalline alloys, respectively.

Table 1. Best plasticity parameters of MA2-1 and MA14 magnesium alloys and their foreign analogs AZ31 and ZK60 for deformation temperatures 150–300°C

Alloy	Production technology	Deformation rate, s^{-1}	Deformation temperature, °C	Elongation to failure, %	References
MA2-1	ECAP + annealing	3×10^{-3}	225	380	This study
MA2-1	Rolling	–	250	30	[4]
AZ31	Rolling	–	225	88	[5]
AZ31	Rolling	1×10^{-4}	250	140	[6]
MA14	ECAP	3×10^{-3}	260	810	This study
MA14	Rolling	–	150	36	[7]
ZK60	ECAP	1×10^{-3}	200	420	[8]
ZK60	Extrusion	1×10^{-3}	300	400	[9]

Note: Chemical composition of alloys.
Ma2-1: Mg—3.8–5.0 wt % Al—0.8–1.5 wt % Zn—0.3–0.7 wt % Mn.
Ma14: Mg—5.0–6.0 wt % Zn—0.3–0.9 wt % Zr.
AZ31: Mg—2.5–3.5 wt % Al—0.6–1.4 wt % Zn—0.2 wt % Mn.
ZK60: Mg—4.8–6.2 wt % Zn—0.5 wt % Zr.

Table 2. Same as in Table 1 but for room temperature

Alloy	Production technology	Deformation rate, s^{-1}	Elongation to failure, %	Tensile strength, MPa	References
MA2-1	ECAP	3×10^{-3}	65	265	This study
MA2-1	Rolling	–	14	260	[4]
AZ31	ECAP	–	38	240	[10]
AZ31	ECAP	1×10^{-3}	46	265	[11]
MA14	ECAP	3×10^{-3}	45	260	This study
MA14	Rolling	–	14	320	[7]
ZK60	Casting	–	5	275	[12]
ZK60	Extrusion	–	18	370	[12]

nential factor of the grain-boundary diffusivity, G is the shear modulus, k is the Boltzmann constant, Q is the activation energy for the strain-rate boundary diffusion, R is the molar gas constant, $p = 2$, and $A = 100$. The parameter n is inverse to the strain-rate sensitivity coefficient $m = \frac{\partial \ln \sigma}{\partial \ln \dot{\varepsilon}}$, is determined from the analysis of the experimental dependence $\sigma(\dot{\varepsilon})$, and is equal to $n = 2$ and 2.8 in the case under consideration for MA14 and MA2-1 alloys, respectively. From the above expression for $\dot{\varepsilon}$, the activation energy for the process of grain-boundary diffusion is easily expressed as $Q = \frac{Y - n \ln \sigma}{RT}$ (Y is the constant). The activation energy is equal to 66 and 60 kJ/mol in MA14 and MA2-1 alloys, respectively. For these Q values, the grain-boundary diffusivity $D_b = D_{b0} \exp\left(-\frac{Q}{RT}\right)$ for temperatures 240–260°C is larger than the value $D_b = 8 \times 10^{-10}$ cm^2/s calculated on the basis of standard data by a factor of about 350 ($D_{b0} = 8 \times 10^{-3}$ m^2/s and $Q = 92$ kJ/mol [14]).

Thus, to explain the results, the classical model of superplastic flow has to be completed by the conception on changes in the parameters of the grain-boundary diffusion under superplastic deformation. A variation in D_b as a function of the superplastic-strain rate can be calculated in the model that was described in [15] and based on the theory of nonequilibrium grain boundaries in metals [3]. According to [15], the quantity $D_b(\dot{\varepsilon})$ can be represented in the form

$$D_b(\dot{\varepsilon}) = D_b(1 + M_1 \ln(1 + M_2 \dot{\varepsilon})).$$

The parameters M_1 and M_2 are calculated on the basis of models [3] and are equal to $M_1 = 520$ and $M_2 = 300$

for magnesium (at $T = 260°C$). Substituting these values into the expression for $D_b(\dot{\varepsilon})$, we find that the ratio $\frac{D_b(\dot{\varepsilon})}{D_b}$ representing the diffusion-acceleration coefficient is equal to 330 for $\dot{\varepsilon} = 3 \times 10^{-3}$ s^{-1}. Thus, taking into account that the grain boundaries are nonequilibrium, we can explain the possibility of superplasticity in magnesium high-strength alloys for relatively low temperatures 200–260°C.

ACKNOWLEDGMENTS

This work was supported by the Russian Foundation for Basic Research (project nos. 02-03-33043 and 03-02-16923), the Ministry of Education of Russian Federation (project no. E02-4.0-131), the program "Basic Research and Higher Education" (BRHE), and the Research and Education Center "Physics of Solid Nanostructures" at the Nizhni Novgorod State University.

REFERENCES

1. V. M. Segal, V. I. Reznikov, V. I. Kopylov, *et al.*, *Processes of Plastic Structure Formation of Metals* (Nauka i Tekhnika, Minsk, 1994).
2. V. I. Kopylov, NATO ASI Ser. 3: High Technology **80**, 23 (2000).
3. V. N. Chuvil'deev, V. I. Kopylov, and W. Zeiger, Ann. Chim. (Paris) **27** (3), 55 (2002).
4. P. G. Miklyaev, *Mechanical Characteristics of Light Alloys at Temperatures and Velocities of Treatment by Pressure. Handbook* (Metallurgiya, Moscow, 1994).
5. J. Enss, T. Evertz, and T. Reier, in *Proceedings of 2nd International Conference on Magnesium Science and Technology, Israel, 2000*, p. 19.
6. J. Tan and M. Tan, Scr. Mater. **47**, 101 (2002).
7. *Magnesium Alloys. Handbook*, Vol. 1: *Metallurgical Science of Magnesium and Its Alloys*, Ed. by M. B. Al'tman, M. E. Drits, M. V. Timonov, and M. V. Chukhrov (Metallurgiya, Moscow, 1978).
8. H. Watanabe, T. Mukai, K. Ishikawa, and K. Higashi, Scr. Mater. **46**, 851 (2002).
9. H. Watanabe, T. Mukai, and K. Higashi, Scr. Mater. **40** (4), 477 (1999).
10. S. Kamado, T. Ashie, and H. Yamada, Mater. Sci. Forum **350**/**351**, 65 (2000).
11. T. Mukai, M. Yamanoi, H. Watanabe, and K. Higashi, Scr. Mater. **45**, 89 (2001).
12. K. Kubota, M. Mabuchi, and K. Higashi, J. Mater. Sci. **34**, 2255 (1999).
13. T. G. Nieh, J. Wadsworth, and O. D. Sherby, *Superplasticity in Metals and Ceramics* (Cambridge Univ. Press, Cambridge, 1997).
14. G. G. Frost and M. F. Eshbi, *Deformation-Mechanism Maps* (Pergamon, Oxford, 1982; Metallurgiya, Chelyabinsk, 1989).
15. V. N. Chuvil'deev and A. V. Petryaev, Fiz. Met. Metalloved. **89** (2), 24 (2000).

Translated by V. Bukhanov

Doklady Physics, Vol. 48, No. 7, 2003, pp. 347–352. Translated from Doklady Akademii Nauk, Vol. 391, No. 2, 2003, pp. 179–184.

TECHNICAL PHYSICS

Thermal Surface Decomposition of Condensed Systems Near the Boundary of Their Thermodynamic Stability: Intrinsic Features of the Process

O. F. Shlenskiĭ and N. N. Lyasnikova

Presented by Academician V.V. Osiko February 18, 2003

Received March 5, 2003

The upper temperature of the phase-state boundary for which a substance conserves thermodynamic stability in its condensed state can be attained as a result of both intense heating and pressure drop [1, 2]. From the practical standpoint, the most urgent problem is to describe the thermal processes that accompany decomposition of materials in extreme conditions of intense one-sided surface heating. We imply, in particular, the processes of both decomposition of heat-resistant coatings and combustion [3, 4]. Regularities of changes in the structure of materials under thermal decomposition as the phase-state boundary is approached were analyzed previously [5, 6].

In this paper, the problem of estimating the parameters of a surface thermal-decomposition zone for a material, i.e., the zone depth and the time of residence of a reacting substance in the zone, is set for the first time. Further analysis is performed on the basis of data available in the literature and novel experimental results.

In thermodynamics, the position of the phase-state boundary is determined from the condition of vanishing of the second derivatives of one of the thermodynamic potentials, e.g., $\delta^2 G = 0$, where G is the Gibbs free energy [1]. At the stability boundary, the derivatives $\frac{\partial p}{\partial v}$ and $\frac{\partial T}{\partial v}$ vanish, which makes it possible to calculate the parameters of the phase-state boundary from the equation of state [7]. The position of the phase-state boundary can be determined experimentally with a high degree of precision by pulse methods according to temperatures T_l of attainable superheating of samples [2].

In order to study the kinetics of thermal decomposition in the vicinity of the phase-state boundary, methods of physical experiments, which use thermal-vision and laser diagnostics, have been developed [8]. In the case under consideration, samples having the form of thin (7–10 μm) substance layers were deposited onto a metallic substrate preliminary heated to a constant temperature. The intensity of the thermal decomposition of the substance in the vicinity of the phase-state boundary is determined by registering the infrared (IR) radiation of the samples. In Fig. 1, an IR spectral thermogram for the radiation of a low-density polyethylene sample is presented as an example. In this thermogram, a gradual decrease in the signal intensity along the sample length as a result of thermolysis of the substance is seen.

As was shown by the tests of [8, 9], at high temperatures, kinetic curves of the thermal decomposition acquire the form of inclined straight lines (Fig. 2). This result implies that, at a constant temperature, the thermolysis process proceeds at a constant velocity W defined, in the main, by the first stage of the reaction. In this case, the heat-absorption (heat-release) function $F(T)$ can be represented in the form $F(T) = \rho Q W(T)$, where Q is the thermal yield of the reaction. The effect of rectification of kinetic curves is associated to a large

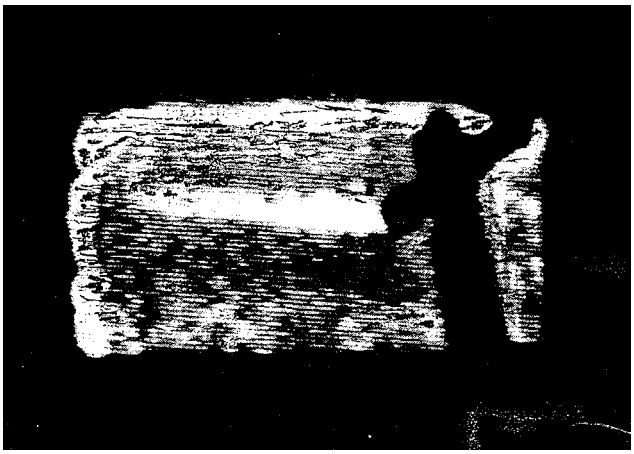

Fig. 1. Thermogram obtained in the IR spectral region for the surface of a metallic substrate with a thin melt of a substance. The dark band is the original sample fixed at a holder and the light band is the melt.

Russian Mendeleev University of Chemical Technology, Miusskaya pl. 9, Moscow, 125820 Russia

1028-3358/03/4807-0347$24.00

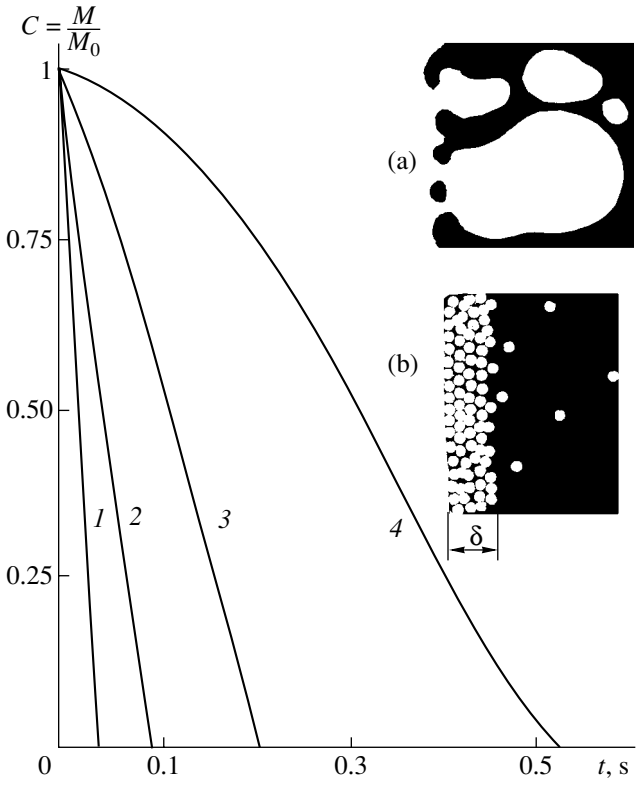

Fig. 2. Kinetic curves for the relative loss of the substance mass $\frac{M}{M_0}$. Curves *1* and *2* are obtained by the method of contact thermal analysis using laser diagnostics; curves *3* and *4* are obtained by IR-spectroscopy methods: (*1*) polyethylene siloxane PEG-400, T = 842 K; (*2*) polyethylene siloxane PEG-400, T = 833 K; (*3*) high-pressure polyethylene, T = 789 K; (*4*) low-pressure polyethylene, T = 758 K. On the right: variation of the substance structure, while forming (a) heterogeneous nuclei and (b) homogeneous nuclei.

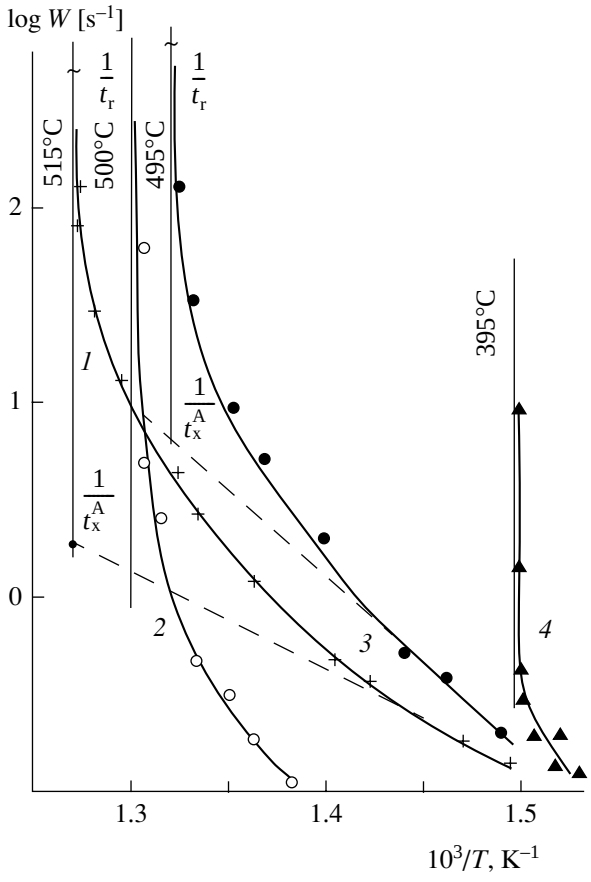

Fig. 3. Temperature curves for the thermal decomposition rate defined as $W = \frac{1}{t_r}$ for certain substances. The curves are determined by the contact thermal-analysis method. (*1*) PMMA; (*2*) polyethylene; (*3*) PChA; and (*4*) colemanite mineral.

measure with the processes of arising nuclei and evaporating thermolysis products, which change with increasing temperature. At moderate temperatures, the number of nuclei arising on structure defects is small and varies negligibly. The nuclei gradually grow, merge, and reach the sample surface.

In this case, gaseous thermolysis products are removed from the sample (Fig. 2a). The development of these nuclei, called heterogeneous, is studied by microscopy methods [10]. At high temperatures, heterogeneous nucleation is replaced by the formation of homogeneous nuclei, which is accompanied by a higher activation barrier [2]. The volume of the substance is uniformly filled with homogeneous micronuclei having a radius on the order of 50×10^{-10} m at a pressure of 0.5–1 MPa [2] (Fig. 2b). As a result of the mutually contacting walls of the micronuclei, particles of the substance that are not coupled to each other appear. These particles are carried on the sample surface, causing the formation of a foam and a dispersal of condensed systems [10].

Logarithms of the inverse thermolysis time as a function of inverse absolute temperature are plotted in Fig. 3. The analysis of this figure shows that the Arrhenius dependence (i.e., the rectilinear segments of the plots) is valid only at moderate temperatures. In the vicinity of the phase-state boundary, an increase in the thermolysis process rate is observed, which is stipulated by weakening of the intermolecular interaction [8]. Below, we employ the obtained results for mathematical simulation of the process of material decomposition under nonuniform heating.

We now consider the one-dimensional process of thermal decomposition of a half-space ($0 < x < \infty$), which proceeds in accordance with the heat-conduction equation

$$\lambda\frac{d^2T}{d^2x} + \rho u C_p\frac{dT}{dx} + F(T) = 0 \qquad (1)$$

under the following boundary conditions: $T = T_s$ at $x = 0$ and $\frac{dT}{dx} = 0$ as $x = \infty$. Here, u is the surface-motion velocity, λ is heat conduction of the material, and other denotations are traditional. Equation (1) describes the temperature profile in which we can distinguish a zone of heating of the initial substance and a chemical-reaction zone [3, 4]. We define the depth (thickness) of the latter by the coordinate $x = \delta$ for which the reaction rate at a temperature $T = T_\delta$ decreases by a factor of e compared to its value on the heated surface. In the case when the Arrhenius law is valid, it follows from this definition that

$$W(T_\delta) = \frac{1}{e}B\exp\left(-\frac{E}{RT_s}\right),$$

where B and E are parameters. From this relation, we obtain

$$T_\delta = \frac{T_s}{1+\frac{RT_s}{E}}, \quad T_s - T_\delta \approx \frac{RT_s^2}{E}, \quad \delta = (T_s - T_\delta)\frac{dx}{dT}.$$

We determine the thickness δ for the case where $W(T)$ does not correspond to the Arrhenius equation. To that end, we integrate Eq. (1) after replacing the variables $\frac{dT}{dx} = \varphi$ and denoting $\left.\frac{dT}{dx}\right|_{x=0} = \varphi_s$:

$$\frac{\varphi^2}{2} - \frac{\varphi_s^2}{2} = \int_{T_s}^{T}\left(-\frac{1}{\lambda}\right)W(T)dT - \int_{T_s}^{T}\frac{u}{a}\varphi dT. \qquad (2)$$

From here, it follows that

$$\frac{dT}{dx} = \pm\sqrt{\varphi_s^2 + \frac{2\rho Q}{\lambda}\int_{T}^{T_s}W(T)dT + \frac{2u}{a}\int_{T}^{T_s}\varphi dT}. \qquad (3)$$

After the variables have been separated, as a result of approximate integration, we arrive at the expression

$$x(T) = \int_{T}^{T_s}\frac{dT}{\sqrt{\varphi_s^2 + \frac{2\rho Q}{\lambda}\int_{T}^{T_s}W(T)dT + \frac{2u}{a}\int_{T}^{T_s}\varphi(T)dT}}. \qquad (4)$$

Since integral (4) cannot be expressed in terms of elementary functions, we find its approximate value. In the narrow interval $T_s - T$, we perform the replacement

$$\int_{T}^{T_s}W(T)dT = W_a(T_s - T), \quad \int_{T}^{T_s}\varphi(T)dT = \varphi_a(T_s - T),$$

where W_a and φ_a are certain average values of the functions W and φ within the interval indicated.

For example,

$$W_a = \frac{W_s + W(T)}{2}, \quad \varphi_a = \frac{\varphi_s + \varphi(T)}{2}.$$

As a result, we have

$$x(T) = \int_{T}^{T_s}\frac{dT}{\sqrt{b - cT}},$$

where

$$c = \frac{2\rho QW}{\lambda} + \frac{2u}{a}\varphi_a, \quad b = \varphi_a^2 + cT_s.$$

Substituting $T = T_\delta$ for the lower limit of the integral, we find

$$\delta = \frac{2}{c}\left(\sqrt{\varphi_s^2 + c(T_s - T_\delta)} - \varphi_s\right). \qquad (5)$$

It is worth noting that, as a result of double integration of expression (4), inaccuracies in the description of the function $W(T)$ are appreciably smoothed. The temperature T_δ can also be determined from the condition of conjugation of two zones, which is reduced to the equality of two heat fluxes and temperature gradients $\left.\frac{dT}{dx}\right|_{\delta+0} = \left.\frac{dT}{dx}\right|_{\delta-0}$:

$$\sqrt{\varphi_s^2 + \frac{2}{\lambda}\int_{T_\delta}^{T_s}F(T)dT + \frac{2u}{a}\int_{T_\delta}^{T_s}\varphi dT} = \frac{\rho u C_p}{\lambda}(T_\delta - T_0) = \frac{u}{a}(T_\delta - T_0). \qquad (6)$$

In other words, passing to the usual denotations, we have

$$\sqrt{b - cT_\delta} = \frac{u}{a}(T_\delta - T_0),$$

whence we can find T_δ:

$$T_\delta = \frac{b_1}{2} \pm \sqrt{\frac{b_1^2}{4} - c_1},$$

where

$$b_1 = 2T + \frac{ca^2}{u^2}, \quad c_1 = T_0^2 - \frac{ba^2}{u^2}.$$

In the case of exothermic processes, the temperature T_δ can be determined from the condition of vanishing of

Table 1. Experimental and calculated data for parameters of the PMMA thermal decomposition

Thermal flux $\lambda\varphi_s$, cal cm^{-2} s^{-1}	Sample surface motion velocity u, 10^2 cm s^{-1}	Temperature		Thickness of the sample surface layer δ, 10^{-3} cm		Time	
		T_s, K	T_δ, K	experimental	calculated	t_r, s	t_x^A, s
Radiation heating of the surface [1]							
12.0	2.2	740	715	1.04	1.13	6.3×10^{-2}	1.75
10.0	1.8	710	687	1.15	1.15	6.4×10^{-1}	6
7.0	1.4	650	630	1.43	1.60	0.10	10
5.1	1.1	600	583	1.67	1.72	0.15	1
Linear pyrolysis [4]							
Linear structure	10	785	757	–	0.62	6.2×10^{-2}	3.39
"	3	772	754	–	0.60	2×10^{-2}	3.28
Netlike structure	10	885	853	–	0.61	6.1×10^{-2}	3.1

the second derivative $\frac{d^2T_\delta}{dx^2}$ at the point of inflection of the temperature profile, as well as by the formula $T_\delta = T_1 - (T_1 - T_s)\sqrt{e}$. Below, we present examples of the calculations and compare their results with available experimental data taken from the literature.

In Table 1, experimental data related to thermal-decomposition parameters for polymethyl methacrylate (PMMA) samples of the linear and net like structure are given in the case of the action on their surface of an intense radiation flux [11]. The samples are prepared by the linear-pyrolysis method [4]. The data calculated according to the Arrhenius equation are presented for both the thickness δ and chemical-reaction time t_x^A. The characteristics of linear PMMA $\left(\frac{E}{R} = 21300\text{ K}, B = 10^{12.47}\text{ s}^{-1}, a = 1 \times 10^{-3}\text{ cm}^2\text{ s}^{-1}, \rho = 1.2\text{ g cm}^{-3}, Q = 2200\text{ kJ kg}^{-1}\right)$ and netlike PMMA $\left(\frac{E}{R} = 21000\text{ K and } B = 10^{12.3}\text{ s}^{-1}\right)$ are taken from [3, 4].The time of residence in the reaction zone $t_r = \frac{\delta}{u}$ is estimated according to the obtained values of the reaction zone thickness.

As follows from Table 1, the calculated value of the reaction zone thickness almost coincides with its experimental value determined by the thermal flux incoming to the sample surface. This is done according to the relation $\delta = \frac{T_s - T_\delta}{\varphi_s}$, which testifies to a reasonably high precision of the relationships obtained. As is shown in [11], a certain difference between t_r and t_x^A (the superscript "A" implies the correspondence to the Arrhenius equation) is caused by the decomposition of PMMA as a result of the penetrating action of the radiation on a transparent polymer. However, the significant (by orders of magnitude) difference between t_r and t_x^A in the case of linear pyrolysis cannot be explained by experimental causes. As is established in [5, 6], this difference is determined by the fact that the temperature of the sample surface approaches the phase-state boundary (the temperature T_l in the case of linear PMMA structure equals 788 K).

In Table 2, we demonstrate an example of the calculation of combustion parameters for ammonium perchlorate (PChA). The kinetic characteristics of PChA in calculating the reaction time according to the results of tests by the method of linear pyrolysis $\left[\frac{E}{R} = 15100\text{ K and } B = 10^{6.8}\text{ s}^{-1}\right.$ (see the first number in the last column) and $\frac{E}{R} = 13500\text{ K and } B = 10^{8.2}\text{ s}^{-1}$ (see the second number in the penultimate column)$\left.\right]$ are taken from [10]. The values of δ are taken from the experimental data of [12] or are obtained as a result of the calculations.

As in the first example, the time of residence for the substance in the reaction zone is many orders of magnitude shorter than the calculated time of occurrence of the chemical reaction. However, this time is determined according to kinetic parameters found at moderate temperatures without allowance for the acceleration of the process in the vicinity of the phase-state boundary. This

Table 2. Experimental and calculated data for parameters of the PChA thermal decomposition

Pressure P, MPa	Sample surface motion velocity u, cm s^{-1}	Temperature		Thickness of the sample surface layer δ, 10^{-3} cm		Time		
		T_s, K	T_δ, K	experimental	calculated	t_r, s	t_x^A, s	t_x, s
0.1	0.02–0.03	750–770	710–730	–	1.9	1.4×10^{-2}–8×10^{-2}	1.44×10^{2}	8×10^{-2}
							3.4×10^{-1}	–10^{-2}
5.0	0.6	670–700	640–630	1.5	0.93	0.05×10^{-2}	1×10^{3}	~10^{-2}
						1.67×10^{-2}	4.7	
10.0	1.0	~613	~588	1.0	1.2	0.2×10^{-3}–1×10^{-3}	7.9×10^{3}	~10^{-3}
							30.1	
15.0	1.5	~603	~580	1.0	1.3	0.14×10^{-3}	1.98×10^{4}	~10^{-3}
						1.54×10^{-3}	6.94	

discrepancy was indicated in due time by the authors of [12].

In order to allow for the acceleration of the thermal-decomposition process in the vicinity of the phase-state boundary with the heterogeneous nucleation and homogeneous nucleation taken into account, the relationship

$$W = B(\nu_{het} + \nu_{hom})^{\beta} k_{chem}^{\lambda}$$

was suggested. However, a simpler and more obvious representation is attained in the case of immediately using experimental data (see Fig. 3). These data were obtained in the regime of sample heating, which is close to the conditions of heating of a substance in the reaction zone. Inclined dashed lines in Fig. 3 correspond to the Arrhenius equation. They extrapolate data of low-temperature tests to the high-temperature region. The points of intersection of the dashed lines with the T_1 vertical lines determine the ordinates $\frac{1}{t_x^A}$. As is shown in Fig. 3, for high temperatures close to the phase-state boundary, both ordinates are more than two orders of magnitude lower than the experimental value $\frac{1}{t_x}$ (without the superscript) of this physical quantity. Hence, the true values of the times t_x marked with the subscript are more than two orders of magnitude lower than the time t_x^A calculated using the Arrhenius equation. Thus, this equation carries no information on the phase-state boundary and does not allow us to describe thermal decomposition of condensed systems at high heating rates adequate to actual processes. At the same time, values of t_x calculated with allowance for the phase-state boundary in the case of both PMMA (~6×10^{-2} s) and PChA, which are given in the last column of Table 2, closely correspond to the residence time t_r. The dependence of temperature T_l on pressure is determined by both experimental and calculation methods [2, 7, 8]. The results obtained testify to the fact that parameters of the phase-state boundary should be necessarily involved in calculations.

CONCLUSIONS

In this paper, relationships for determining chemical-reaction zone parameters such as zone thickness, temperature gradients, and the time of substance residence in the vicinity of the phase-state boundary are obtained.

The results of mathematical modeling of thermal-decomposition processes in PMMA and PChA samples under their intense heating are confirmed by experimental data. An explanation of the discrepancy between the kinetics of the low-temperature decomposition and gasification of these substances under intense heating in the vicinity of the phase-state boundary is suggested.

A significant effect of destruction kinetics near the phase-state boundary on the thermal-decomposition rate for condensed systems at high temperatures is shown. The allowance for parameters of the phase-state boundary makes it possible to considerably increase the precision of calculating the thermal-decomposition rate of condensed systems under intense heating.

REFERENCES

1. A. Münster, *Chemische Thermodynamik* (Academie, Berlin, 1969; Mir, Moscow, 1971).
2. V. P. Skripov, E. N. Sinitsyn, P. A. Pavlov, *et al.*, *Thermal and Physical Properties of Liquids in a Metastable State* (Atomizdat, Moscow, 1980).

3. Yu. V. Polezhaev and F. B. Yurevich, *Thermal Defense* (Énergiya, Moscow, 1976).
4. R. M. Aseeva and G. E. Zaikov, *Combustion of Polymeric Materials* (Nauka, Moscow, 1981).
5. O. F. Shlenskiĭ, Dokl. Akad. Nauk **380**, 614 (2001) [Dokl. Phys. **46**, 317 (2001)].
6. O. F. Shlenskiĭ and A. S. Lyapin, Dokl. Akad. Nauk **383**, 184 (2002) [Dokl. Phys. **47**, 176 (2002)].
7. I. V. Lomonosov, K. V. Khishchenko, V. E. Fortov, and O. F. Shlenskiĭ, Dokl. Akad. Nauk **349**, 322 (1996) [Phys. Dokl. **41**, 304 (1996)].
8. O. F. Shlenskiĭ, N. V. Afanas'ev, and A. G. Shashkov, *Thermal Decomposition of Materials* (Énergoatomizdat, Moscow, 1996).
9. D. N. Yundev, A. A. Lash, O. F. Shlenskiĭ, *et al.*, Teplofiz. Vys. Temp. **27** (2), 369 (1989).
10. G. B. Manelis, G. N. Nazin, Yu. N. Rubtsov, and V. A. Strunin, *Thermal Decomposition and Combustion of Explosive Substances and Powders* (Nauka, Moscow, 1996).
11. N. P. Novikov and A. A. Kholodilov, Inzh.-Fiz. Zh. **22** (4), 618 (1972); Inzh.-Fiz. Zh. **22** (2), 257 (1972).
12. V. K. Bobolev, A. P. Glazkova, A. A. Zenin, and O. I. Leĭpunskiĭ, Prikl. Mekh. Tekh. Fiz., No. 3, 153 (1964).
13. M. E. Brown, D. Dollimore, and A. K. Galwey, *Reactions in the Solid State*, *Comprehensive Chemical Kinetics*, Ed. by C. H. Bamford and C. F. H. Tipper (Elsevier, Amsterdam, 1980; Mir, Moscow, 1983).

Translated by G. Merzon

Doklady Physics, Vol. 48, No. 7, 2003, pp. 353–354. Translated from Doklady Akademii Nauk, Vol. 391, No. 1, 2003, pp. 51–52.

MECHANICS

Nonintegrability of a Restricted Two-Body Problem for an Elastic-Interaction Potential on a Sphere

S. L. Ziglin

Presented by Academician V.V. Kozlov March 5, 2003

Received March 7, 2003

A restricted two-body problem for an elastic-interaction potential on a unit-radius sphere has two degrees of freedom and is described by the Hamiltonian

$$H = \frac{1}{2}\left(p_\theta^2 + \frac{p_\phi^2}{\sin^2\theta}\right)$$

$$+ \omega(p_\theta\cos\phi - p_\phi\sin\phi\cot\theta) + \gamma\tan^2\theta$$

(cf. [1–5]). Here, θ and ϕ are the spherical coordinates in the moving system associated with a body of nonzero mass, p_θ and p_ϕ are the corresponding momentum components, ω is the angular velocity of the body, and γ is a constant.

The system described by the Hamiltonian H is considered in the complexified phase space M^4. This space is the direct product of the complexified circle S^1_C, which is specified by the coordinate $\theta(\mathrm{mod}2\pi)$ and the deleted points $\frac{n\pi}{2}$, where n is an integer number, the complexified circle S^1_C corresponding to the coordinate ϕ, and the two complex straight lines C^1 corresponding to the coordinates p_θ and p_ϕ.

At $\gamma = 0$ and $\omega = 0$, the system under consideration has an additional (i.e., functionally independent of the Hamiltonian) analytic first integral.

Remark. *Generalization of the last fact to the case of three motionless centers situated at the vertices of an equilateral spherical right triangle is presented in* [2].

Theorem. *If* $\gamma \neq 0$, $x = \frac{\omega}{\sqrt{2\gamma}}$ *is an irrational number, and* $\sqrt{1+x^2}$ *is a noninteger number, then the system described by the Hamiltonian H has no additional meromorphic first integral in the phase space M.*

Institute of Radio Engineering and Electronics, Russian Academy of Sciences, ul. Mokhovaya 18, Moscow, 103907 Russia

Proof. *The Hamiltonian H is invariant with respect to the involutive symplectic diffeomorphism*

$$J : M \longrightarrow M, \quad J : (\theta, \phi, p_\theta, p_\phi) \mapsto (\theta + \pi, \phi, p_\theta, p_\phi).$$

In the quotient manifold $\bar{M} = M/J$, the induced Hamiltonian system has a phase curve Γ that does not represent an equilibrium position and is given by the relations

$$\phi = p_\phi = 0, \quad p_\theta + \omega = \sqrt{-2\gamma}\tan\theta \neq 0.$$

We consider the variable $z = \cot\theta$ as a coordinate in the phase curve Γ and, to contract the notation, denote $d\phi$ by ϕ, dp_ϕ by p_ϕ, and the derivative with respect to z by a prime. Then, in variations along Γ, the reduced system of equations, i.e., the restriction of the system in normal variations along this phase curve to the zero-level surface of its first integral dH (cf. [6]), takes the form

$$\begin{aligned}\phi' &= -\frac{z}{\sqrt{-2\gamma}(1+z^2)}(-\omega z\phi + (1+z^2)p_\phi),\\ p'_\phi &= -\frac{z}{\sqrt{-2\gamma}(1+z^2)}\left(\omega\left(\frac{\sqrt{-2\gamma}}{z} - \omega\right)\phi + \omega z p_\phi\right).\end{aligned} \tag{1}$$

This system has three singular points $z = \pm i, \infty$. In addition, when passing around the points $z = \pm i$, the eigenvalues of the transformations under the action of this system are equal to $\exp(\pm\pi i x)$.

To find the eigenvalues of the transformations under the action of this system when passing around the point $z = \infty$, we represent the system as

$$\phi'' + a(z)\phi' + b(z)\phi = 0, \tag{2}$$

where

$$a(z) = \frac{a_0}{z}, \quad b(z) = \frac{\omega z^2}{2\gamma(1+z^2)^2}\left(\frac{\sqrt{-2\gamma}}{z} - \omega\right)$$

$$= \frac{b_0}{z^2} + O\left(\frac{1}{z^3}\right), \quad a_0 = -1, \quad b_0 = -\frac{\omega^2}{2\gamma}.$$

1028-3358/03/4807-0353$24.00

The determining equation [7]

$$r(r-1) + a_0 r + b_0 = 0$$

at the point $z = \infty$ has the roots $r = 1 \pm \sqrt{1 + x^2}$. Consequently, when passing around this point, the eigenvalues of the transformation under the action of Eq. (2) are equal to $\exp(2\pi i\sqrt{1 + x^2})$.

Let the system described by the Hamiltonian H have an additional meromorphic first integral. Then, according to the lemma from item 1.5 in [6], the induced system also has an additional (functionally independent of H) meromorphic first integral in the quotient manifold $\overline{M}$. According to conditions of the theorem, the eigenvalues of the transformations under the action of system (1) when passing around the points $z = \pm i$ are not equal to roots of unity. Therefore, according to theorem 2 from [6], the monodromy group of this system is commutative. As a result,

$$\pm\sqrt{1 + x^2} = \frac{x}{2} \pm \frac{x}{2} + n,$$

where n is an integer number. According to the conditions of the theorem, the last equation cannot be satisfied for any sign choice. The theorem is proven.

ACKNOWLEDGMENTS

I am grateful to A.V. Borisov for the formulation of the problem and to Academician V.V. Kozlov for stimulating discussions.

REFERENCES

1. V. V. Kozlov and A. O. Harin, Celest. Mech. Dyn. Astron. **54**, 393 (1992).
2. V. V. Kozlov and Yu. N. Fedorov, Mat. Zametki **58** (3), 74 (1993).
3. V. V. Kozlov, Vestn. Mosk. Univ., Ser. 1: Mat., Mekh., No. 2, 28 (1994).
4. V. V. Kozlov, Vestn. Mosk. Univ., Ser. 1: Mat., Mekh., No. 5, 43 (2000).
5. A. V. Borisov and I. S. Mamaev, *Poisson Structures and Lee Algebras in Hamilton Mechanics* (Udmurt Univ., Izhevsk, 1999).
6. S. L. Ziglin, Funkts. Anal. Prilozh. **16** (3), 30 (1982).
7. V. V. Golubev, *Analitic Theory of Differential Equations* (Gostekhizdat, Moscow, 1950).

Translated by Yu. Verevochkin

Doklady Physics, Vol. 48, No. 7, 2003, pp. 355–358. Translated from Doklady Akademii Nauk, Vol. 391, No. 2, 2003, pp. 185–188.

MECHANICS

Nonlinear Effects Observed in the Flow of a Fluid out of Vibrating Vessels

I. I. Blekhman, L. I. Blekhman, L. A. Vaĭsberg, V. B. Vasil'kov, and K. S. Yakimova

Presented by Academician N.F. Morozov February 10, 2003

Received March 20, 2003

Two peculiar nonlinear phenomena are considered in this work. The first of them, called the *vibro-jet effect*, has been known for a comparatively long time [1]. It is the appearance of slow flows of a fluid in the direction of the narrowing of conic holes in a plate vibrating in the fluid. The vibro-jet effect is successfully used in a number of technical devices [1–3]. At the same time, this phenomenon was possibly responsible for some fatal air crashes when fuel stopped coming from tanks due to vibration; i.e., *vibration locking of the holes* occurred. In this case, the pressure facilitating the discharge of the fuel was balanced by the vibration-induced counterpressure. The second phenomenon—*vibrational injection of a gas into a fluid*—was discovered quite recently [4]. It is the suction of the gas through a hole in the bottom of a fluid-filled vessel vibrating in the gas. Moreover, injection also occurs when the vessel vibrates in the fluid; i.e., there is vibrational injection of a fluid into a fluid.

The theory of the vibro-jet effect was considered in [1, 3]. We propose here a general explanation comprising the theory of both phenomena as special cases and give the experimental results.

We consider a vessel (Fig. 1) that contains fluid *1* and is situated in either fluid or gas *2*. The vessel can be either open or closed and vibrates vertically according to the law $y = -A\sin\omega t$, where A and ω are the amplitude and frequency of vibrations, respectively. The hole is at the bottom of the vessel.

The volume discharge of the fluid or gas steadily outflowing through the hole in the thin wall of the immovable vessel is determined by the well-known hydraulic formula [5]

$$Q = \mu F\sqrt{\frac{2\Delta P}{\rho}}. \qquad (1)$$

Here, ΔP is the pressure difference between the inlet and outlet of the hole, ρ is the density of the outflowing medium, F is the area of the hole, and μ is the so-called discharge coefficient of the hole. For $\mu = 1$ and free discharge of the fluid into the atmosphere from the open vessel with the fluid column of height h, $\Delta P = \rho g h$ (g is the gravitational acceleration) and formula (1) corresponds to the Torricelli formula. We make the assumption, which will be experimentally tested (see below), that formula (1) is also valid for the instantaneous discharge at a time-dependent pressure difference $|\Delta p|$. In this case, the coefficient μ is assumed to depend both on the direction of the outflow, which can be caused by the shape of the hole channel, and on the properties of the outflowing fluid. The pressure difference for the vibrating vessel is expressed as

$$\Delta p = \Delta P - \rho_1 h\ddot{y} = \Delta P(1 - w\sin\tau). \qquad (2)$$

Here, $\Delta P = P_1 - P_2 > 0$ is the static pressure difference at the hole, ρ_1 is the density of fluid *1*, h is the height of the fluid in the vessel, $\tau = \omega t$, and

$$w = \frac{\rho_1 h A\omega^2}{\Delta P} \qquad (3)$$

is the "overload parameter," i.e., the ratio of the ampli-

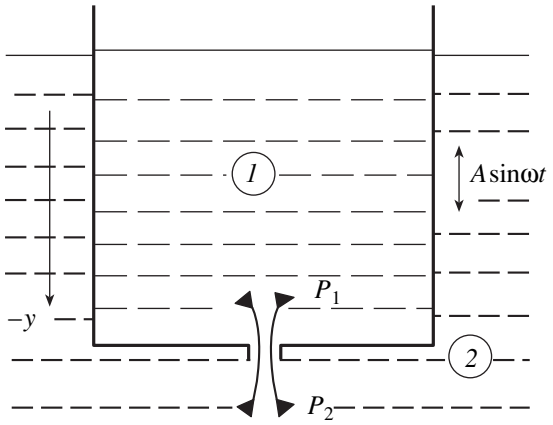

Fig. 1. General scheme of the system "a vessel that contains a fluid, has a hole, and vibrates in air or fluid."

Institute of Problems of Mechanical Engineering, Russian Academy of Sciences, Vasil'evskiĭ Ostrov, Bol'shoi pr. 61, St. Petersburg, 199178 Russia

OAO Mekhanobr-Tekhnika, Vasil'evskiĭ Ostrov, 22 liniya 3, korp. 5, St. Petersburg, 199106 Russia

e-mail: blekhman@vibro.ipme.ru

1028-3358/03/4807-0355$24.00 © 2003 MAIK "Nauka/Interperiodica"

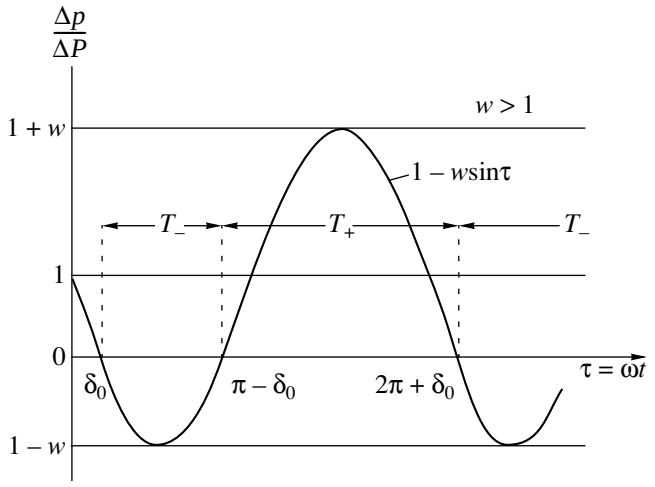

Fig. 2. Time dependence of the pressure difference.

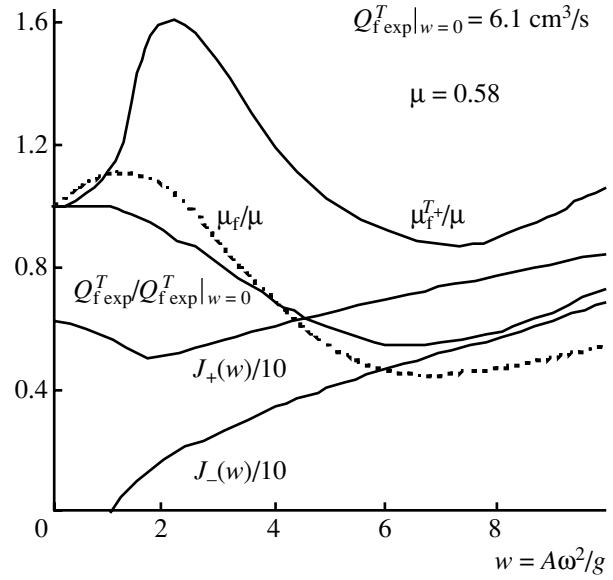

Fig. 3. Water discharges $Q^T_{f\,exp}$ through the hole, the functions J_+ and J_-, and the discharge coefficients μ_f and $\mu_f^{T_+}$ vs. the overload parameter *w*.

tude of the dynamic pressure to the static pressure difference.

For $w > 1$ (Fig. 2), in the interval $\delta_0 < \tau < \pi - \delta_0$, where $\delta_0 = \arcsin\frac{1}{w}$, we have $\frac{\Delta p}{\Delta P} < 0$ and fluid or gas *2* flows into the vessel, while in the interval $\pi - \delta_0 < \tau < 2\pi + \delta_0$, we have $\frac{\Delta p}{\Delta P} > 0$ and fluid *1* flows out of the vessel. Periods of inflow and outflow are equal to $T_- = \frac{\pi - 2\delta_0}{\omega}$ and $T_+ = \frac{\pi + 2\delta_0}{\omega}$, respectively.

The outflowing and inflowing volume discharges per second that are averaged over the period $T = \frac{2\pi}{\omega} = T_+ + T_-$ are given by the expressions

$$Q_+^T = \frac{\omega}{2\pi}\mu_+ F\sqrt{\frac{2\Delta P}{\rho_+}}\int\limits_{\frac{\pi-\delta_0}{\omega}}^{\frac{2\pi+\delta_0}{\omega}}\sqrt{1-w\sin\omega t}\,dt,$$

$$Q_-^T = -\frac{\omega}{2\pi}\mu_- F\sqrt{\frac{2\Delta P}{\rho_-}}\int\limits_{\frac{\delta_0}{\omega}}^{\frac{\pi-\delta_0}{\omega}}\sqrt{w\sin\omega t-1}\,dt, \quad (4)$$

$$w \geq 1,$$

respectively. Here, μ_+ and μ_- are the discharge coefficients for the outflow and inflow, respectively, and $\rho_+ = \rho_1$ and $\rho_- = \rho_2$ are the densities of fluids *1* and *2*, respectively.

For $0 \leq w \leq 1$, we always have $\Delta P > 0$, and fluid *1* always flows from the vessel. Therefore, $T_- = 0$, $T_+ = T = \frac{2\pi}{\omega}$. In this case,

$$Q_+^T = \frac{\omega}{2\pi}\mu_+ F\sqrt{\frac{2\Delta P}{\rho_+}}\int\limits_0^{\frac{2\pi}{\omega}}\sqrt{1-w\sin\omega t}\,dt, \quad (5)$$

$$Q_-^T = 0, \quad 0 \leq w \leq 1.$$

Expressions (4) and (5) can be represented as

$$Q_\pm^T = \pm\frac{1}{2\pi}\mu_\pm F\sqrt{\frac{2\Delta P}{\rho_\pm}}J_\pm(w), \quad (6)$$

$$J_\pm(w) = 4\sqrt{2w}[\mathbf{E}(k_\pm) - (1-k_\pm)\mathbf{K}(k_\pm)], \quad w \geq 1,$$

$$J_+(w) = 4\sqrt{1+w}\,\mathbf{E}\left(\frac{1}{k_+}\right), \quad J_-(w) = 0, \quad (7)$$

$$0 \leq w \leq 1,$$

where $k_\pm = \sqrt{\frac{w \pm 1}{2w}}$ and **K** and **E** are the complete elliptic integrals of the first and second kinds, respectively. The plots of the functions $J_\pm(w)$ are presented in Fig. 3. For practical calculations, one can use the approximate formula

$$J_\pm(w) = \frac{4}{3}\sqrt{w \pm 1}\left(\frac{\pi}{2} \pm \arcsin\frac{1}{w}\right), \quad w \geq 1, \quad (8)$$

obtained by the parabolic approximation of the integrands in formula (5).

For comparison with experimental data, the discharges

$$Q_+^{T_+} = \frac{Q_+^T T}{T_+}, \quad Q_-^{T_-} = \frac{Q_-^T T}{T_-}, \tag{9}$$

averaged over the outflow and inflow times T_+ and T_-, respectively, are also of interest.

It is easy to show that relations (6) can be written in the form of the equation of vibrational hydraulics [2], which is an analogue of the Bernoulli equation for the "slow" components of the velocity and pressure under vibration.

In the case of the vibro-jet effect, the fluids inside and outside the vessel are the same, so that $\rho_+ = \rho_- = \rho$, $w > 1$, and the total average discharge is determined by the formula

$$Q^T = Q_+^T + Q_-^T$$
$$= \frac{1}{2\pi} F \sqrt{\frac{2\Delta P}{\rho}} [\mu_+ J_+(w) - \mu_- J_-(w)]. \tag{10}$$

When the inequality $\frac{\mu_+}{\mu_-} < \frac{J_-(w)}{J_+(w)}$ is satisfied, the fluid flows into the vessel (more fluid per period flows in than flows out) in spite of the positive static pressure difference $\Delta P = p_1 - p_2 > 0$. When $\frac{\mu_+}{\mu_-} = \frac{J_-(w)}{J_+(w)}$, *the vibration locking of the vessel* occurs as described above. For $w > 5$, the condition of the appearance of the inverse flow and the condition of the vibration locking can be represented as $\frac{\mu_+}{\mu_-} < 1 - \frac{2.27}{w}$ and $\frac{\mu_+}{\mu_-} = 1 - \frac{2.27}{w}$, respectively, with an accuracy of about 5% by using formulas (8).

In the case of *vibrational injection of a gas into a fluid*, we consider an open vessel where the pressure of the gas on the surface of the fluid is equal to the pressure at the outlet from the hole. Then, $\Delta P = \rho_1 g h$ and formulas (6) for the gas and liquid discharges $Q_+^T = Q_\mathrm{f}^T$ and $Q_-^T = Q_\mathrm{g}^T$ averaged over the period T take the form

$$Q_+^T = Q_\mathrm{f}^T = \frac{1}{2\pi} \mu_\mathrm{f} F \sqrt{2gh} J_+(w),$$
$$Q_-^T = Q_\mathrm{g}^T = -\frac{1}{2\pi} \mu_\mathrm{g} F \sqrt{\frac{2gh\rho_\mathrm{f}}{\rho_\mathrm{g}}} J_-(w). \tag{11}$$

Here, contrary to Eqs. (6), subscripts "f" and "g" refer to the fluid and gas, respectively, and $w = \frac{A\omega^2}{g}$.

Vibrational injection takes place only when the volume of the gas entering the vessel in the time T_- during every vibration period is sufficient to form a bubble with the diameter of the hole (see below). This condition leads to the demand that the height of the column of the fluid in the vessel must exceed a certain critical value h_*. Calculations show that h_* is not large when vibration is strong enough ($w > 3$), but it can be large for $w < 1.5$ when J_- is small (Fig. 3).

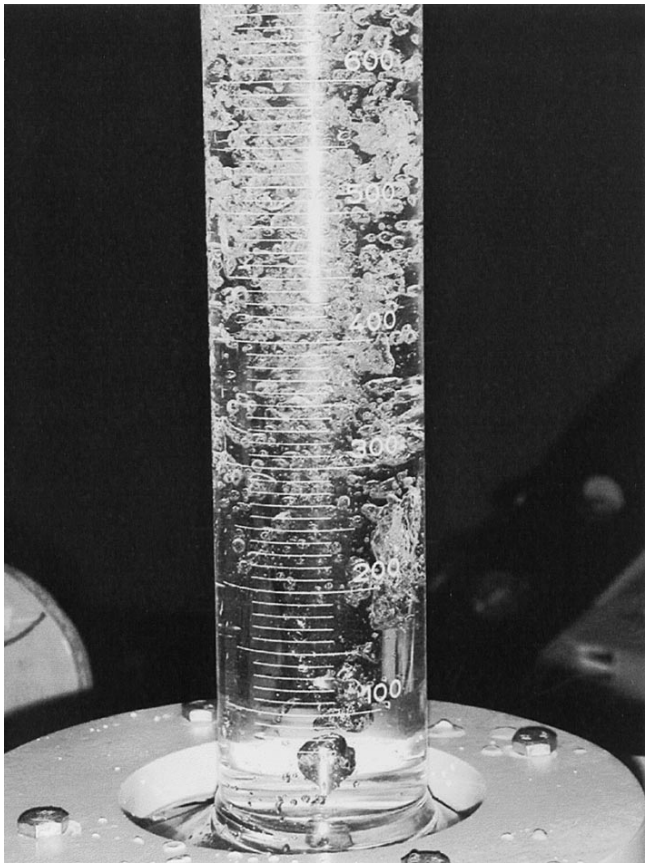

Fig. 4. Vibrational injection of a gas into a fluid.

The experiments on studying the vibrational injection were carried out on a 157 A-UC vibration bench at the Mekhanobr Institute. An open cylindrical glass vessel 300 mm in height and 58 mm in inner diameter was fixed on the table of the bench. The vessel had a round hole at the center of the bottom. A certain level of water was kept in the vessel. The vessel vibrated vertically with a frequency and amplitude that could be changed. Observation in stroboscopic light revealed that one bubble of air was sucked into the vessel and one drop of water flowed out during every oscillation period. Figure 4 shows a photo of the vibrating vessel with air rapidly sucked into it.

The average volume discharge of outflowing water Q_fexp^T was measured as a function of the parameter w for the oscillation amplitude $A = 2.5$ mm, the height of the water column in the vessel $h = 200$ mm, and the hole diameter $d = 2.6$ mm (Fig. 3). As is seen, with an

increase in w from $w = 1$, the discharge first decreases and then begins to increase. This behavior, as well as the behavior of $J_+(w)$, can be easily explained by relations (7) and (11).

According to Fig. 3 and formula (11), the dependence of the air discharge $Q_g^T(w)$, as well as the $J_-(w)$ dependence, is monotonic. A sufficiently rapid suction of air into the vessel was observed in the experiment beginning with $w \approx 2.5$. At the same time, according to the theory presented above, it must begin at w somewhat exceeding 1. This can be explained by the surface-tension effect on the formation of bubbles.

To compare the theoretical results with the experimental data, it is interesting to compare the discharge coefficient μ_f with its value μ for the stationary flow of the fluid through the hole. We calculated the μ_f values by formula (11) using the experimental data and the $\mu_f^{T_+}$ values using the average discharges calculated by formula (9) including the actual time of the outflow. These quantities are shown in Fig. 3 by the dotted and solid lines, respectively. As is seen, the $\mu_f^{T_+}$ values for $w > 4$ differ only moderately from the μ value. This fact seems to corroborate the elements of the above theory of the phenomenon.

REFERENCES

1. *Vibration in Technology. Handbook in 6 Volumes* (Mashinostroenie, Moscow, 1978–1981), Vol. 4.
2. I. I. Blekhman, *Vibrational Mechanics: Nonlinear Dynamic Effect, General Approach, Applications* (Fizmatlit, Moscow, 1994; World Scientific, Singapore, 2000).
3. I. I. Blekhman, L. A. Vaĭsberg, and A. N. Korovnikov, in *Inter-Department Collection of Scientific Works* (Mekhanobr., Leningrad, 1988), pp. 35–46.
4. I. I. Blekhman, L. I. Blekhman, L. A. Vaĭsberg, *et al.*, in *Scientific Discoveries* (Akad. Estestv. Nauk, Moscow, 2002), pp. 60–61.
5. R. R. Chugaev, *Hydraulics* (Énergoizdat, Leningrad, 1982).

Translated by I. Blekhman

Doklady Physics, Vol. 48, No. 7, 2003, pp. 359–363. Translated from Doklady Akademii Nauk, Vol. 391, No. 2, 2003, pp. 189–193.

MECHANICS

Nonuniqueness and Stability in Problems of Equilibrium of Elastic Two-Phase Bodies

V. A. Eremeev*, A. B. Freidin, and L. L. Sharipova****

Presented by Academician N.F. Morozov March 3, 2003

Received March 19, 2003

Interfaces in martensitic transformations can be treated as strain-discontinuity surfaces, where, in addition to the ordinary kinematic and force conditions, an additional thermodynamic condition must be satisfied [1–4]. This condition restricts the geometry of the interfaces [5–8].

Being a problem with an unknown boundary, the problem of determination of equilibrium two-phase configurations has as a rule several solutions; i.e., different equilibrium two-phase structures can correspond to the same boundary conditions. In this case, locally stable (metastable) states, as well as states providing the global minimum of the energy functional, are of interest. A certain state is realized depending on the initial conditions and kinetics of a phase transition. However, various equilibrium solutions can be *a priori* estimated disregarding transition kinetics by analyzing the stability of two-phase fields of strains and energy changes induced by phase transitions.

In this paper, the nonuniqueness and stability of two-phase states are analyzed by an example of centrosymmetric two-phase strain fields. The equilibrium of a two-phase ball on the class of solutions with one spherical interface was previously analyzed in [6–9]. In these works, the possibility of two or more equilibrium interfaces, as well as the stability of two-phase states under arbitrary disturbances, was not studied. The results presented below continue investigations begun in [10, 11].

1. EQUILIBRIUM CENTROSYMMETRIC STRAINS

For small strains, the problem of equilibrium two-phase configurations of an elastic body reduces [7, 12] to the problem of determination of an interface Γ and displacement field $\mathbf{u}(x)$, which is quite smooth for $x \notin \Gamma$, is continuous on Γ, and satisfies the boundary conditions and equilibrium conditions

$$x \notin \Gamma: \quad \nabla \cdot \sigma = 0, \quad \theta = \text{const}, \tag{1}$$

$$x \in \Gamma: \quad [\mathbf{u}] = 0, \quad [\sigma] \cdot \mathbf{n} = 0, \quad [f] - \sigma : [\varepsilon] = 0. \tag{2}$$

Here, x is a point of the body; the volume density f of the free energy is approximated by the quadratic functions

$$f(\varepsilon, \theta) = \min_{-,+}\{f^-(\varepsilon, \theta), f^+(\varepsilon, \theta)\},$$
$$f^\pm(\varepsilon, \theta) = f_0^\pm(\theta) + \frac{1}{2}(\varepsilon - \varepsilon_\pm^p) : C_\pm : (\varepsilon - \varepsilon_\pm^p). \tag{3}$$

ε and σ are the strain tensor and stress tensor, respectively; θ is the temperature; $\mathbf{n}$ is the unit vector normal to the interface Γ; $C_\pm$ are the positive definite tensors of the elastic moduli of the phases; $f_0^\pm$ and $\varepsilon_\pm^p$ are, respectively, the free-energy densities and strain tensors for the phases in unstressed state; $[\cdot] = (\cdot)_+ - (\cdot)_-$; and subscripts + and – mean the material in different phase states. Mass forces, thermoelastic stresses, and surface energy are ignored.

Thermodynamic condition (2) reduces to an equation determining a one-parameter family of normals to the interface depending on strains on the one side of the interface [5]. If the tensor $C_1 = C_+ - C_-$ is nondegenerate, this equation is represented in the q space as

$$\chi(q_\pm, \mathbf{n}) \triangleq \gamma_* + \frac{1}{2}(q_\pm : C_1^{-1} : q_\pm \pm q_\pm : K_\mp(\mathbf{n}) : q_\pm) = 0, \tag{4}$$

$$q = -C_1 : \varepsilon + [C : \varepsilon^p], \tag{5}$$

$$K_\pm(\mathbf{n}) = \{\mathbf{n} \otimes G_\pm \otimes \mathbf{n}\}^s, \quad G_\pm = (\mathbf{n} \cdot C_\pm \cdot \mathbf{n})^{-1},$$
$$\gamma_* = \gamma + \frac{1}{2}[\varepsilon^p] : B_1^{-1} : [\varepsilon^p], \quad B_\pm = C_\pm^{-1},$$
$$B_1 = B_+ - B_-,$$

* *Rostov State University, ul. Zorge 5, Rostov-on-Don, 344090 Russia*
e-mail: eremeyev@math.rsu.su

** *Institute of Problems of Mechanical Engineering, Russian Academy of Sciences, Vasil'evskiĭ Ostrov, Bol'shoi pr. 61, St. Petersburg, 199178 Russia*
e-mail: freidlin@mechanics.ipme.ru

1028-3358/03/4807-0359$24.00

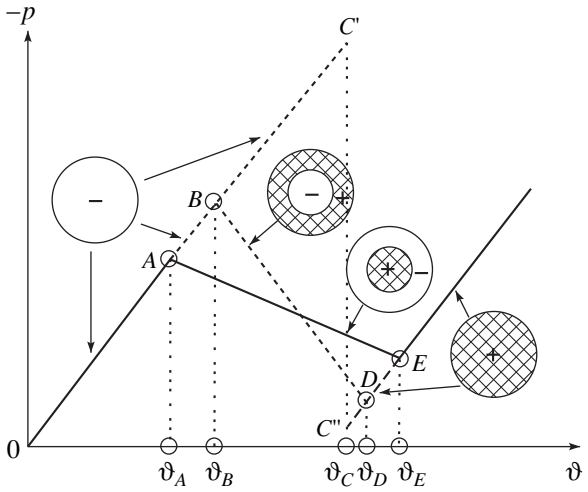

Fig. 1. Pressure vs. volume strain for $\mu_+ > \mu_-$, where μ_+ and μ_- are the shear moduli of the respective phases.

where the superscript *s* means symmetrization: $K_{ijkl} = n_{(i}\, G_{j)(k}\, n_{l)}$.

The following statement for an isotropic material can be proved by analyzing the possibility of satisfaction of equilibrium condition (4) at several interfaces.

Statement. *For the class of centrosymmetric equilibrium two-phase solutions, only one spherical interface for a solid body and no more than two interfaces in a body with a spherical cavity can exist.*

This statement is valid for any type of boundary conditions on the cavity surface.

2. STABILITY. THE LINEARIZED BOUNDARY VALUE PROBLEM FOR A TWO-PHASE BODY

We consider a certain initial equilibrium two-phase state and a state infinitesimally different from it. The displacement and radius vector of the interface in the perturbed state are given by the formulas

$$\mathbf{u} = \mathbf{u}^0 + \mathbf{w}, \quad \mathbf{r} = \mathbf{r}^0 + \eta\mathbf{n}, \tag{6}$$

where $\mathbf{w}$ is the vector of small additional displacements, η is the perturbation of the interface in the $\mathbf{n}$ direction, and $\mathbf{u}^0$ and $\mathbf{r}^0$ are the displacement vector and radius vector of the interface in the initial state, respectively. We consider quasistatic perturbations; i.e., the field of displacements depends on time as on a parameter through the time dependence of the interface.

When the interface moves quasistatically, $\chi \neq 0$ is the thermodynamic force. In the linear thermodynamic approximation, the normal component of the interface velocity is determined by the equation

$$v_n^\Gamma = -k\chi(q_+, \mathbf{n}), \quad k > 0, \tag{7}$$

where the normal is out of the domain occupied by the + phase and *k* is the kinetic coefficient.

The linearization of the boundary value problem specified by Eqs. (1) and (2) provides the set of equations for $\mathbf{w}$ and η

$$x \notin \Gamma: \quad \nabla \cdot \sigma_\pm(\mathbf{w}) = 0, \quad \sigma_\pm(\mathbf{w}) = C_\pm : \nabla\mathbf{w}, \tag{8}$$
$$x \in \Omega_1 \cup \Omega_2: \quad \mathbf{w}|_{\Omega_1} = 0, \quad \mathbf{n} \cdot \sigma(\mathbf{w})|_{\Omega_2} = 0,$$
$$x \in \Gamma: \quad [\mathbf{w}] = -\eta[\mathbf{n} \cdot \nabla\mathbf{u}^0],$$

$$\mathbf{n} \cdot [\sigma(\mathbf{w})] = \nabla\eta \cdot [\sigma^0(\mathbf{u}^0)] - \eta\mathbf{n} \cdot [\mathbf{n} \cdot \nabla\sigma^0(\mathbf{u}^0)], \tag{9}$$

$$q_+ : (C_1^{-1} + K_-(\mathbf{n})) : q_+ + \eta\mathbf{n} \cdot \nabla\chi = -\frac{1}{k}\frac{d\eta}{dt}, \tag{10}$$

$$q_+ \triangleq -C_1 : \varepsilon(\mathbf{w}),$$

where $\Omega_1 \cup \Omega_2$ is the outer boundary of the body. Relation (10) follows from master equation (7) and describes the evolution of initial perturbations of the interface. If the initial state includes several interfaces, consistency conditions (9) and (10) are imposed at each of them.

The operator generated by the boundary value problem specified by Eqs. (8) and (9) is uniquely solvable with respect to $\mathbf{w}$, because additional displacements $\mathbf{w}$ are expressed in terms of the interface perturbation η as $\mathbf{w} = \mathcal{A}\eta$, where $\mathcal{A}$ is a certain linear integral operator. The substitution of this expression into master equation (10) provides the integro-differential equation for η

$$-\frac{1}{k}\frac{d\eta}{dt} = \mathcal{L}\eta. \tag{11}$$

For several interfaces, the solution of Eqs. (8)–(10) leads to the set of integro-differential equations for perturbations of the interfaces.

The analysis of the stability of equilibrium solutions reduces to the determination of the bifurcation points of Eq. (11) and behavior of its small solutions. Bifurcation points are determined from the existence condition of stationary nonzero solution of the equation $\mathcal{L}\eta = 0$. If the operator $\mathcal{L}$ is positive definite, Eq. (11) (set of equations) admits only solutions decreasing with time. In this case, the initial two-phase solution is stable. Otherwise, undamped perturbations exist and, therefore, the solution is unstable.

3. STABILITY OF CENTROSYMMETRIC EQUILIBRIUM STATES

Figure 1 [6, 7] shows pressure p on the surface of a solid ball as a function of $\vartheta = \frac{3u_0}{R}$, where u_0 are radial displacements at the ball boundary and R is the outer radius of the ball.

The solution changes qualitatively at the points A, B, D, and E, where the topology of the solution changes and an internal interface can appear. Single-phase solutions presented by intervals AC' and $C''E$ in Fig. 1 are locally stable on the class of one-phase deformations. At the same time, both two-phase solutions presented by intervals AE and BD are energetically favorable over the single-phase solution and are stable on the class of centrosymmetric solutions, where only the interface radius is perturbed for given ϑ values [7].

Analysis of energy changes accompanying the appearance of new-phase domains shows that centrosymmetric two-phase states energetically favorable over one-phase states even disregarding the thermodynamic equilibrium condition first appear when achieving ϑ_A (loading) and ϑ_E (discharge). This means that the single-phase solution is metastable with respect to two-phase solutions, i.e., is unstable with respect to finite two-phase perturbations. Therefore, the points ϑ_A and ϑ_B can be called points of topological instability (bifurcation).

For a body with a spherical cavity, similar dependences can be plotted for equations with one and two interfaces and for various phase alternating. For two-phase solutions, the new-phase domain expands and pressure decreases with an increase in ϑ.

We consider the stability of the above solutions with respect to axisymmetric perturbations.

Equilibrium conditions for the solid ball admit two two-phase solutions. It is shown that a solution where the phase with the higher shear modulus occupies the outer spherical layer is unstable (interval BD in Fig. 1) [10, 11]. When the harder phase is located at the center of the ball, loss of stability is not observed (interval AE). Solid lines in Fig. 1 are solutions for the solid ball that are locally stable and energetically favorable. Dashed lines are unstable or metastable solutions.

Equilibrium conditions for the ball with the cavity admit solutions with one and two interfaces and various phase alternating. The analysis of stability, when the bulk moduli of materials of phases are identical, for zero stresses or displacements on the cavity surface provides the following conclusions.

(i) When the cavity is small, only a solution with one interface, where the phase with the higher shear modulus forms the inner layer, can be stable. Other solutions, including those with two interfaces, are unstable.

(ii) When the radius of the cavity exceeds a certain value, all two-phase solutions are unstable.

Comparison of results for the stability of the solid ball and ball with the cavity reveals the passage to the limit: the stable solution for the ball with the cavity passes to the stable solution for the solid ball when the cavity radius tends to zero.

4. TWO-PHASE STRAIN FIELDS AND PHASE-TRANSITION ZONE

We compare the strain fields in various two-phase configurations of the ball with the phase-transition zone formed in the strain space by all strains that can coexist at the equilibrium interface [8, 12–14].

For centrosymmetric two-phase fields, spherical and axisymmetric fields of the q tensor arise in the body. In the principal-value space q_1, q_2, and q_3 of the q tensor, these fields lie on the $q_2 = q_3$ plane. Figure 2 shows the sections of the phase-transition zone by this plane. The two solutions of the problem for the solid ball correspond to jumps aa' and bb' at the interface.

For $\mu_1 > 0$, the AE solution (Fig. 1), where the inner + phase has higher shear modulus, corresponds to the strain distribution shown in Fig. 2a by the point a (+ phase in the hydrostatic state) and interval $a'e$ (strains in the ball layer formed by the – phase). When the point e in the z_0e path is achieved, the + phase can originate at the center of the ball and an interface with the strain jump aa' can arise. The interface expands with further deformation of the ball. The strain of the inner + phase remains unchanged (point a). Strains in the ball layer of the – phase are represented by the points of the interval $a'e$, but the point e is shifted to a' with deformation.

The second solution (BD in Fig. 1) is represented in Fig. 2a by the jump bb' and interval $b'd$.

For $\mu_1 < 0$, as the point a is achieved, the + phase originates on the ball surface with the strain a' at the interface (Fig. 2b). With the transformation of the ball, strains in the ball layer of the + phase are distributed over the interval $a'e$. The second solution is represented in Fig. 2b by the jump bb' and interval $b'd$.

Thus, various two-phase states of the ball can correspond to strain fields of the following two types.

(i) Strains at the interface correspond to the outer boundary of the phase-transition zone, and strains at other points of the body lie beyond the phase-transition zone (interval $a'e$ in Fig. 2).

(ii) At least in a part of the body, strains correspond to inner domains of the phase-transition zone (interval db'), and a jump occurs form the nonconvex part of the boundary of the phase-transition zone (point b).

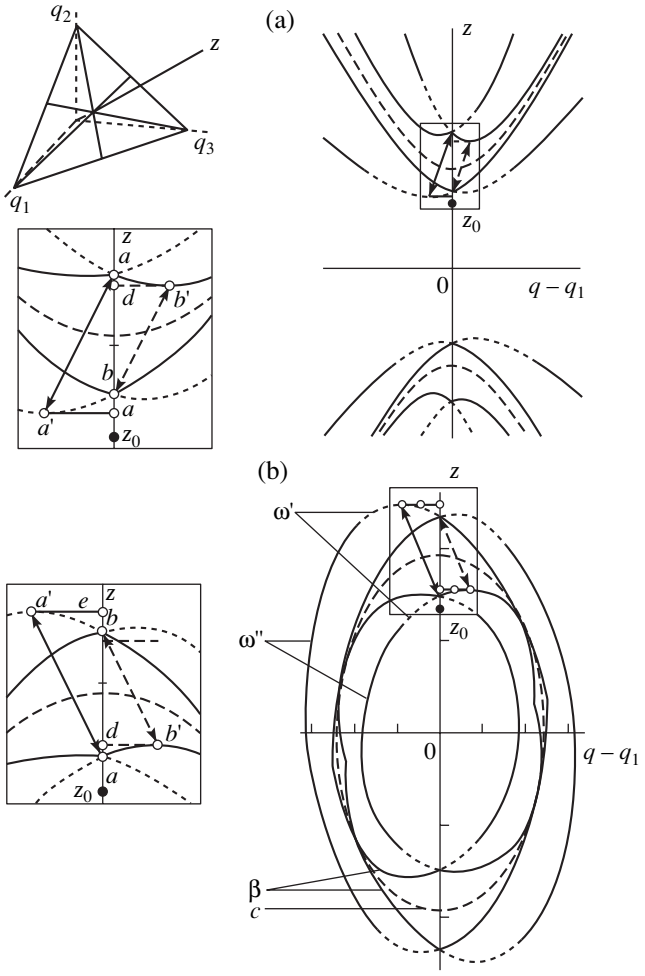

Fig. 2. Section of the phase-transition zone by the $q_2 = q_3 = q$ plane for (a) $\mu_1 > 0$ and $K_1 < 0$ and (b) $\mu_1 < 0$ and $K_1 < 0$: ω' and ω'' are the outer boundaries of the zone, β are the inner boundaries, c is the surface, where the derivatives of the function $f(\varepsilon)$ are discontinuous, $z = \dfrac{I_1(q)}{\sqrt{3}}$, and z_0 is the initial undeformed state.

In the case considered above, the unstable solution corresponds to the second type of two-phase strains.

5. CONCLUSIONS

The above analysis reveals a number of fundamental features of the formulation and solution of boundary value problems for bodies that undergo phase transitions under deformation and, therefore, have an additional degree of freedom associated with an interface.

(i) Since the boundary value problem specified by Eqs. (1) and (2) is nonlinear due to the presence of an unknown interface, the solution is not unique.

(ii) The new degree of freedom significantly affects the stability of elastic two-phase bodies. In the absence of a phase transition ($\eta = 0$), the problem specified by Eqs. (8) and (9) is a well-known homogeneous boundary value problem for a composite, linearly elastic body and has only zero solutions. In this case, the centrosymmetric strain field is stable for any radius of the fixed interface.

(iii) The appearance of a cavity, i.e., an additional outer boundary, is responsible for a destabilizing action independent of the type of boundary conditions imposed at it.

(iv) Solutions of the problem of equilibrium two-phase configurations of elastic bodies can substantially differ from solutions obtained when designing two-phase composites of the optimal structure. Centrosymmetric solutions providing the global minimum of the energy functional of the two-phase body for a fixed fraction of one of the phases were considered in [15]. The phases differed only in the elastic moduli; i.e., this case corresponds to $\varepsilon^p = 0$. A solution providing the global minimum for the solid ball was shown to correspond to a structure where the harder phase is concentrated at the center of the ball and is surrounded by the softer phase. This conclusion coincides with the results of the above stability analysis.

However, for the ball with the cavity, when the bulk moduli of materials of the phases are identical, a solution in the form of the three-layered shell, whose middle layer is formed by the hard phase, is optimal (energetically favorable on the class of states satisfying the isoperimetric condition of the constant content). As was shown above, this solution is unstable under phase transitions, which mean the appearance of the additional degree of freedom associated with the change in the relative phase content.

ACKNOWLEDGMENTS

This work was supported by the Ministry of Industry, Science, and Technology of the Russian Federation (project no. 40.010.1 1.1195), the Russian Foundation for Basic Research (project nos. 01-01-00324, 02-01-06263), and the Competitive Center for Fundamental Natural Sciences at St. Petersburg State University (project no. E00-4.0-185).

REFERENCES

1. M. A. Grinfel'd, *Methods of Continuum Mechanics in the Theory of Phase Transitions* (Nauka, Moscow, 1990).
2. R. D. James, Arch. Ration. Mech. Anal. **77**, 143 (1981).
3. M. E. Gurtin, Arch. Ration. Mech. Anal. **84**, 1 (1983).
4. V. G. Osmolovskiĭ, *Variational Problem of Phase Transitions in Continuum Mechanics* (S.-Peterburg. Gos. Univ., St. Petersburg, 2000).
5. L. B. Kublanov and A. B. Freidin, Prikl. Mat. Mekh. **52** (3), 493 (1988).

6. N. F. Morozov, I. R. Nazyrov, and A. B. Freidin, Dokl. Akad. Nauk **346**, 188 (1996) [Phys. Dokl. **41**, 40 (1996)].
7. I. R. Nazyrov and A. B. Freidin, Izv. Akad. Nauk, Mekh. Tverd. Tela **5**, 52 (1998).
8. N. F. Morozov and A. B. Freidin, Tr. Mat. Inst., Ross. Akad. Nauk **223**, 220 (1998).
9. V. A. Eremeev and L. M. Zubov, Izv. Akad. Nauk, Mekh. Tverd. Tela **2**, 56 (1991).
10. L. L. Sharipova, V. A. Eremeev, and A. B. Freidin, Izv. Vyssh. Uchebn. Zaved., Sev.-Kavk. Reg., Estestv. Nauki, Special Issue: *Mathematical Simulation and Numerical Experiments in Mechanics and Physics* (2001), pp. 166–169.
11. V. A. Eremeev, A. B. Freidin, and L. L. Sharipova, *Problems of Mechanics of Deformable Body* (S.-Peterburg. Gos. Univ., St. Petersburg, 2002), pp. 111–122.
12. A. B. Freidin, Issled. Uprugosti Plast. **18**, 266 (1999).
13. A. B. Freidin and A. M. Chiskis, Izv. Akad. Nauk, Mekh. Tverd. Tela **29** (4), 91 (1994).
14. A. B. Freidin, E. N. Vilchevskaya, and L. L. Sharipova, Theor. Appl. Mech. **28**–**29**, 149 (2002).
15. R. Fosdick and G. F. Royer-Carfagni, J. Elast. **42**, 49 (1996).

Translated by R. Tyapaev

Doklady Physics, Vol. 48, No. 7, 2003, pp. 364–367. Translated from Doklady Akademii Nauk, Vol. 391, No. 2, 2003, pp. 194–198.

MECHANICS

Multidimensional Distributions of Fluctuations in the Motion of the Earth's Pole

Yu. G. Markov and I. N. Sinitsyn

Presented by Academician V.V. Kozlov March 17, 2003

Received March 18, 2003

Measurements of the motion of the Earth's pole have been statistically analyzed in numerous papers (see, e.g., review [1]). Analytical stochastic models of the motion of the Earth's pole were developed in [2–4] on the basis of celestial mechanics. Stationary and nonstationary one-dimensional distributions of fluctuations in the motion of the Earth's pole were studied in [5]. In this paper, we continue that investigation and consider multidimensional distributions for the deformable Earth by using the equations for multidimensional distribution densities and characteristic functions.

1. The notation and assumptions in this paper are the same as in [5].

(i) The state vector is denoted by $\mathbf{Y} = [Y_1 Y_2 Y_3]^{\mathrm{T}}$, where $Y_1 = p_t$, $Y_2 = q_t$, and $Y_3 = r_t$ are the projections of the instantaneous angular velocity of the Earth's rotation on the Earth's axes.

(ii) We assume that the components of the inertia tensor $\mathcal{J} = \{J_{ij}\}$, $i, j = p, q, r$ (i.e., the axial and centrifugal moments of inertia of the deformable Earth $A = J_{pp}$, $B = J_{qq}$, and $C = J_{rr}$, with $J_{pq} = J_{qp}$, $J_{qr} = J_{rq}$, and $J_{rp} = J_{pr}$) in the daily time interval $T_* = 2\pi r_*^{-1}$ can be represented in the form

$$J_{ij} = J_{ij}^* + J'_{ij,1}\sin r_* t + J''_{ij,1}\cos r_* t + J'_{ij,2}\sin 2r_* t + J''_{ij,2}\cos 2r_* t,$$

where higher harmonics are disregarded.

(iii) The dimensionless combinations of the axial moments of inertia

$$u_1 = \langle (C - B)A^{*-1}\cos\varphi\rangle,$$

$$u_2 = \langle (C - A)B^{*-1}\sin\varphi\rangle, \text{ and } u_3 = \langle (B - A)C^{*-1}\sin 2\varphi\rangle,$$

averaged over the daily time interval $T_* = 2\pi r_*^{-1}$ are referred to as effective daily humps. Here, $\langle\ldots\rangle$ means averaging over the time interval $T_* = 2\pi r_*^{-1}$, $\varphi = r_* t$, $u_1 \sim u_2$, and $u_3 \ll u_{1,2}$.

(iv) The dimensionless combinations of the centrifugal moments of inertia,

$$u_4 = \langle J_{qr}A^{*-1}\rangle, \quad u_5 = \langle J_{qr}C^{*-1}\sin\varphi\rangle,$$

$$u_6 = \langle J_{qr}A^{*-1}\cos 2\varphi\rangle,$$

$$u_7 = \langle J_{qr}B^{*-1}\sin 2\varphi\rangle, \quad u_8 = \langle J_{pr}B^{*-1}\rangle,$$

$$u_9 = \langle J_{pr}C^{*-1}\cos\varphi\rangle,$$

$$u_{10} = \langle J_{pr}B^{*-1}\cos 2\varphi\rangle, \quad u_{11} = \langle J_{pr}A^{*-1}\sin 2\varphi\rangle,$$

$$u_{12} = \langle J_{pq}C^{*-1}\rangle,$$

$$u_{13} = \langle J_{pq}A^{*-1}\sin\varphi\rangle, \quad u_{14} = \langle J_{pq}B^{*-1}\cos\varphi\rangle,$$

$$\text{and } u_{15} = \langle J_{pq}C^{*-1}\cos 2\varphi\rangle,$$

averaged over the daily time interval $T_* = 2\pi r_*^{-1}$ will be referred to as effective daily spikes, where $u_{4-7} \sim u_3$, $u_{8-11} \ll u_{4-7}$, and $u_{12-15} \ll u_{8-11}$.

(v) We allow for only the moments of gravitational forces of the Sun with respect to the Earth's axes [6, 7]. It is important to note that the amplitude of the gravitational moment induced by the Moon is larger than that induced by the Sun by a factor of 2–3. However, since the natural frequency differs significantly from the forcing frequency, the amplitude of monthly oscillations induced by the Moon is one twentieth to one fifteenth that of annual oscillations. Therefore, monthly oscillations of the Earth's pole are not manifested in observations.

(vi) We allow for the moments of external random and dissipative forces:

$$M_1^{\mathrm{rd}} = V_{1t} - D_1 p_t, \; M_2^{\mathrm{rd}} = V_{2t} - D_2 q_t,$$
$$\text{and } M_3^{\mathrm{rd}} = V_{3t} - D_3 r_t.$$

Here, V_{1t}, V_{2t}, and V_{3t} are the specific moments of external random forces, and $D_{1,2,3}$ are the coefficients of the specific moments of dissipative forces.

Institute for Problems of Informatics, Russian Academy of Sciences, ul. Vavilova 30/6, Moscow, 117900 Russia

1028-3358/03/4807-0364$24.00

(vii) Finally, $\mathcal{P} = \mathcal{P}(t, p_t, q_t, r_t, \mathbf{u}, \mathbf{V})$, $\mathcal{Q} = \mathcal{Q}(t, p_t, q_t, r_t, \mathbf{u}, \mathbf{V})$, and $\mathcal{R} = \mathcal{R}(t, p_t, q_t, r_t, \mathbf{u}, \mathbf{V})$ denote the specific moments of external perturbing forces, which depend on time, the state vector, the constant parameters $\mathbf{u} = [u_1 u_2 \ldots u_{n_1}]^{\mathrm{T}}$, and the random parameters $\mathbf{V} = [V_{1t} V_{2t} V_{3t} \ldots V_{n_2 t}]^{\mathrm{T}}$, where $n_{1,2} \geq 3$.

Under assumptions (i)–(vii), the equations of the Earth's motion have the form [5]

$$\dot{p}_t + N_* q_t = \mathcal{P}_1 + \mathcal{P}_2 \mathbf{V}, \quad p_{t_0} = p_0, \tag{1}$$

$$\dot{q}_t - N_* p_t = \mathcal{Q}_1 + \mathcal{Q}_2 \mathbf{V}, \quad q_{t_0} = q_0, \tag{2}$$

$$\dot{r}_t = \mathcal{R}_1 + \mathcal{R}_2 \mathbf{V}, \quad r_{t_0} = r_0, \tag{3}$$

where

$$\mathcal{P}_1 = 3u_1 b\omega_*^2 \cos\omega_* t - \frac{3}{2}u_4\omega_*^2(1 - 3b_1^2\cos^2\omega_* t) - \frac{3}{2}u_6\omega_*^2(1 - b_1^2\cos^2\omega_* t) - \frac{3}{2}u_{11}\omega_*^2(1 - b_1^2\cos^2\omega_* t) + \frac{3}{2}u_{13}\omega_*^2 b\cos\omega_* t - u_4 r_t^2 - D_1 p_t, \tag{4}$$

$$\mathcal{P}_2 V = V_{1t} + \bar{\mathcal{P}}_2(t, p_t, q_t, r_t, \mathbf{u})V, \tag{5}$$

$$\mathcal{Q}_1 = -3u_2 b\omega_*^2 \cos\omega_* t + \frac{3}{2}u_7\omega_*^2(1 - b_1^2\cos^2\omega_* t) + \frac{3}{2}u_8\omega_*^2(1 - 3b_1^2\cos^2\omega_* t) - \frac{3}{2}u_{10}\omega_*^2(1 - b_1^2\cos^2\omega_* t) - 3u_{14}b\omega_*^2\cos\omega_* t + u_8 r_t^2 - D_2 q_t, \tag{6}$$

$$\mathcal{Q}_2 V = V_{2t} + \bar{\mathcal{Q}}_2(t, p_t, q_t, r_t, \mathbf{u})V, \tag{7}$$

$$\mathcal{R}_1 = \frac{3}{2}u_3\omega_*^2(1 - b_1^2\cos^2\omega_* t) - \frac{3}{2}u_5 b\omega_*^2\cos\omega_* t + 3u_9 b\omega_*^2\cos\omega_* t + 3u_{15}\omega_*^2(1 - b_1^2\cos^2\omega_* t) - D_3 r_t, \tag{8}$$

$$\mathcal{R}_2 V = V_{3t} + \bar{\mathcal{R}}_3(t, p_t, q_t, r_t, \mathbf{u})V. \tag{9}$$

Here, $N_* = (C^* - B^*)A^{*-1}\omega_*$, $r_* = 365\omega_*$; the quantities u_{1-3} and u_{4-15} are defined in (iii) and (iv), respectively; and b and $b_1 \approx b$ are known parameters such that $4 \leq b \leq (4/3)\pi^{-1}$ [7]. Terms involving the squares and products of $\mathbf{u}$, p_t, q_t, and $r_t - r_*$, as well as the averaged (over the time interval T_*) rates of variation of the axial and centrifugal moments of inertia, are omitted in the functions $\mathcal{P}_1$, $\mathcal{Q}_1$, and $\mathcal{R}_1$. The specific moments of external random–dissipative forces are denoted by $\mathcal{P}_2$, $\mathcal{Q}_2$, and $\mathcal{R}_2$; they are nonlinear in $\mathbf{u}$, p_t, q_t, and r_t and depend on the parameters $\mathbf{V}$.

2. We first consider the general case of non-Gaussian parameters $\mathbf{V}$ with zero mathematical expectations ($M\mathbf{V} = 0$) and known one-dimensional distribution of the independent increments $\mathbf{W}$ ($\dot{\mathbf{W}} = \mathbf{V}$). The corresponding one-dimensional characteristic function and its logarithmic derivative are denoted by

$$h_1 = h_1(\mu; t) = M\exp(i\mu^{\mathrm{T}}W), \quad \chi = \chi(\mu; t) = \frac{\partial}{\partial t}\ln h_1(\mu; t), \tag{10}$$

respectively. According to [8, 9], Eqs. (1)–(3) treated in the sense of θ-differentials reduce to the Ito form

$$d_\theta Y = a(Y, t)dt + b(Y, t)d_\theta W, \quad Y(t_0) = Y_0, \tag{11}$$

where

$$a = a(Y, t) = [a_1 a_2 a_3]^{\mathrm{T}} = \bar{a} + \theta\left[\left(\frac{\partial}{\partial\eta}\right)^{\mathrm{T}} b(Y, t)\nu(t)b(\eta, t)^T\right]^{\mathrm{T}}_{\eta = Y}, \tag{12}$$

$$\bar{a} = \bar{a}(Y, t) = [\bar{a}_1\bar{a}_2\bar{a}_3], \quad \bar{a}_1 = -N_* q_t + \mathcal{P}_1, \quad \bar{a}_2 = N_* p_t + \mathcal{Q}_1, \quad \bar{a}_3 = \mathcal{R}_1, \tag{13}$$

$$b = b(Y, t) = \mathrm{diag}[\mathcal{P}_2, \mathcal{Q}_2, \mathcal{R}_2]. \tag{14}$$

If the parameters $\mathbf{V}$ represent broadband Markov processes, Eqs. (1)–(3) should be treated as nonlinear stochastic differential equations in the sense of θ-differentials [8, 9] (e.g., in the Stratonovich sense, $\theta = \frac{1}{2}$). In the case of self-correlated noise, Eqs. (1)–(3) or (11) should be completed by the equations of linear shaping filters generated by white noise [8, 9].

3. We denote the one- and multidimensional probability densities and characteristic functions of the state vector $\mathbf{Y}$ by $f_n = f_n(y_1, y_2, \ldots, y_n; t_1, t_2, \ldots, t_n)$ and $g_n = g_n(\lambda_1, \lambda_2, \ldots, \lambda_n; t_1, t_2, \ldots, t_n)$, respectively ($n = 1, 2, 3, \ldots$). Then, according to Eq. (11), the stochastic models of fluctuations in the Earth's motion are described by the

Pugachev linear integro-differential equations under the corresponding initial conditions [8, 9]:

$$\frac{\partial g_n}{\partial t_n} = \frac{1}{(2\pi)^{3n}}\int_{-\infty}^{\infty}\dots\int_{-\infty}^{\infty}[i\lambda_n^{\mathrm{T}}a((y_n, t_n) + \chi(b(y_n, t_n)^{\mathrm{T}}\lambda_n; t_n)]\exp\left\{i\sum_{l=1}^{n}(\lambda_l^{\mathrm{T}} - \mu_l^{\mathrm{T}})y_l\right\} \times g_n(\mu_1, \mu_2, \dots, \mu_n; t_1, t_2, \dots, t_n) \times d\mu_1 d\mu_2 \dots d\mu_n dy_1 dy_2 \dots dy_n, \quad (15)$$

$$g_n(\lambda_1, \lambda_2, \dots, \lambda_n; t_1, t_2, \dots, t_{n-1}, t_{n-1}) = g_{n-1}(\lambda_1, \lambda_2, \dots, \lambda_{n-2}, \lambda_{n-1} + \lambda_n; t_1, t_2, \dots, t_{n-1}), \quad (16)$$
$$g_1(\lambda; t_0) = g_0(\lambda);$$

$$\frac{\partial f_n}{\partial t_n} = \frac{1}{(2\pi)^{3n}}\int_{-\infty}^{\infty}\dots\int_{-\infty}^{\infty}[i\lambda_n^{\mathrm{T}}a(\eta_n, t_n) + \chi(b(\eta_n, t_n)^{T}\lambda_n; t_n)]\exp\left\{i\sum_{l=1}^{n}\lambda_l^{\mathrm{T}}(\eta_l^{\mathrm{T}} - y_l^{\mathrm{T}})\right\} \times f_n(\eta_1, \eta_2, \dots, \eta_n; t_1, t_2, \dots, t_n) \times d\eta_1 d\eta_2 \dots d\eta_n d\lambda_1 d\lambda_2 \dots d\lambda_n, \quad (17)$$

$$f_n(y_1, y_2, \dots, y_{n-1}, y_n; t_1, t_2, \dots, t_{n-1}, t_{n-1}) = f_{n-1}(y_1, y_2, \dots, y_{n-1}; t_1, t_2, \dots, t_{n-1})\delta(y_n - y_{n-1}), \quad (18)$$
$$f_1(y; t_0) = f_0(y).$$

Here, $y_n = [p_{t_n} q_{t_n} r_{t_n}]^{\mathrm{T}}$ and $\lambda_n = [\lambda_{pn}\lambda_{qn}\lambda_{rn}]^{\mathrm{T}}$; the function $\chi(\mu; t)$ is given by Eq. (10); and $f_0(y)$ and $g_0(t)$ are the probability density and the characteristic function for the initial state $y_0 = [p_{t0} q_{t0} r_{t0}]^{\mathrm{T}}$, respectively. The δ function enters into the right-hand side of the last equation because the quantity Y_{t_n} for $t_n = t_{n-1}$ is very close to $Y_{t_{n-1}}$.

If the parameters **V** are Gaussian random variables characterized by the intensity matrix $\nu(t) = [\nu_{lh}(t)]$ ($l, h = 1, 2, \dots, n_2$) with zero mathematical expectations, Eqs. (17) and (18) for $n = 1$ reduce either to the Fokker–Planck–Kolmogorov equation [see Eq. (14) in [5]] or to the equation for one-dimensional probability density given in [5]. The transition density $f = f(y; t \mid \eta; \tau)$ satisfies the same equation under the initial condition $f(y; \tau \mid \eta; \tau) = \delta(y - \eta)$. Using the recurrence relation [8, 9]

$$f_n(y_1, y_2, \dots, y_n; t_1, t_2, \dots, t_n) = f_1(y_1; t_1) f(y_2; t_2 \mid y_1; t_1)\dots f(y_n; t_n \mid y_{n-1}; t_{n-1}), \quad (19)$$

we obtain the desired multidimensional probability densities f_n.

4. Using the orthogonal expansion method [8, 9], we present both one-dimensional ($n = 1$) and multidimensional ($n > 1$) kinetic models in the form

$$f_1(y; t) \approx w_1^{\mathrm{st}}(y)\left[1 + \sum_{l=3}^{n^*}\sum_{|\mu| = l} c_{\mu t} p_\mu(y)\right], \quad (20)$$

$$f_n(y_1, y_2, \dots, y_n; t_1, t_2, \dots, t_n) \approx w_n^{\mathrm{st}}(y_1, y_2, \dots, y_n) \times \left[1 + \sum_{l=3}^{n}\sum_{|\mu_1| + \dots + |\mu_n| = l} c_{\mu_1, \mu_2, \dots, \mu_n} \times p_{\mu_1, \mu_2, \dots, \mu_n}(y_1, y_2, \dots, y_n)\right]. \quad (21)$$

Here, $\{p_\mu(y), q_\mu(y)\}$ and $\{p_{\mu_1, \mu_2, \dots, \mu_n}(y_1, y_2, \dots, y_n), q_{\mu_1, \mu_2, \dots, \mu_n}(y_1, y_2, \dots, y_n)\}$ are the known sets of orthogonal polynomials, and the functions $w_n^{\mathrm{st}} = w_n^{\mathrm{st}}(y_1, y_2, \dots, y_n)$ belong to the known standard consistent sequence of probability densities (for $n \geq 1$). Since the first- and second-order moments of w_n^{st} are identical to those of f_n, the functions w_n^{st} depend on the mathematical expectation m_t, covariance matrix K_t, coefficients $c_{\mu t}$, and covariance function $K(t', t'')$ of the vector **Y** for $t', t'' = t_1, t_2, \dots, t_n$. The parameters m_t, K_t, $c_{\mu t}$, $K(t', t'')$, $c_{\mu_1\mu_2}$, and $c_{\mu_1, \dots, \mu_n}$ entering into Eqs. (20) and (21) obey a set of ordinary differential equations, which are generally nonlinear in m_t and K_t but linear in the coefficients of the consistent orthogonal expansions.

In particular, for non-Gaussian parameters **V** in the Gaussian approximation (normal approximation method [8, 9]), the two-dimensional nonlinear kinetic model is described (in terms of probability densities) by the equations

$$f_1 = f_1(y, m_t, K_t; t) = [(2\pi)^3|K_t|]^{-1/2} \times \exp\{-(y - m_t)^{\mathrm{T}}K_t^{-1}(y - m_t)\}; \quad (22)$$

$$\dot{m}_t = M_N a(Y, t), \quad m_{t_0} = m_0; \quad (23)$$

$$\dot{K}_t = M_N[a(Y, t)(Y^{\mathrm{T}} - m_t^{\mathrm{T}}) + (Y - m_t)a(Y, t)^{\mathrm{T}} + \sigma(Y, t)],$$
$$\sigma(Y, t) = b(Y, t)\nu(t)b(Y, t)^{\mathrm{T}}, \quad K_{t_0} = K_0; \tag{24}$$

$$f_2 = f_2(y_1, y_2, m_{t_1}, m_{t_2}, K_{t_1}, K_{t_2}, K(t_1, t_2); t_1, t_2)$$
$$= [(2\pi)^2|\bar{K}_2|]^{-1/2}\exp\left\{-\frac{1}{2}(\bar{y}_2^{\mathrm{T}} - \bar{m}_2^{\mathrm{T}})\bar{K}_2^{-1}(\bar{y}_2 - \bar{m}_2)\right\}; \tag{25}$$

$$\bar{y}_2 = [y_{t_1}^{\mathrm{T}} y_{t_2}^{\mathrm{T}}]^{\mathrm{T}}, \quad \bar{m}_2 = [m_{t_1}^{\mathrm{T}} m_{t_2}^{\mathrm{T}}]^{\mathrm{T}},$$
$$\bar{K}_2 = \begin{bmatrix} K(t_1, t_1) & K(t_1, t_2) \\ K(t_2, t_1) & K(t_2, t_2) \end{bmatrix}; \tag{26}$$

$$\frac{\partial K(t_1, t_2)}{\partial t_2} = M_N[(Y_{t_1} - m_{t_1})a(Y_{t_2}, t_2)^{\mathrm{T}}],$$
$$K(t_1, t_1) = K(t_1). \tag{27}$$

Here, the subscript N implies that the mathematical expectation is calculated for equivalent normal distribution (22) or (25) with unknown parameters m_t, K_t, and $K(t_1, t_2)$. With known one- and two-dimensional Gaussian distributions, the probability densities f_n for $n > 2$ are calculated by the normal approximation method.

5. In conclusion, we make two remarks.

For Gaussian parameters **V** with $n = 1$, the kinetic model described by Eqs. (15)–(18) coincides with the model developed in [5]. In this case, it is advisable to use the Pugachev linear operator equation [8, 9]

$$\frac{\partial q_1}{\partial t} = \left[i\lambda^T a\left(\frac{\partial}{i\partial\lambda}, t\right) - \frac{1}{2}\lambda^{\mathrm{T}}\sigma\left(\frac{\partial}{i\partial\lambda}, t\right)\lambda_1\right]g_1, \tag{28}$$
$$i^2 = -1$$

under initial condition (19) for the one-dimensional characteristic function rather than the Fokker–Planck–Kolmogorov equation for the polynomials $a(y, t)$ and $\sigma(y, t) = b(y, t)\nu(t)b(y, t)^{\mathrm{T}}$. However, the method of parameterization [8, 9] is more efficient in practical calculations particularly for $n > 1$.

Integro-differential equation (15) allows us, first, to formulate the following exact differential criterion of the equivalence (with respect to the distribution of **V**) of stochastic differential equations (1)–(3) or (11) for both Gaussian and non-Gaussian parameters **V**:

$$\chi(b(y, t)^{\mathrm{T}}\lambda; t) = -\frac{1}{2}[b(y, t)^{\mathrm{T}}\lambda]^{\mathrm{T}}\nu_{\mathrm{eq}}(t)[b(y, t)^{\mathrm{T}}\lambda], \tag{29}$$

where $\nu_{\mathrm{eq}}(t)$ is the intensity matrix for equivalent white noise. Second, in the normal approximation method [8, 9], the approximate criterion of equivalence, $\nu(t) = \nu_{\mathrm{eq}}(t)$, follows from Eq. (24) [10, 11]. Third, it is possible to formulate integral (spectral and dispersion) criteria of equivalence [10, 11]. Specific differential and integral criteria of the replacement of stochastic equations (1)–(3) or (11) with non-Gaussian parameters **V** by equivalent equations with Gaussian parameters can be formulated on the basis of the above models. For example, when analyzing the motion of the Earth's pole by means of Eqs. (1) and (2), terms containing r_t must be replaced by equivalent perturbations. This is very important for the choice and identification of the parameters **u** entering into Eqs. (1)–(3). The problem of identification of the motion regimes of the Earth's pole was first deterministically formulated in [12] and solved in [7, 13, 14].

ACKNOWLEDGMENTS

This work was support by the Russian Foundation for Basic Research, project nos. 01-02-17250 and 01-01-00758.

REFERENCES

1. M. Araty, *Linear Stochastic Systems with Constant Coefficients* (Springer-Verlag, Berlin, 1982; Nauka, Moscow, 1989).
2. Yu. G. Markov and I. N. Sinitsyn, Dokl. Akad. Nauk **385**, 189 (2002).
3. Yu. G. Markov and I. N. Sinitsyn, Dokl. Akad. Nauk **387**, 482 (2002).
4. Yu. G. Markov and I. N. Sinitsyn, Astron. Zh. **80** (2), 186 (2003).
5. Yu. G. Markov and I. N. Sinitsyn, Dokl. Akad. Nauk **390** (3), 343 (2003).
6. W. Munk and G. Macdonald, *The Rotation of the Earth* (Cambridge Univ. Press, Cambridge, 1960; Mir, Moscow, 1964).
7. L. D. Akulenko, S. A. Kumakshev, and Yu. G. Markov, Dokl. Akad. Nauk **382**, 199 (2002) [Dokl. Phys. **47**, 78 (2002)].
8. V. S. Pugachev and I. N. Sinitsyn, *Stochastic Differential Systems: Analysis and Filtering* (Wiley, New York, 1987; Nauka, Moscow, 1990).
9. V. S. Pugachev and I. N. Sinitsyn, *Stochastic Systems: Theory and Applications* (Logos, Moscow, 2000; World Scientific, River Edge, NJ, 2001).
10. I. N. Sinitsyn, Dokl. Akad. Nauk **348**, 327 (1996) [Phys. Dokl. **41**, 218 (1996)].
11. I. N. Sinitsyn, Mekh. Tverd. Tela, No. 6, 14 (1996).
12. G. S. Kurbasova and L. V. Rykhlova, Astron. Zh. **75**, 632 (1998) [Astron. Rep. **42**, 558 (1998)].
13. L. D. Akulenko, S. A. Kumakshev, and Yu. G. Markov, Dokl. Akad. Nauk **379**, 191 (2001) [Dokl. Phys. **46**, 508 (2001)].
14. L. D. Akulenko, S. A. Kumakshev, Yu. G. Markov, and L. V. Rykhlova, Astron. Zh. **79**, 952 (2002) [Astron. Rep. **46**, 858 (2002)].

Translated by V. Chechin

Doklady Physics, Vol. 48, No. 7, 2003, pp. 368–371. Translated from Doklady Akademii Nauk, Vol. 391, No. 2, 2003, pp. 199–202.

MECHANICS

Interaction of a Shock Wave with a Spherical Bubble Cluster in a Liquid

Academician V. E. Nakoryakov and V. E. Dontsov

Received February 10, 2003

Propagation of pressure waves in a liquid containing gas bubbles was investigated in detail by theoretical and experimental methods [1–5]. In particular, a finite-duration nonlinear perturbation propagating in a liquid with gas bubbles was shown to decay into solitary waves (solitons). The evolution, structure, and attenuation of these solitons have been studied in detail. New types of wave structures, multisolitons, have been discovered and investigated in a liquid containing gas bubbles of two different dimensions for various ratios of bubble radii [6, 7]. The effect of both the heterogeneity of a gas–liquid mixture and compressibility of the liquid on the pressure-wave structure was investigated in [8, 9]. The attenuation and structure of moderate-amplitude pressure waves propagating either in a liquid containing bubbles of two different gases or in stratified bubble media were studied experimentally in [10, 11]. Generation of high-power pressure pulses by spherical bubble clusters was investigated numerically in [12].

In this work, we experimentally investigate the interaction of a plane shock wave with a spherical bubble cluster in a liquid.

The experiments were carried out on a shock-tube setup. Its working section represented a vertical thick-walled steel tube with an inner diameter and length of 53 mm and 1 m, respectively. A thin stainless wire (1 mm in diameter) whose ends were fixed to walls of the working section was situated along the working-section axis. A part of the working section was filled with a working liquid (distilled water). A foam-rubber ball, which was filled with the liquid containing gas bubbles and which served as a bubble cluster, was put on the wire through its center. The upper cluster end was spaced from the surface of the liquid by about 10 mm. In the experiments, we used foam-rubber balls 30 and 45 mm in diameter.

The bubble cluster was prepared on an additional setup. We placed the foam-rubber ball in an active volume of the setup and saturated it with distilled water under vacuum. Then, air bubbles were pumped through the liquid in the active volume at static pressure exceeding atmospheric pressure. As a result, the liquid in the active volume reached equilibrium air saturation at the given static pressure and the gas dissolved inside the foam-rubber ball due to diffusion. When the active volume was depressurized down to the atmospheric static pressure, gas bubbles were released and grew in the liquid. Adhering to the foam-rubber skeleton, these bubbles formed the gas–liquid cluster. In the investigated range of the volume gas content, the bubble diameter increased up to $d \sim 0.1$ mm [13]. However, we observed gas bubbles with diameters up to $d \sim 0.5$ mm on the cluster surface that could be caused by the coalescence of bubbles during their growth. Varying the drop of the static pressure, we changed the initial volume content φ of the gas in the cluster. This was determined by measuring both the cluster volume and the increase in the volume of the liquid with a decrease in the initial static pressure in the medium [13].

Since the porosity of the foam-rubber ball was high (98%) and its rigidity was low, the porous skeleton did not affect the propagation of the pressure wave [13].

A step-shaped pressure wave was generated in air by breaking a diaphragm, which separated the high-pressure chamber and the working section, and then allowed to propagate into the liquid. Pressure-wave profiles were measured by piezoelectric pressure sensors, which were situated on the lateral surface ($D1$–$D5$) and at the bottom ($D6$) of the working section. Signals generated by the sensors were transmitted to an analog-to-digital converter and then processed on a computer.

Figure 1 shows the profiles of pressure waves in the liquid behind the bubble cluster at various distances X from the shock-wave entry into the medium for two initial wave amplitudes. The amplitudes of the waves, as well as the time scale, are shown above their profiles; ΔP_0 is the amplitude of the shock wave entering the liquid; ΔP is the pressure-wave amplitude in the liquid; P_0 is the static pressure in the liquid ahead of the wave. The sensor situated at a distance of 0.495 m from the wave entry into the medium is flush with the working-section bottom and measures the shock wave reflected

Kutateladze Institute of Thermal Physics, Siberian Division, Russian Academy of Sciences, pr. Lavrent'eva 1, Novosibirsk, 630090 Russia

1028-3358/03/4807-0368$24.00

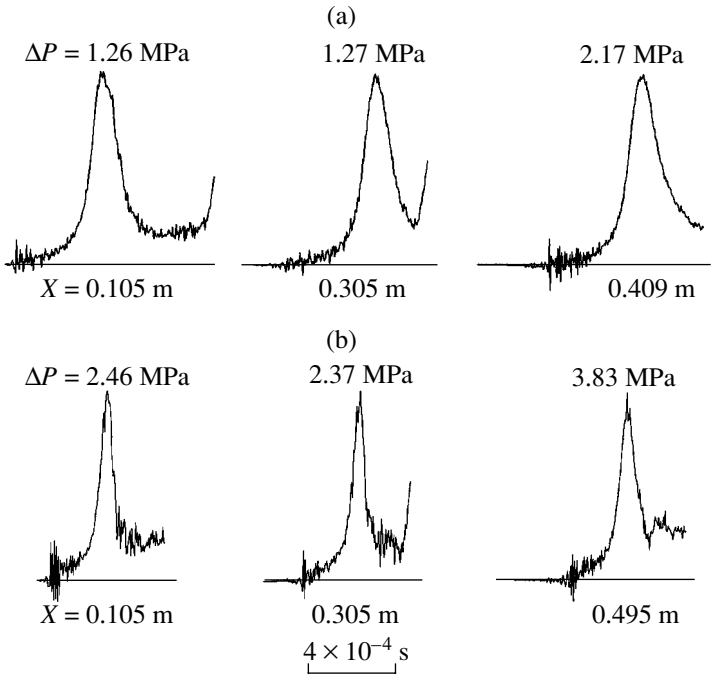

Fig. 1. Profiles of pressure waves in the liquid behind the bubble cluster 30 mm in diameter for P_0 = 0.1 MPa, φ = (a) 12 and (b) 8.9%, and ΔP_0 = (a) 0.36 and (b) 0.69 MPa.

from the bottom. It is seen that the bubble cluster transforms the initial step-shaped wave into a solitary pressure wave. It propagates in the liquid with the speed of sound almost without variation in its shape and amplitude (Fig. 1a, X = 0.105 and 0.305 m). The amplitude of the solitary pressure wave considerably exceeds the amplitude of the incident shock wave. Reflecting from the rigid bottom, the solitary wave virtually doubles its amplitude (Fig. 1a, X = 0.495 m). The solitary profile is formed due to the re-emission of the refracted shock wave preliminarily absorbed by the cluster [12]. High-frequency oscillations at the front edge of the solitary wave are mainly caused by vibrations of gas bubbles in the cluster. With an increase in the amplitude of the shock wave entering the medium, the width of the forming solitary wave decreases and its amplitude increases (Fig. 1b). As in the case of high-amplitude solitons propagating in a homogeneous gas–liquid medium [14], this transformation of the solitary pressure wave is accompanied by the sharpening of its profile. An increase in the amplitude of the solitary wave intensifies its attenuation in the liquid.

Figure 2 shows the measured amplitude of the solitary pressure wave formed by the bubble cluster versus the amplitude of the shock wave entering the medium for various parameters of the gas–liquid cluster. Here, open (*1*, *3*, *5*) and closed (*2*, *4*, *6*) points correspond to atmospheric and lowered static pressures in front of the wave, respectively. In addition, points *1–4* show the amplitude of the solitary wave formed by the cluster, and points *5*, *6* show the amplitude of the solitary wave reflected from the rigid bottom. According to the data plotted in Fig. 2, with an increase in the amplitude of the shock wave entering the medium, the relative soli-

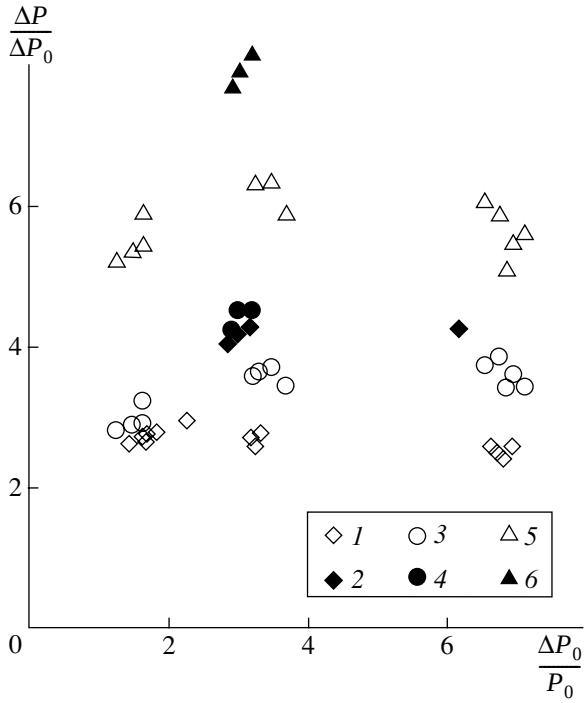

Fig. 2. Relative amplitude of the solitary pressure wave formed by the bubble cluster 30 mm in diameter vs. the amplitude of the shock wave entering the medium for P_0 = 0.1 MPa and φ = (*1*) 4.8, (*3*, *5*) 12% and P_0 = 0.05 MPa and φ = (*2*) 11.2, (*4*, *6*) 24%.

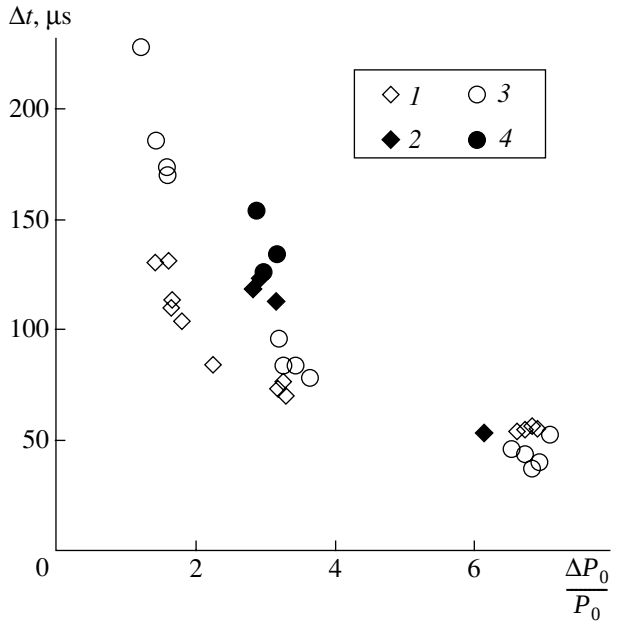

Fig. 3. Same as in Fig. 2, but for the half-width of the solitary pressure wave.

tary-wave amplitude $\frac{\Delta P_0}{P_0}$ increases and decreases for small and large $\frac{\Delta P}{\Delta P_0}$ values, respectively. The maximum of the relative amplitude $\frac{\Delta P}{\Delta P_0}$ apparently lies in the range $\frac{\Delta P_0}{P_0} \sim 5$–10, which agrees with the numerical calculations [12]. Comparison of experimental points *1* and *3*, which are obtained at different initial volume gas contents φ, shows that the amplitude of the solitary wave increases with increasing φ in the cluster. A decrease in the initial static pressure P_0 in the cluster ahead of the wave also increases the amplitude of the solitary wave (points *3* and *2*). Both a decrease in P_0 and an increase in φ in the cluster increase its compressibility. As a result, cluster compression in the shock wave and therefore the amplitude of the solitary wave increase. Reflecting from the rigid wall, the solitary waves virtually double their amplitudes (points *3* and *5*, *4* and *6*). The most substantial deviation from the linear reflection law is observed for large wave amplitudes (points *3* and *5*, $\frac{\Delta P_0}{P_0} \sim 7$), when dissipative loss in the liquid becomes large.

Figure 3 presents the measured half-width of the solitary pressure wave propagating in the liquid versus the amplitude of the shock wave entering the medium for various parameters of the gas–liquid cluster. The half-width of the solitary wave was measured as for the classical Korteweg–de Vries or Boussinesq soliton [3]. According to this approach, Δt is the wave width from the level $0.42\Delta P$ to the pressure maximum in the wave ΔP. The resulting wave widths for the corresponding amplitudes are much larger than those for solitons calculated by using bubble dimensions in the cluster [3, 14] and much smaller than those for the wave generated by vibrations of the gas bubble whose size is equal to the size of the cluster. As is seen, the width of the solitary wave decreases with increasing the amplitude $\frac{\Delta P_0}{P_0}$. For small amplitudes of the shock wave, Δt depends strongly on both the initial volume gas content φ and the static pressure ahead of the wave P_0. An increase in φ (points *1* and *3*) and a decrease in P_0 (points *3* and *2*) both increase the width of the solitary wave. This effect occurs because, at small $\frac{\Delta P_0}{P_0}$, the duration of cluster compression and, consequently, the width of the solitary wave formed by the cluster are mainly determined by the time of propagation of the refracted shock wave through the cluster. As the amplitude $\frac{\Delta P_0}{P_0}$ increases, the inertial properties of the cluster become substantial for its compression. As a result, the width of the solitary wave for $\frac{\Delta P_0}{P_0} > 6$ is almost independent of the cluster parameters φ and P_0 and is determined by the wave amplitude as for solitons propagating in bubble media [3, 14].

It is shown that the growth of the cluster increases both the amplitude and width of the solitary pressure wave formed by the cluster.

Thus, the interaction of a plane shock wave with a spherical bubble cluster situated in a liquid was shown to cause the formation of a solitary pressure wave, which propagates in the liquid and whose amplitude considerably exceeds the amplitude of the shock wave.

ACKNOWLEDGMENTS

This work was supported by the Russian Foundation for Basic Research (project no. 03-01-00211) and Foundation of the President of Russian Federation for the Support of Leading Scientific Schools (mathematics and mechanics, project no. NSh-523.2003.1).

REFERENCES

1. G. K. Batchelor, Mechanik **109**, 67 (1968).
2. L. van Wijngaarden, J. Fluid Mech. **33**, 465 (1968).
3. V. E. Nakoryakov, B. G. Pokusaev, and I. R. Shreĭber, *Wave Dynamics of Gas- and Vapor-Liquid Atmosphere* (Énergoatomizdat, Moscow, 1990).

4. R. I. Nigmatulin, *Dynamics of Multiphase Atmospheres* (Nauka, Moscow, 1987), Vol. 1/2.
5. M. Watanabe and A. Prosperetti, J. Fluid Mech. **274**, 349 (1994).
6. V. E. Nakoryakov and V. E. Dontsov, Dokl. Akad. Nauk **378**, 483 (2001) [Dokl. Phys. **46**, 422 (2001)].
7. V. E. Nakoryakov, V. E. Dontsov, and V. G. Gasenco, in *Proceedings of 2nd Biot Conference on Poromechanics, 26–28 August, Grenoble, 2002*, p. 715.
8. A. E. Beylich and A. Gulhan, Phys. Fluids A **2**, 1412 (1990).
9. M. Kameda, N. Shimaura, F. Higashino, and Y. Matsumoto, Phys. Fluids **10**, 2661 (1998).
10. V. E. Nakoryakov and V. E. Dontsov, Dokl. Akad. Nauk **382**, 637 (2002) [Dokl. Phys. **47**, 153 (2002)].
11. V. E. Nakoryakov and V. E. Dontsov, Dokl. Akad. Nauk **386**, 48 (2002).
12. V. K. Kedrinskiĭ, Yu. I. Shokin, V. A. Vshivkov, *et al.*, Dokl. Akad. Nauk **381**, 773 (2001) [Dokl. Phys. **46**, 856 (2001)].
13. V. E. Dontsov and V. E. Nakoryakov, Int. J. Multiphase Flow **27** (12), 2023 (2001).
14. V. E. Nakoryakov, V. E. Kuznetsov, V. E. Dontsov, and P. G. Markov, Int. J. Multiphase Flow **16** (5), 741 (1990).

Translated by Yu. Verevochkin

Doklady Physics, Vol. 48, No. 7, 2003, pp. 372–375. Translated from Doklady Akademii Nauk, Vol. 391, No. 3, 2003, pp. 327–330.

MECHANICS

Thermal Wave Generated by a Given Boundary Regime

S. P. Bautin

Presented by Academician G.G. Chernyĭ March 31, 2003

Received February 10, 2003

A thermal-wave solution is considered for the nonlinear heat conduction equation (which is simultaneously the equation of nonstationary filtration of a gas in porous soil) in the plane-symmetric case. A thermal wave that is generated by a given boundary regime, continuously adjoins the cold background, and propagates through it with a finite velocity is considered. For the gas-filtration process, such a boundary regime specifies pressure at a fixed bed point from which the filtration front propagates with a finite velocity. It is proved that the boundary value problem, where a function specifying the boundary condition is analytic and equal to zero at the initial time, while its derivative is positive at this time, has a unique analytic solution, which is the corresponding thermal wave.

To successfully realize controlled thermonuclear fusion, it is necessary to simulate complex gas flows, including those in the presence of equilibrium radiation and Compton scattering of photons [1, 2]. The simple inclusion of these phenomena leads to the necessity of the study of nonlinear heat-transfer processes for the case where a thermal wave propagates through a cold background with a finite velocity [3]. The problem formulated by A.D. Sakharov for the construction of the thermal wave generated by a given boundary regime [4] is the most interesting and physically natural for description of such processes. This problem also describes the finite-rate filtration of a gas in porous soil under a given boundary regime of an increase in pressure in the bed [5–7].

For the one-dimensional case, with a power temperature dependence of the heat conductivity, this problem is formulated as follows. For the equation

$$u_t = uu_{xx} + \frac{1}{\sigma}u_x^2, \quad \sigma = \text{const} > 0, \tag{1}$$

the boundary condition

$$u(t, x)|_{x=0} = f(t), \quad f(0) = 0, \quad f'(0) = f_1 > 0 \tag{2}$$

is imposed. Here, $u(t, x)$ is the desired function related to temperature T as $u = T^\sigma$.

The condition $f(0)$ ensures the continuous joining of the desired solution $u(t, x) \geq 0$ and the cold background $u \equiv 0$ for $t \geq 0$ and enables one to construct a thermal wave propagating, for definiteness, from left to right

$$u_*(t, x) = \begin{cases} u(t, x) & \text{for } x \leq a(t) \\ 0 & \text{for } x \geq a(t). \end{cases}$$

The function $a(t)$ specifies the thermal-wave front; i.e.,

$$u(t, x)|_{x=a(t)} = 0, \quad a(0) = 0, \quad a'(0) > 0. \tag{3}$$

Figure shows the composite surface $u_*(t, x)$ for $t \geq 0$ and $x \geq 0$.

The theorem concerning the conditions on the coefficients of the power series for the function $f(t)$ under which the problem specified by Eqs. (1) and (2) has a unique solution in the form of a convergent double series in powers of t and x was formulated in [8]. The existence of a formal power series solving the problem specified by Eqs. (1) and (2) was proved in [9], where the convergence of this series was not shown (see [4, p. 10]).

In this study, the theorem of existence and uniqueness of the analytic solution of the problem specified by

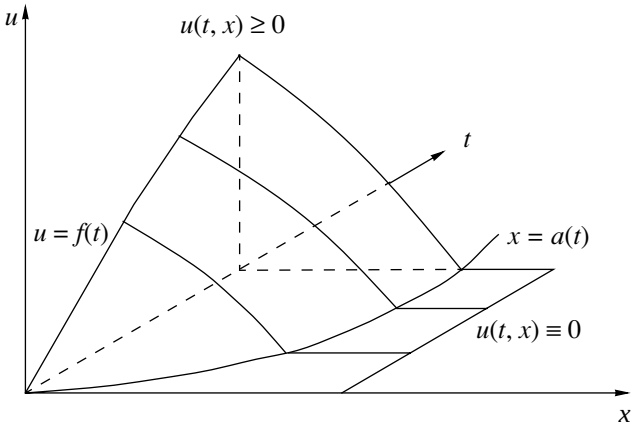

Figure.

Ural State Railway University, ul. Kolmogorova 66, Yekaterinburg, 620034 Russia

** e-mail: SBautin@math.usart.ru*

1028-3358/03/4807-0372$24.00 © 2003 MAIK “Nauka/Interperiodica”

Eqs. (1) and (2) is proved. To this end, the problem reduces to that for which the theorem of existence and uniqueness was already proved [10]. In [10], the problem of a thermal wave determined by its specified front, i.e., the problem specified by Eqs. (1) and (3) for a given analytic function $a(t)$, was analyzed.

Theorem. *If the function $f(t)$ such that $f(0) = 0$ and $f'(0) = f_1 > 0$ is analytic in a certain vicinity of the point $t = 0$, the problem specified by Eqs.* (1) *and* (2) *has a unique analytic solution near the origin.*

Note. In contrast to the theorem proved in [8], this theorem imposes no additional restrictions on the coefficients of the power series for the function $f(t)$.

Proof. We introduce one more unknown function $a(t)$ such that $a(0) = 0$ and $a'(0) > 0$, which presents an unknown front of the thermal wave. The problem specified by Eqs. (1)–(3) is considered for unknown functions $u(t, x)$ and $a(t)$.

Then, we change variables as

$$z = x - a(t), \quad \tau = t$$

with the Jacobian equal to unity for a finite function $a'(t)$. After this change, the unknown thermal-wave front is the new coordinate axis $z = 0$. In the new variables, Eqs. (1)–(3) take the form

$$u_\tau - a'(\tau)u_z = uu_{zz} + \frac{1}{\sigma}u_z^2,$$

$$u(\tau, z)|_{z = -a(\tau)} = f(\tau),$$

$$u(\tau, z)|_{z = 0} = 0,$$

respectively.

Further, we change the dependent and independent variables, i.e.,

$$z = z(t, u), \quad \tau = t,$$

where the new desired function z depends on t and u. The Jacobian of this transformation is determined as

$$J = -z_u = -\frac{1}{u_z}.$$

Since

$$u_z(0, 0) = -\sqrt{f_1\sigma} \neq 0,$$

the latter change is nonsingular at the point $\tau = 0$, $z = 0$ and near it. As a result, we arrive at the problem

$$z_u^2[z_t + a'(t)] = uz_{uu} - \frac{1}{\sigma}z_u,$$

$$z(t, u)|_{u = f(t)} = -a(t),$$

$$z(t, u)|_{u = 0} = 0.$$

The second relation is satisfied for $t = 0$ due to the third relation and the relations $f(0) = a(0) = 0$. Therefore, the second relation can be replaced by its derivative with respect to t

$$[z_t + z_u f'(t)]|_{u = f(t)} = -a'(t).$$

This relation makes it possible to exclude the unknown function $a(t)$ from the first equation.

Thus, it is necessary to prove the existence and uniqueness of the analytic solution of the problem

$$z_u^2\{z_t - [z_t(t, u)|_{u = f(t)}] - f'(t)[z_u(t, u)|_{u = f(t)}]\}$$

$$= uz_{uu} - \frac{1}{\sigma}z_u,$$

$$z(t, u)|_{u = 0} = 0.$$

In this problem, we change variables

$$\nu = u, \quad \zeta = u - f(t)$$

so that the $u = f(t)$ line, as well as the $u = 0$ line, becomes a coordinate axis. The Jacobian of this transformation is equal to $-f'(t)$ and is nonzero at the point $t = 0$ and near it. The old variables are expressed in terms of the new ones as

$$u = \nu, \quad t = \varphi(\nu - \zeta),$$

where φ is the inverse function of f. Then,

$$\varphi(0) = 0, \quad \varphi'(0) = \frac{1}{f'(0)} = \frac{1}{f_1} > 0,$$

and, if the function $f(t)$ is analytic near the point $t = 0$, the function φ is also analytic near the origin.

We introduce the analytic function

$$F(\nu - \zeta) = -f'(\varphi(\nu - \zeta)),$$

which is obtained by substituting the expression $t = \varphi(\nu - \zeta)$ into the function $f'(t)$. In this case, $F(0) = -f'(0) = -f_1$.

As a result, the unknown function $z(\zeta, \nu)$ satisfies the equation

$$\{F(\nu - \zeta)z_\zeta + [F(\nu - \zeta) - F(\nu)](z_\zeta|_{\zeta = 0})$$

$$+ F(\nu - \zeta)(z_\nu|_{\zeta = 0})\}(z_\nu + z_\zeta)^2$$

$$= \nu(z_{\nu\nu} + 2z_{\nu\zeta} + z_{\zeta\zeta}) - \frac{1}{\sigma}(z_\nu + z_\zeta) \qquad (4)$$

and the initial condition

$$z(\zeta, \nu)|_{\nu = 0} = 0. \qquad (5)$$

For $\nu = 0$, $\zeta = 0$, Eq. (4) provides

$$z_1(0) = \pm\frac{1}{\sqrt{\sigma f_1}}.$$

According to the physical meaning of the problem under consideration (thermal wave propagating from left to right), we take the minus sign, i.e.,

$$z_1(0) = -\frac{1}{\sqrt{\sigma f_1}}.$$

Then, Eq. (4) for $\nu = 0$ uniquely provides the coefficient

$$z_1(\zeta) = \sqrt{\frac{f_1}{\sigma}}\frac{1}{F(-\zeta)}, \quad (6)$$

which is an analytic function near the point $\zeta = 0$ because $F(0) \neq 0$.

Taking into account relations (5) and (6), we replace the desired function $z(\zeta, t)$ with the new unknown function $Z(\zeta, t)$ according to the relation

$$z(\zeta, \nu) = \sqrt{\frac{f_1}{\sigma}}\frac{1}{F(-\zeta)}\nu + \nu^2 Z(\zeta, \nu).$$

If the function $Z(\zeta, \nu)$ is analytic, the function $z(\zeta, \nu)$ is also analytic.

Equation (4) transforms to the equation

$$2\left(1 + \frac{1}{\sigma}\right)Z + \left(4 + \frac{1}{\sigma}\right)\nu Z_\nu + \nu^2 Z_{\nu\nu}$$

$$-\frac{2f_1}{\sigma F(-\zeta)}(Z|_{\zeta=0}) - \frac{f_1}{\sigma F(-\zeta)}\nu(Z_\nu|_{\zeta=0})$$

$$= g_0 + \nu g_1 + \nu^2 g_2 \equiv g$$

for the new unknown function, where

$$g_0 = g_0(\zeta, \nu),$$

$$g_1 = g_1(\zeta, \nu, Z, Z|_{\zeta=0}, Z_\zeta, Z_\zeta|_{\zeta=0}),$$

$$g_2 = g_2(\zeta, \nu, Z, Z|_{\zeta=0}, Z_\zeta, Z_\zeta|_{\zeta=0}, Z_\nu, Z_\nu|_{\zeta=0}, Z_{\zeta\zeta}, Z_{\zeta\nu}),$$

are analytic functions, where the unknown function $Z(\zeta, \nu)$ and its derivatives enter in the polynomial form.

We seek the solution of the equation for the function $Z(\zeta, \nu)$ in the form of the power series

$$Z(\zeta, \nu) = \sum_{k=0}^{\infty} Z_k(\zeta)\frac{\nu^k}{k!}, \quad Z_k(\zeta) = \left.\frac{\partial^k Z}{\partial \nu^k}\right|_{\nu=0}, \quad (7)$$

whose coefficients are uniquely determined as the analytic functions

$$Z_0(\zeta) = \frac{1}{2\left(1 + \frac{1}{\sigma}\right)}\left[g^{(0)}(\zeta) + \frac{f_1}{\sigma F(-\zeta)}\frac{g^{(0)}(0)}{1 + \frac{2}{\sigma}}\right],$$

$$Z_1(\zeta) = \frac{1}{3\left(2 + \frac{1}{\sigma}\right)}\left[g^{(1)}(\zeta) + \frac{f_1}{\sigma F(-\zeta)}\frac{g^{(1)}(0)}{2\left(1 + \frac{1}{\sigma}\right)}\right],$$

$$Z_k(\zeta) = \frac{1}{\left[k(k-1) + k\left(4 + \frac{1}{\sigma}\right) + 2\left(1 + \frac{1}{\sigma}\right)\right]}\left\{g^{(k)}(\zeta) + \frac{f_1}{\sigma F(-\zeta)}\frac{(k+2)g^{(k)}(0)}{k(k-1) + k\left(4 + \frac{1}{\sigma}\right) + 2\left(1 + \frac{1}{\sigma}\right) + \frac{k+2}{\sigma}}\right\}.$$

Here, $k \geq 2$ and

$$g^{(l)}(\zeta) = \left.\frac{\partial^l g}{\partial \nu^l}\right|_{\nu=0}$$

for $l \geq 0$.

The convergence of series (7) is proved by the classical majorant method. We take the standard majorizing functions

$$\Phi(\zeta) \gg \frac{f_1}{\sigma F(-\zeta)}, \quad W_0(\zeta) \gg Z_0(\zeta), \quad W_1(\zeta) \gg Z_1(\zeta);$$

$$G_0(\zeta, \nu) \gg g_0(\zeta, \nu),$$

$$G_1(\zeta, \nu, W, W_\zeta) \gg g_1(\zeta, \nu, Z, Z|_{\zeta=0}, Z_\zeta, Z_\zeta|_{\zeta=0}),$$

$$G_2(\zeta, \nu, W, W_\zeta, W_\nu, W_{\zeta\nu}, W_{\zeta\zeta})$$

$$\gg g_2(\zeta, \nu, Z, Z|_{\zeta=0}, Z_\zeta, Z_\zeta|_{\zeta=0}, Z_\nu, Z_\nu|_{\zeta=0}, Z_{\zeta\zeta}, Z_{\zeta\nu})$$

and introduce the function

$$G = G_0 + \nu G_1 + \nu^2 G_2 \gg g = g_0 + \nu g_1 + \nu^2 g_2.$$

If

$$W_k(\zeta) = \frac{G^{(k)}(\zeta) + \Phi(\zeta)G^{(k)}u(\zeta)}{k(k-1) + k\left(4 + \frac{1}{\sigma}\right) + 2\left(1 + \frac{1}{\sigma}\right)},$$

$$G^{(k)}(\zeta) = \left.\frac{\partial^k G}{\partial \nu^k}\right|_{\nu = 0}$$

for $k \geq 2$, then

$$W_k(\zeta) \gg Z_k(\zeta), \quad k \geq 2,$$

and the convergence of series (7) follows from the convergence of the series

$$W(\zeta, \nu) = \sum_{k=0}^{\infty} W_k(\zeta)\frac{\nu^k}{k!}, \quad W_k(\zeta) = \left.\frac{\partial^k W}{\partial \nu^k}\right|_{\nu = 0}. \quad (8)$$

The construction of series (8) by the above formulas is equivalent to the construction of the solution of the equation

$$2\left(1 + \frac{1}{\sigma}\right)W + \left(4 + \frac{1}{\sigma}\right)\nu W_\nu + \nu^2 W_{\nu\nu}$$

$$= [1 + \Phi(\zeta)][G_0 + \nu G_1 + \nu^2 G_2].$$

The existence of the analytic majorizing zero solution of the last equation follows from the theorem proved in [10].

Thus, the theorem of the existence and uniqueness of the analytic solution of the problem specified by Eqs. (1) and (2) has been proved.

The analytic function $a(t)$ specifying the thermal-wave front is determined in the form

$$a(t) = \frac{f(t)}{\sqrt{\sigma f_1}} - \sum_{k=0}^{\infty} Z_k(0)\frac{[f(t)]^{k+2}}{k!}.$$

The proved theorem is generalized for the multidimensional case.

ACKNOWLEDGMENTS

This work was supported by the Russian Foundation for Basic Research, project no. 02-01-01122.

REFERENCES

1. E. I. Zababakhin and I. E. Zababakhin, *Phenomena of Unlimited Cumulation* (Nauka, Moscow, 1988).
2. I. E. Zababakhin and V. A. Simonenko, Prikl. Mat. Mekh. **42** (3), 573 (1978).
3. O. A. Oleĭnik, A. S. Kalashnikov, and Yuĭ-Lin Chzhou, Izv. Akad. Nauk SSSR, Ser. Mat. **22**, 667 (1958).
4. A. F. Sidorov, *Selected Papers: Mathematics, Mechanics* (Fizmatlit, Moscow, 2001).
5. G. I. Barenblat, Prikl. Mat. Mekh. **16** (1), 67 (1952).
6. L. S. Leĭbenzon, *Collection of Scientific Papers*, Vol. 2: *Underground Hydrodynamics* (Akad. Nauk SSSR, Moscow, 1953).
7. G. I. Barenblat and Ya. B. Zel'dovich, Usp. Mat. Nauk **26** (2), 115 (1971).
8. A. F. Sidorov, Dokl. Akad. Nauk SSSR **280**, 47 (1985).
9. V. V. Vasin and A. F. Sidorov, Izv. Vyssh. Uchebn. Zaved., Mat., No. 7/254, 13 (1983).
10. S. P. Bautin, Chislennye Metody Mekh. Sploshnoĭ Sredy **16** (5), 16 (1985).

Translated by R. Tyapaev

Doklady Physics, Vol. 48, No. 7, 2003, pp. 376–378. Translated from Doklady Akademii Nauk, Vol. 391, No. 3, 2003, pp. 331–333.

MECHANICS

A Concentrated Force in an Elastic Porous Half-Space

E. V. Grachev*, N. M. Zhabborov, and Kh. Kh. Imomnazarov*****

Presented by Academician A.S. Alekseev January 14, 2003

Received January 28, 2003

The equations of motion for a porous liquid-saturated medium were derived in terms of displacements [1, 2] and displacement velocities [3, 4]. In the first case, the Frenkel'–Biot model [1, 2] is described by four elastic constants. Moreover, these equations do not go over to the equations of motion of the medium in the single-velocity model (e.g., if the elastic-skeleton displacements coincide with those of the liquid in pores, the equations of motion have to go over to the Euler equations in the absence of energy dissipation).

In [3, 4], a nonlinear mathematical model of motion of a liquid in an elastically deformed porous medium was constructed on the basis of the conservation laws and the Galilean principle of relativity. In this approach, the reversible reactions induced by interacting components are correctly taken into account. The resulting dynamic equations of motion of heterogeneous media are hyperbolic [5]. Moreover, the model proposed by Dorovsky involves three elastic constants in the case of isotropic elastic porous media [5, 6].

Mindlin and Chen' [7, 8] considered the problem of strains arising in an elastic half-space under the action of a concentrated force. Using the Galerkin vector, they obtained the formula for calculating the displacement vector and the stresses for various simple forces.

In this study, we consider a similar problem for an elastic porous half-space $x_3 > 0$; i.e., we calculate the displacement of an elastic porous solid, stresses, and pressure for simple forces. The $x_3 = 0$ surface is considered to be free of stresses and the pressure.

* *Institute of Inorganic Chemistry, Siberian Division, Russian Academy of Sciences, pr. Akademika Lavrent'eva 3, Novosibirsk, 630090 Russia*

** *Tashkent State University, Universitetskaya ul. 95, Vuzgorodok, Tashkent, 700095 Uzbekistan*

*** *Institute of Computational Mathematics and Mathematical Geophysics, Siberian Division, Russian Academy of Sciences, pr. Akademika Lavrent'eva 6, Novosibirsk, 630090 Russia*

e-mail: imom@omzg.sscc.ru

1. FORMULATION OF THE PROBLEM

We consider the static boundary value problem for determining the displacements and pressure for an elastic porous medium in the half-space $x_3 > 0$ [9]:

$$\mu\Delta\mathbf{U} + \left(\lambda + \mu + \alpha\rho_s^2 - 2K\frac{\rho_s}{\rho}\right)\nabla\mathrm{div}\mathbf{U} - \rho_l\left(\frac{K}{\rho} - \rho_s\alpha\right)\nabla\mathrm{div}\mathbf{V} + \rho_s\mathbf{f} = 0, \quad (1)$$

$$-\rho_l\left(\frac{K}{\rho} - \rho_s\alpha\right)\nabla\mathrm{div}\mathbf{U} + \rho_l^2\alpha\nabla\mathrm{div}\mathbf{V} + \rho_l\mathbf{f} = 0, \quad (2)$$

$$\sigma_{13}\big|_{x_3=0} = \sigma_{23}\big|_{x_3=0} = \sigma_{33}\big|_{x_3=0} = \frac{\rho_l}{\rho}p\big|_{x_3=0} = 0. \quad (3)$$

Here, $\mathbf{U}$ and $\mathbf{V}$ are the displacements of the elastic porous solid and a liquid with the partial densities ρ_s and ρ_l, respectively; $\mathbf{f}$ is the volume force; λ, μ, and $\alpha = \rho\alpha_3 + \frac{K}{\rho^2}$ are the constants entering into the equation of state [4, 5]; $\rho = \rho_s + \rho_l$; $K = \lambda + \frac{2\mu}{3}$;

$$\sigma_{ik} = \mu\left(\frac{\partial U_k}{\partial x_i} + \frac{\partial U_i}{\partial x_k}\right) + \left(\lambda - \frac{\rho_s}{\rho}K\right)\delta_{ik}\mathrm{div}\mathbf{U} - \frac{\rho_l}{\rho}K\delta_{ik}\mathrm{div}\mathbf{V} - p\delta_{ik}, \quad (4)$$

where δ_{ik} is the Kronecker delta; and

$$p = (K - \rho\rho_s\alpha)\mathrm{div}\mathbf{U} - \rho\rho_l\alpha\mathrm{div}\mathbf{V}. \quad (5)$$

2. REDUCTION OF PROBLEM (1)–(3) TO TWO INDEPENDENT PROBLEMS

Eliminating $\nabla\mathrm{div}\mathbf{V}$ from Eq. (1) and using Eq. (2), we obtain [8]

$$\mu\Delta\mathbf{U} + (\tilde{\lambda} + \mu)\nabla\mathrm{div}\mathbf{U} + (\alpha\rho_0)^{-1}K\mathbf{f} = 0, \quad (6)$$

where $\tilde{\lambda} = \lambda - (\rho^2\alpha)^{-1}K^2$.

1028-3358/03/4807-0376$24.00 © 2003 MAIK "Nauka/Interperiodica"

We eliminate $\operatorname{div}\mathbf{V}|_{x_3=0}$ from boundary conditions (3) and, using definitions (4) and (5) for the stress tensor and the threshold pressure, obtain

$$\mu\left(\frac{\partial U_1}{\partial x_3}+\frac{\partial U_3}{\partial x_1}\right)\Big|_{x_3=0}=0,\quad \mu\left(\frac{\partial U_2}{\partial x_3}+\frac{\partial U_3}{\partial x_2}\right)\Big|_{x_3=0}=0,$$
$$2\mu\frac{\partial U_3}{\partial x_3}+\tilde{\lambda}\operatorname{div}\mathbf{U}|_{x_3=0}=0. \quad (7)$$

Eliminating $\operatorname{div}\mathbf{V}$ from (4) and using (5), we arrive at the formula

$$\sigma_{ik}=\mu\left(\frac{\partial U_k}{\partial x_i}+\frac{\partial U_i}{\partial x_k}\right)+\tilde{\lambda}\delta_{ik}\operatorname{div}\mathbf{U}-\left(1-\frac{K}{\alpha\rho^2}\right)\delta_{ik}p \quad (8)$$

relating the stress tensor to the displacement vector for the elastic porous solid and pressure in pores. If the porosity disappears, formula (8) goes over to the relationships of Hooke's law [10] for a homogeneous elastic isotropic solid because $\rho^2\alpha_3 \longrightarrow \frac{K_s}{\rho_s^f}$ [5], where K_s and ρ_s^f are the bulk modulus and the density of the homogeneous elastic isotropic solid, respectively.

Now, we take the divergence of both sides of Eq. (2). With allowance for Eqs. (3) and (5), we arrive at the Dirichlet problem for the Poisson equation:

$$\Delta p=\rho\operatorname{div}\mathbf{f},\quad x_3>0, \quad (9)$$

$$p|_{x_3=0}=0. \quad (10)$$

Thus, for simple forces ($\mathbf{f}=\mathbf{F}\delta(\mathbf{x}-\mathbf{x}^0)$, where $\mathbf{F}$ is a constant vector and $\mathbf{x}^0$ is the coordinate of the source), initial boundary value problem (1)–(3) splits into two independent problems: the Mindlin–Chen' problem specified by Eqs. (6) and (7) and the Dirichlet problem specified by Eqs. (9) and (10) for the Poisson equation.

3. FORMULAS FOR SOLVING PROBLEM (1)–(3) FOR SIMPLE FORCES

Similar to [8], we find the displacement vector in terms of the Galerkin vector $\mathbf{G}$:

$$\mathbf{U}=\frac{1}{2\mu}[2(1-\tilde{\nu})\Delta\mathbf{G}-\nabla\operatorname{div}\mathbf{G}].$$

Substituting these expressions into Eq. (8), we obtain the stress tensor in the form

$$\sigma_{11}=2(1-\tilde{\nu})\frac{\partial}{\partial x_1}\Delta G_1+\left(\tilde{\nu}\Delta-\frac{\partial^2}{\partial x_1^2}\right)\operatorname{div}\mathbf{G}-\left(1-\frac{K}{\alpha\rho^2}\right)p,$$

$$\sigma_{22}=2(1-\tilde{\nu})\frac{\partial}{\partial x_2}\Delta G_2+\left(\tilde{\nu}\Delta-\frac{\partial^2}{\partial x_2^2}\right)\operatorname{div}\mathbf{G}-\left(1-\frac{K}{\alpha\rho^2}\right)p,$$

$$\sigma_{33}=2(1-\tilde{\nu})\frac{\partial}{\partial x_3}\Delta G_3+\left(\tilde{\nu}\Delta-\frac{\partial^2}{\partial x_3^2}\right)\operatorname{div}\mathbf{G}-\left(1-\frac{K}{\alpha\rho^2}\right)p,$$

$$\sigma_{12}=(1-\tilde{\nu})\Delta\left(\frac{\partial}{\partial x_2}G_1+\frac{\partial}{\partial x_1}G_2\right)-\frac{\partial^2}{\partial x_1\partial x_2}\operatorname{div}\mathbf{G},$$

$$\sigma_{13}=(1-\tilde{\nu})\Delta\left(\frac{\partial}{\partial x_1}G_3+\frac{\partial}{\partial x_3}G_1\right)-\frac{\partial^2}{\partial x_1\partial x_3}\operatorname{div}\mathbf{G},$$

$$\sigma_{23}=(1-\tilde{\nu})\Delta\left(\frac{\partial}{\partial x_3}G_2+\frac{\partial}{\partial x_2}G_3\right)-\frac{\partial^2}{\partial x_2\partial x_3}\operatorname{div}\mathbf{G},$$

$$\Delta^2\mathbf{G}=\frac{1}{\tilde{\nu}-1}(\alpha\rho)^{-1}K\mathbf{f}.$$

Here, $\tilde{\nu}=\dfrac{\tilde{\lambda}}{2(\tilde{\lambda}+\mu)}$ is the Poisson-type ratio.

Solving Dirichlet problem (9), (10) for simple forces, we determine the pressure in pores in the form

$$p=\rho\left[\frac{(\mathbf{F},\mathbf{x}-\mathbf{x}^0)}{|\mathbf{x}-\mathbf{x}^0|^3}-\frac{(\mathbf{F},\mathbf{x}_--\mathbf{x}^0)}{|\mathbf{x}-\mathbf{x}_-^0|^3}\right], \quad (11)$$

where $\mathbf{x}_-=(x_1, x_2, -x_3)$.

Thus, the problem of displacements in an elastic porous liquid-saturated half-space under the action of concentrated forces can be solved by using the formulas from [8] after replacing Poisson's ratio ν with $\tilde{\nu}$. The components of the shear-stress tensor can be calculated as in [8] by replacing Poisson's ratio ν with $\tilde{\nu}$. The components of the normal-stress tensor can also be

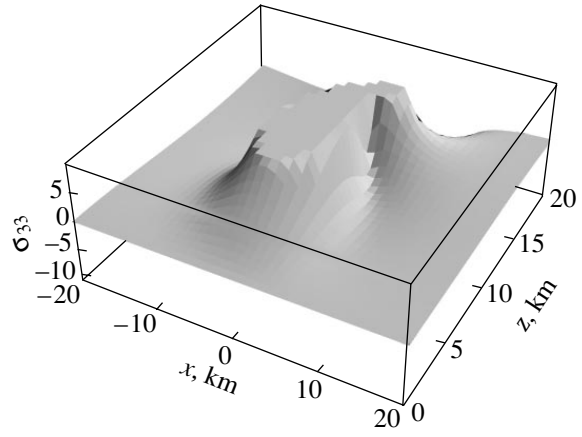

Fig. 1.

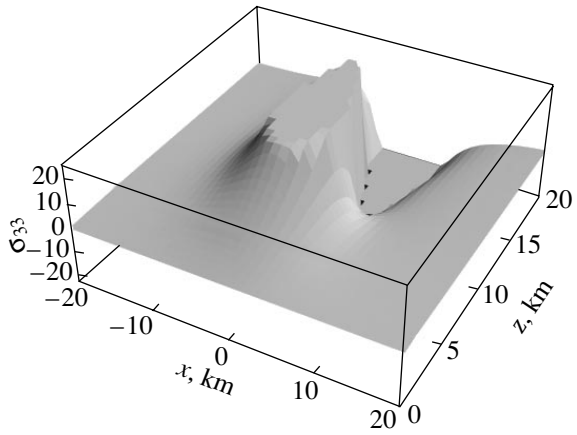

Fig. 2.

obtained by the formulas from [8] by replacing Poisson's ratio ν with $\tilde{\nu}$ and adding Eq. (11).

Figures 1 and 2 show the vertical component of the stress tensor as a function of coordinates (*x*, *z*) for porosities $d_0 = 0.01$ and 10%, respectively. In this case, the elastic coefficients λ, μ, and α were calculated by formulas taken from [6] for the velocities v_{p_1} = 6000 m/s, $v_s = \frac{v_{p_1}}{\sqrt{3}}$, and v_{p_2} = 600 m/s and partial densities $\rho_s = \rho_s^f (1 - d_0)$, $\rho_l = \rho_l^f d_0$, ρ_l^f = 2900 kg/m^3, and ρ_l^f = 900 kg/m^3. The force was specified as $\mathbf{F} = F(\cos\phi, \sin\phi)$, $F = 5 \times 10^6$ N, $\phi = 30°$ and its source was located at a depth of 15 km.

ACKNOWLEDGMENTS

This work was supported by the Russian Foundation for Basic Research, project no. 02-05-64939.

REFERENCES

1. Ya. I. Frenkel', Izv. Akad. Nauk SSSR, Ser. Geogr. Geofiz. **8** (4), 133 (1944).
2. M. A. Biot, J. Acoust. Soc. Am. **28** (2), 168 (1956).
3. V. N. Dorovsky, Geol. Geofiz., No. 7, 39 (1989).
4. V. N. Dorovsky, Yu. V. Perepechko, and E. I. Romenskiĭ, Fiz. Goreniya Vzryva, No. 1, 100 (1993).
5. A. M. Blokhin and V. N. Dorovsky, *Mathematical Modelling in the Theory of Multivelocity Continuum* (Nova Sci., New York, 1995).
6. Kh. Kh. Imomnazarov, Dokl. Akad. Nauk **373**, 536 (2000).
7. R. D. Mindlin, Physics (N.Y.) **7**, 195 (1936).
8. R. Mindlin and D. Chen', Mekhanika, No. 4/14, 118 (1952).
9. Kh. Kh. Imomnazarov, Bull. Novosibirsk Comput. Center, Ser. Mat. Model. Geofiz. **4**, 75 (1998).
10. L. D. Landau and E. M. Lifshitz, *Course of Theoretical Physics*, Vol. 7: *Theory of Elasticity* (Nauka, Moscow, 1982; Pergamon, New York, 1986).

Translated by V. Bukhanov

Doklady Physics, Vol. 48, No. 7, 2003, pp. 379–381. Translated from Doklady Akademii Nauk, Vol. 391, No. 3, 2003, pp. 334–336.

MECHANICS

Estimate of the Life of a Material under Creep Conditions in the Phase-Transition Theory

N. A. Zharkova and L. R. Botvina*

Presented by Academician O.A. Bannykh March 4, 2003

Received March 5, 2003

The prediction of the strength of materials under long-term loading is among the important current problems of the mechanics of deformable solids.

During long-term creep tests, prevailing fracture mechanisms change with stress σ and loading time t, fracture under high stresses ($\sigma > \sigma_{cr1}$) is intragranular, fracture for medium stresses ($\sigma_{cr1} > \sigma > \sigma_{cr2}$) is intergranular and occurs due to the development of wedge cracks, and fracture for low stresses ($\sigma < \sigma_{cr2}$) is intergranular and occurs due to the formation and development of pores along grain boundaries (Fig. 1). The change of the fracture mechanisms is responsible for the appearance of kinks in the long-term strength curve for stresses σ_{cr1} and σ_{cr2}. Known temperature–time parametric methods of the life prediction (Larson–Miller, Dorn, Marrey, Manson–Succop, Manson–Haferd, etc.) are based on relations with fixed determining constants in wide ranges of temperature and fracture duration, which ignore the change of fracture mechanisms. Therefore, these methods are not necessarily reliable.

In this work, we propose a new method for estimating the material life under creep conditions. This method is based on the theory of phase transitions and on similarity in fracture mechanisms.

It was shown in [1] that fracture processes could be considered in the theory of phase transitions by analogy with the liquid–vapor phase transition. For this consideration, it is necessary to find the order parameter for such a transition and to find its dependence on the determining factor. For creep fracture, the following power dependence of the reduced order parameter on the reduced stress was determined in [1]:

$$\frac{t_{II} - t_{cr}}{t_{cr}} = C\left[\frac{\sigma - \sigma_{cr}}{\sigma_{cr}}\right]^n. \quad (1)$$

Here, the duration t_{II} of the steady-state creep stage is taken as the order parameter and t_{cr} is its critical value for the critical stress σ_{cr} corresponding to the disappearance of the steady-state stages in the primary creep curves. Taking into account the similarity of creep curves, one can assume that the similar power dependence

$$\frac{t - t_{cr}}{t_{cr}} = A\left[\frac{\sigma_{cr} - \sigma}{\sigma_{cr}}\right]^m \quad (2)$$

is valid for the total time t until fracture. The critical order parameter t_{cr} in Eq. (2) corresponds to the critical stress σ_{cr} for which the prevailing mechanism of fracture considered as a critical event changes. We have $\sigma_{cr} = \sigma_{cr1}$ and $t_{cr} = t_{cr1}$ for material fracture caused by the formation of wedge cracks and $\sigma_{cr} = \sigma_{cr2}$ and $t_{cr} = t_{cr2}$ for material fracture caused by the formation of pores (Fig. 1). The exponent m and coefficient A in relation (2)

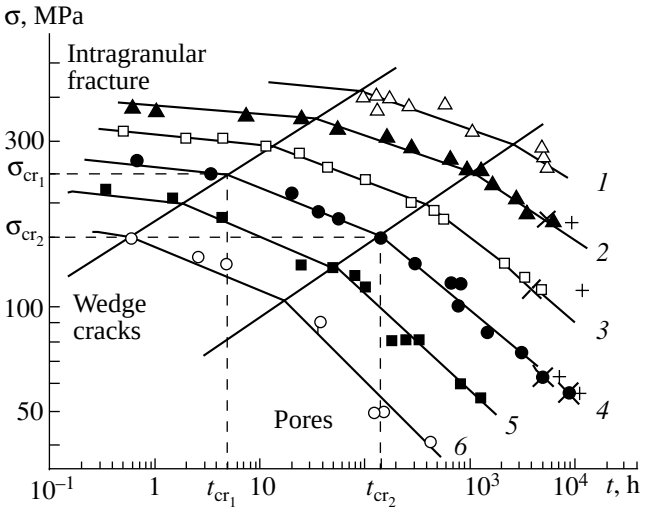

Fig. 1. Long-term strength curves for 1613 steel for temperatures (*1*) 550, (*2*) 600, (*3*) 650, (*4*) 700, (*5*) 750, and (*6*) 800°C with the lines separating the regions with different fracture mechanisms [6]. Points calculated on 10^3-h base by the (+) Larsen–Miller method for C = 12 and (×) proposed method.

Baĭkov Institute of Metallurgy, Russian Academy of Sciences, Leninskiĭ pr. 49, Moscow, 117334 Russia

** e-mail: botvina@ultra.imet.ac.ru*

1028-3358/03/4807-0379$24.00

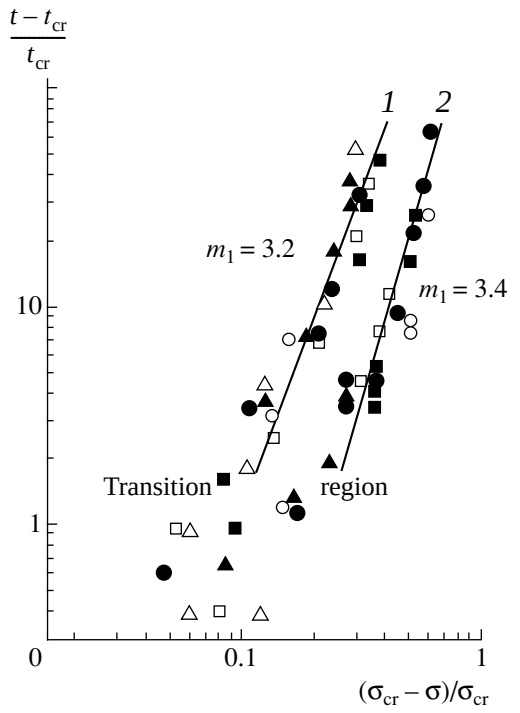

Fig. 2. Reduced order parameter vs. the reduced stress for fracture caused by (*1*) wedge cracks and (*2*) pores for 1613 steel and $T = 550$–800°C.

depend on the material and separated stress range, where a definite fracture mechanism is realized.

Figure 2 shows the reduced order parameter $\frac{t-t_{cr}}{t_{cr}}$ as a function of the reduced stress $\frac{\sigma-\sigma_{cr}}{\sigma_{cr}}$ for CrNiNb 1613 steel and $T = 550$–800°C. Lines *1* and *2* correspond to fracture caused by the growth of wedge cracks and development of pores, respectively. The input data are shown in Fig. 1. As is seen in Fig. 2, $\frac{t-t_{cr}}{t_{cr}}$ as a function of $\frac{\sigma-\sigma_{cr}}{\sigma_{cr}}$ for each fracture type is approximated by one straight line with the angular coefficient m and free term $\log A$ in the logarithmic coordinates over the entire temperature range:

$$\log\frac{t-t_{cr}}{t_{cr}} = m\log\frac{\sigma_{cr}-\sigma}{\sigma_{cr}} + \log A. \qquad (3)$$

According to the proposed method, the coefficients m and $\log A$ are determined from the plot of $\log\frac{t-t_{cr}}{t_{cr}}$ vs. $\log\frac{\sigma_{cr}-\sigma}{\sigma_{cr}}$ for one temperature taken in the similarity interval of fracture mechanisms, e.g., for the highest temperature, which requires the minimum test time. To estimate the life for any temperature from this interval, it is sufficient to substitute the critical stress σ_{cr} and time t_{cr} for this temperature, as well as the stress σ for which the time to fracture is determined, into Eq. (3).

As is seen in Fig. 2, points in the initial part of plots are spread due to the existence of transition regions from one fracture mechanism to another.

The analysis of such plots constructed by using measured long-term strengths for various materials and test temperature ranges (1613 steel, $T = 550$–800°C; S816 steel, $T = 648$–815°C; *E*I617 steel, $T = 750$–880°C; *E*I826 steel, $T = 750$–800°C; *E*P44 steel, $T = 585$–595°C; *E*P17 steel, $T = 700$–750°C; 2.25Cr–1Mo alloy, $T = 600$–650°C) shows that $m = 4$–6 for intragranular fracture, $m = 2$–4 for fracture due to wedge cracks, and $m = 3$–5 for fracture due to the development of pores.

The analysis of experimental data that was made in [2–6] showed that temperature ranges of the similarity of mechanisms of deformation and fracture under creep conditions can be quite wide particularly for materials with a high melting point.

The processing of experimental data shows that logarithms of the critical stresses and logarithms of the critical times depend linearly on temperature in such temperature ranges. This circumstance makes it possible to determine the critical values (t_{cr} and σ_{cr}) for intermediate temperatures. Therefore, the characteristics of long-term strength can be interpolated inside the indicated temperature range.

By analogy with seismic prediction, three types of predictions can be separated. These are (i) short-term predictions in the $\sigma_{cr1} > \sigma > \sigma_{cr2}$ range, (ii) medium-term predictions for $\sigma < \sigma_{cr2}$, and (iii) long-term predictions for $\sigma \ll \sigma_{cr2}$ for lives significantly exceeding the time t_{cr2} corresponding to the second kink in the long-term strength curve. For short-term and medium-term predictions, the critical stress and time are the coordinates of, respectively, the first (σ_{cr1} and t_{cr1}) and second (σ_{cr2} and t_{cr2}) kinks of the long-term strength curve (Fig. 1). For $\sigma \ll \sigma_{cr2}$, one more kink can appear in the long-term strength curve. The coordinates of this kink (σ_{cr3} and t_{cr3}) are the critical stress and time for long-term predictions. For this reason, long-term predictions require the analysis of the structure state of the material with both the inclusion of its phase diagram for a given temperature and the estimation of the diffusion rate of basic and impurity elements. If this analysis shows that the material does not substantially change its structure for indicated temperature and test duration, the life prediction can be made with the critical stress σ_{cr2}. If such changes occur, a new threshold stress σ_{cr3} appropriate for long-term prediction must be estimated.

The accuracy of the linear extrapolation of the lifetime by the proposed method based on the theory of phase transitions is compared with the accuracy of the

Table 1. Measured and calculated (on the base up to 10^3 h) lives for 1613 steel

T, °C	σ, MPa	t_{exp}, h	Proposed method, h	δ, %	Larson–Miller method for $C = 12$, h	δ, %
700	56	8912	8820	–1%	10575	+19%
700	63	5011	5100	+2%	6738	+34%
650	112	4823	3855	–20%	11400	+136%
600	178	6072	5470	–10%	9260	+52%

Larson–Miller method, because it is extensively used to estimate lifetimes. In addition, as was shown in [7], known parametric Larson–Miller, Dorn, Marrey, Trunin, Manson–Succop, and Manson–Haferd approximations being extrapolated to a service life of 2×10^5 h provide almost identical results differing by no more than 3%.

The error of the proposed method is determined by the standard deviation in linearizing the plot of $\log\frac{t - t_{cr}}{t_{cr}}$ vs. $\log\frac{\sigma_{cr} - \sigma}{\sigma_{cr}}$ and by the spread in the input data. For all materials being investigated, the calculated values deviate from experimental data by no more than 20%. At the same time, the Larson–Miller extrapolation gives 20–140% deviation. Table 1 presents the measured and calculated results for the life of 1613 steel. Calculated points are also shown in Fig. 1.

Thus, the proposed method was shown to estimate the time to creep fracture with accuracy higher than the known temperature–time parametric methods. Moreover, the results corroborate that practical problems of estimates of the service life of materials can be solved by generally analyzing kinetic processes in the theory of critical phenomena.

ACKNOWLEDGMENTS

This work was supported in part by the Russian Foundation for Basic Research (project no. 02-05-6531) and INTAS (grant no. 01-0748).

REFERENCES

1. L. R. Botvina, Metalloved. Term. Obrab. Met., No. 8, 2 (1994).
2. I. I. Trunin, Probl. Prochn., No. 9, 9 (1976).
3. E. I. Uryupina, *Instability of Structure and Properties of Boiler-and-Turbine Steels* (Mashinostroenie, Moscow, 1969).
4. K. A. Lanskaya, *Heatproof Steels* (Metallurgiya, Moscow, 1969).
5. V. V. Krivenyuk, *Forecasting of Lasting Strength of High-Melting Metals and Alloys* (Naukova Dumka, Kiev, 1990).
6. V. I. Kovpak, *Forecasting of High-Temperature-Strength of Metallic Materials* (Naukova Dumka, Kiev, 1981).
7. A. É. Ugorskiĭ, Probl. Prochn., No. 1, 40 (1986).

Translated by R. Tyapaev

Doklady Physics, Vol. 48, No. 7, 2003, pp. 382–384. Translated from Doklady Akademii Nauk, Vol. 391, No. 3, 2003, pp. 337–339.

MECHANICS

On the Compression of a Perfectly Plastic Pyramid by a Flat Die

D. D. Ivlev*, A. Yu. Ishlinskiĭ, and R. I. Nepershin*****

Received February 10, 2003

The problem of the compression of a perfectly plastic regular square (or triangular) pyramid by a flat rigid die is solved. A self-similar solution is given by using the full plasticity condition for the Tresca yield criterion (Haar–Karman hypothesis). The full plasticity condition corresponds to the shear mechanism of three-dimensional plastic strain and leads to statically determinate hyperbolic equations [1–3]. A self-similar solution of the inverse problem of the indentation of the regular square (or triangular) pyramid into an ideal-plastic half-space under the full plasticity condition was given in [4]. The geometrically similar problem of the plastic-wedge compression under plane strain was given in [5].

The compression of the perfectly plastic regular square (or triangular) pyramid by a flat die, which moves along the pyramid axis normal to the die, is considered in the Cartesian coordinate system $\{x, y, z\}$. The z axis coincides with both the pyramid axis and the normal to the die plane. The x axis coincides with the normal to the middle point of a side of a square or regular triangle that is the section of the pyramid by the die plane $z = 0$ (Fig. 1).

The plastic-flow region in the regular pyramid compressed by the flat die has planes of symmetry that are orthogonal to the die boundary and pass through the pyramid edges and middles of the faces. The plastic region bounded by the two planes of symmetry and the die boundary is considered. Cartesian coordinates, stresses, and displacement velocities are made dimensionless by dividing them by the die displacement h, the yield stress σ_Y of the plastic material under uniaxial compression, and the die displacement velocity V, respectively. The side length of the regular triangle or square on the pyramid section by the die boundary $z = 0$ is given by

$$L = 2c\cot\alpha, \tag{1}$$

where α is the angle between the pyramid face and the $-z$ axis and $c = \sqrt{3}$ and 1 for the triangular and square pyramids, respectively.

The velocity vector of the plastic flow is assumed to lie on the planes y = const orthogonal to both the pyramid face and the die boundary. This condition is exactly valid on the plane $y = 0$ because of the plastic-flow symmetry. On planes $0 < y < \frac{L}{2}$, this condition leads to the geometric similarity of the plastic flow in all planes y = const. On the plane $y = \frac{L}{2}$, the plastic region shrinks to the point of the intersection of a pyramid edge with the die boundary $z = 0$. The same mode of the plane plastic

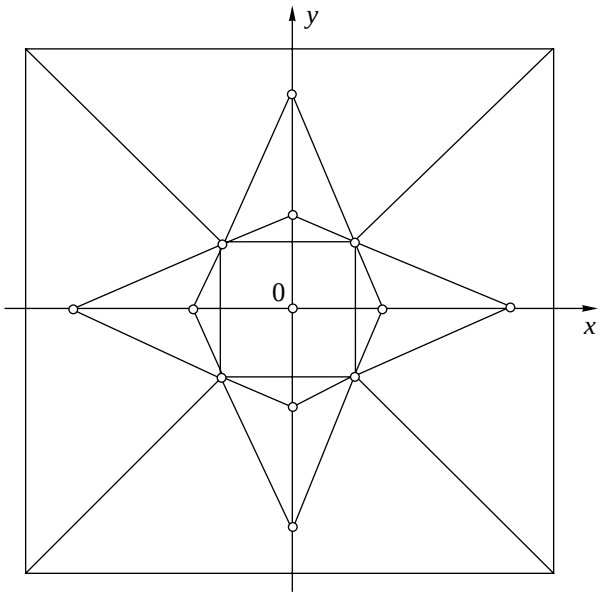

Fig. 1. Contact boundary of the perfectly plastic pyramid with the flat rough die and projection of the plastic boundary on the plane $z = 0$ for $\alpha = \frac{\pi}{4}$.

* *Chuvash State Pedagogical University, ul. Karla Marksa 38, Cheboksary, 428000 Russia*

** *Institute for Problems in Mechanics, Russian Academy of Sciences, pr. Vernadskogo 101, Moscow, 117526 Russia*

*** *Moscow State Academy of Instrument Engineering and Informatics, ul. Stromynka 20, Moscow, 107846 Russia*

e-mail: nepershin_r@pop.mtu.ru

1028-3358/03/4807-0382$24.00

flow on the planes y = const in the inverse self-similar problem of the indentation of the rigid pyramid [4] was corroborated by experiments [6].

The full plasticity condition for the problem under consideration provides the following relations for the principal stresses:

$$\sigma_1 = \sigma_2, \quad \sigma_3 = \sigma_1 - 1, \quad \sigma = \sigma_1 - \frac{1}{3}, \tag{2}$$

where σ is the mean stress.

The stress-tensor components on the planes y = const under condition (2) are given by the relations

$$\sigma_x = \sigma + \frac{1}{3} - \cos^2\theta, \quad \sigma_y = \sigma + \frac{1}{3}, \tag{3}$$

$$\sigma_z = \sigma + \frac{1}{3} - \sin^2\theta,$$

$$\tau_{xz} = -\sin\theta\cos\theta, \tag{4}$$

where θ is the angle between the σ_3-stress direction and the x axis and the stress σ_y coincides with the principal stress σ_2.

The sliplines ξ and η on the plane y = const are defined by the differential equations

$$\frac{dz}{dx} = \tan\varphi \text{ for } \xi, \quad \frac{dz}{dx} = -\cot\varphi \text{ for } \eta \tag{5}$$

with differential relations for the stresses and the displacement velocities. These relations coincide with the Hencky and Geiringer equations [7]

$$d\sigma - d\varphi = 0 \text{ along } \xi, \; d\sigma + d\varphi = 0 \text{ along } \eta, \tag{6}$$

$$dV_\xi - V_\eta d\varphi = 0 \text{ along } \xi,$$
$$dV_\eta + V_\xi d\varphi = 0 \text{ along } \eta, \tag{7}$$

where $\varphi = \theta + \frac{\pi}{4}$ is the angle between the ξ-slipline direction and the x axis and V_ξ and V_η are the projections of the velocity on the sliplines.

Two possible modes of the plastic flow are determined by the die surface conditions. For the rough-die surface (Fig. 2), the rigid region OAD moves with the die along the $-z$ axis. The velocity discontinuity $[V] = \frac{1}{\sqrt{2}}$ along the rigid-plastic boundaries AD and DB arises at the point D. The velocity vector of the region ABC is determined by the relations

$$V_x = \frac{1}{2}(\sin\psi + \cos\psi), \quad V_z = \frac{1}{2}(\sin\psi - \cos\psi), \tag{8}$$

where ψ is the angle of the centered fan of the slipline field.

For a smooth die surface (Fig. 3), the region OAD slides along the die contact boundary. The velocity discontinuity $[V] = \sqrt{2}$ along the rigid-plastic boundary OB arises at the point O. The velocity vector of the region ABC is determined by the relations

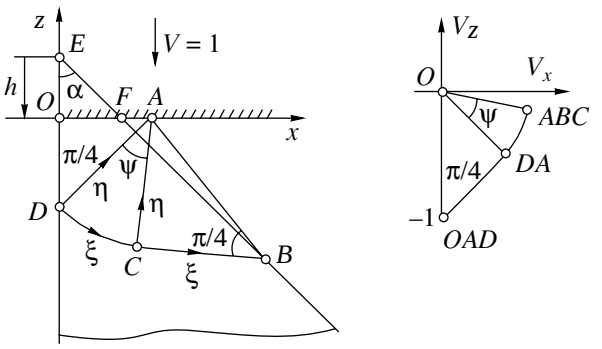

Fig. 2. Slipline field and velocity hodograph on the plane y = const for the rough die.

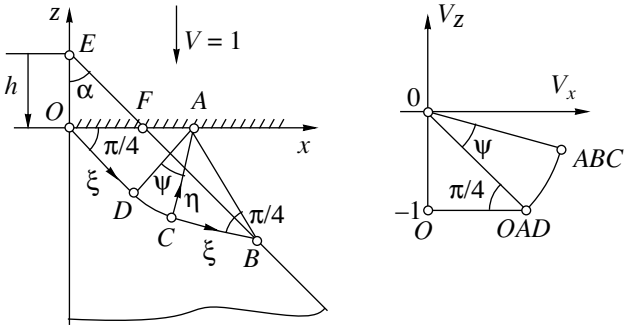

Fig. 3. Same as in Fig. 2, but for the smooth die.

$$V_x = \sin\psi + \cos\psi, \quad V_z = \sin\psi - \cos\psi. \tag{9}$$

The full plasticity condition determines the uniaxial compressive state in the plastic region ABC along the boundary AB

$$\sigma_1 = \sigma_2 = 0, \quad \sigma_3 = -1, \quad \sigma = -\frac{1}{3} \text{ on } AB. \tag{10}$$

The angle ψ and length l of the contact boundary are found from the incompressibility condition for the plane plastic flow on planes y = const as follows. Coordinates of the point B are determined by the relations

$$x_B = l(1 + 2\sin\psi), \quad z_B = -2l\cos\psi \tag{11}$$

for the rough die and by the relations

$$x_B = l(1 + \sin\psi), \quad z_B = -l\cos\psi \tag{12}$$

for the smooth die. The intersection line of the pyramid face with the plane y = const passing through the

point B is determined by the equation

$$x - x_B = \tan\alpha(z_B - z).$$

From this equation, the coordinate x_F of the point F and the coordinate z_E of the point E, which is the height h of the pyramid edge on the plane y = const over the die plane $z = 0$, are found in the form

$$x_F = x_B + z_B\tan\alpha, \quad h = z_B + x_B\cot\alpha, \tag{13}$$

$$h = 1 - \frac{y}{c}\cot\alpha, \quad 0 \le y \le \frac{L}{2}, \tag{14}$$

where L and c are defined by Eq. (1). The incompressibility condition leads to the equality of the areas of the triangles OEF and ABF, and, using Eqs. (11)–(13), we find the relations

$$\tan\alpha = \frac{(1 + 2\sin\psi)^2}{4\cos\psi(1 + \sin\psi)} \tag{15}$$

for the rough die and the relations

$$\tan\alpha = \frac{(1 + \sin\psi)^2}{\cos\psi(2 + \sin\psi)} \tag{16}$$

for the smooth die.

The mean stress σ in the region OAD is found from the boundary condition (10) and relation (6) along the ξ slipline. The die pressure is found from the third of relations (3) for $\theta = -\frac{\pi}{2}$

$$p = 1 + \psi. \tag{17}$$

If $\psi = 0$, the entire plastic region degenerates into the uniaxial-compression state $p = 1$ with the vertical stress-free boundary AB. This condition, along with relations (15) and (16), determines the minimum slope α_{min} of the pyramid face when the plastic region retains geometric similarity. This minimum slope is

$$\alpha_{min} = 0.245 \text{ for the rough die,}$$

$$\alpha_{min} = 0.464 \text{ for the smooth die.}$$

For the compression of the pyramid with a given angle α, it is found that the angle ψ and pressure for the rough die are somewhat larger than the respective values for the smooth die. For $\alpha \longrightarrow \frac{\pi}{2}$, we obtain $p = 1 + \frac{\pi}{2}$ for both the dies. It is the case of the pressure of the flat triangle or square die on the perfectly plastic half-space [7].

The limiting load capacity of the pyramid below the rigid–plastic boundary can be tested by continuing the static slipline field into the rigid region similarly to the problem of the pressure of a flat die on the half-space [8].

Using Eqs. (11)–(14) and the relation $x_F = h\tan\alpha$, we determine the contact boundary length

$$l = \left(\tan\alpha - \frac{y}{c}\right)[1 + 2(\sin\psi - \cos\psi\tan\alpha)]^{-1}, \tag{18}$$

$$l = \left(\tan\alpha - \frac{y}{c}\right)[1 + \sin\psi - \cos\psi\tan\alpha]^{-1}, \quad 0 \le y \le c\tan\alpha \tag{19}$$

for the rough and smooth dies, respectively.

The load Q applied to the die is determined by the relations

$$Q = 4pl_0\tan\alpha \text{ and } Q = 3\sqrt{3}pl_0\tan\alpha \tag{20}$$

for the square and triangle pyramids, respectively, where l_0 is the contact length on the plane $y = 0$.

The contact boundary for the square pyramid compressed by the rough die and the projection of the stress-free boundary of the plastic region on the plane $z = 0$ with $\alpha = \frac{\pi}{4}$ are shown in Fig. 1. For this example, $\psi = 0.673$, $p = 1.673$, $l_0 = 1.466$, and $Q = 9.52$ were found from Eqs. (15), (17), (18), and (20). Similar calculations for the square pyramid with $\alpha = \frac{\pi}{4}$ compressed by the smooth die provide the values $\psi = 0.486$, $p = 1.486$, $l_0 = 1.716$, and $Q = 10.2$. The pressure on the smooth die is lower than the pressure on the rough die, but the contact area for the smooth die is larger, and the pyramid is compressed by the rough die with lower load than by the smooth die for the same die displacement h.

REFERENCES

1. A. Yu. Ishlinskiĭ, Izv. Akad. Nauk SSSR, Otd. Tekh. Nauk, No. 3, 250 (1945).
2. A. Yu. Ishlinskiĭ, *Applied Problems of Mechanics* (Nauka, Moscow, 1986), Vol. 1, pp. 62–83.
3. A. Yu. Ishlinskiĭ and D. D. Ivlev, *Mathematical Theory of Plasticity* (Fizmatlit, Moscow, 2001).
4. D. D. Ivlev, A. Yu. Ishlinskiĭ, and R. I. Nepershin, Dokl. Akad. Nauk **385**, 766 (2002) [Dokl. Phys. **47**, 630 (2002)].
5. V. V. Sokolovskiĭ, *Theory of Plasticity* (Vysshaya Shkola, Moscow, 1969), pp. 300–302.
6. D. S. Dugdale, J. Mech. Phys. Solids **3**, 197 (1955).
7. D. D. Ivlev, A. Yu. Ishlinskiĭ, and R. I. Nepershin, Dokl. Akad. Nauk **381**, 616 (2001) [Dokl. Phys. **46**, 890 (2001)].
8. B. A. Druyanov and R. I. Nepershin, *Theory of Technological Plasticity* (Mashinostroenie, Moscow, 1990).

Translated by R. Nepershin

Doklady Physics, Vol. 48, No. 7, 2003, pp. 385–387. Translated from Doklady Akademii Nauk, Vol. 391, No. 3, 2003, pp. 340–342.

MECHANICS

First Integrals in the Problem of Rolling a Body of Revolution over a Rough Plane

A. S. Kuleshov

Presented by Academician V.V. Rumyantsev March 19, 2003

Received March 21, 2003

We consider the problem of the motion of a heavy rigid dynamically symmetric body bounded by a surface of revolution over a fixed horizontal plane without sliding. The equations of motion are known [1, 2] to have, in addition to the energy integral, two first integrals linear in quasivelocity. However, the explicit form of these integrals has been determined only for several particular cases (for a moving ball or disk). In this study, the explicit form of these integrals is obtained under a certain condition for the surface of the moving body and its mass distribution. It is also shown that a denumerable set of surfaces of moving bodies satisfy this condition.

1. FORMULATION OF THE PROBLEM AND EQUATIONS OF MOTION

Let a body, which has mass m and is symmetric in shape and in mass distribution with respect to the $G\zeta$ axis passing through its center of gravity G, rest on the fixed horizontal plane Oxy at the point M. We introduce the following notation: θ is the angle between the axis of symmetry and a vertical line, β is the angle between the meridian $M\zeta$ of the body and a certain meridian plane, and α is the angle between the horizontal tangent MQ to the meridian $M\zeta$ and the Ox axis. The position of the body is entirely specified by the angles α, β, θ and the coordinates x and y of the point M.

In addition, we introduce the system of coordinates $G\xi\eta\zeta$ moving both in space and in body so that the $G\xi$ axis always lies in the vertical–meridional plane, while $G\eta$ is perpendicular to this plane (figure). Let the velocity $\mathbf{v}$ of the center of mass G, the angular velocity $\boldsymbol{\omega}$ of the body, the angular velocity $\boldsymbol{\Omega}$ of the trihedron $G\xi\eta\zeta$, and the reaction vector $\mathbf{R}$ be given in the coordinate system $G\xi\eta\zeta$ by the components v_ξ, v_η, v_ζ; p, q, r; Ω_ξ, Ω_η, Ω_ζ; and R_ξ, R_η, R_ζ, respectively. The moment of inertia of the body with respect to the $G\xi$ and $G\eta$ axes is denoted by A_1, and its moment of inertia with respect to the axis of symmetry is denoted by A_3.

The distance GQ between the center of gravity and the plane Oxy is a function of the angle θ; i.e., $GQ = f(\theta)$ [1, 2]. The coordinates ξ, η, and ζ of the point of contact M between the body and the plane in the system of coordinates $G\xi\eta\zeta$ also depend only on the angle θ, $\eta = 0$, and

$$\begin{aligned} \xi &= -f(\theta)\sin\theta - f'(\theta)\cos\theta, \\ \zeta &= -f(\theta)\cos\theta + f'(\theta)\sin\theta. \end{aligned} \tag{1.1}$$

Since the $G\zeta$ axis is fixed in the body, $\Omega_\xi = p$ and $\Omega_\eta = q$. The $G\xi\zeta$ plane is always vertical; therefore, $\Omega_\zeta - \Omega_\xi \cot\theta = 0$. The point of contact has zero velocity; therefore,

$$v_\xi + q\zeta = 0, \quad v_\eta + r\xi - p\zeta = 0, \quad v_\zeta - q\xi = 0.$$

After simple transformations, the laws of variation in the momentum component along the $G\eta$ axis and in

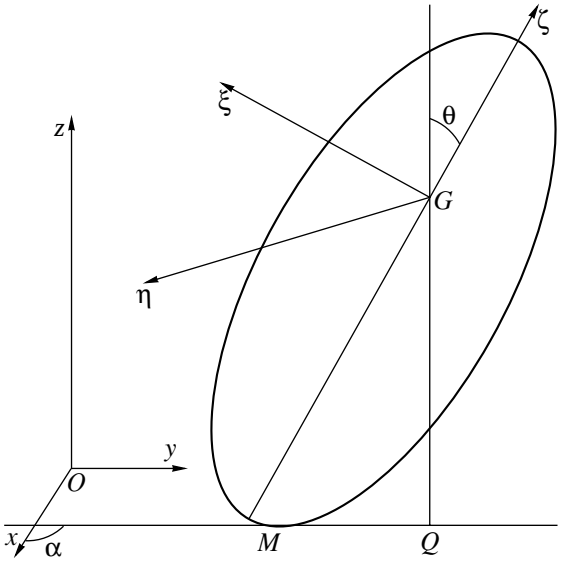

Figure.

Moscow State University,
Vorob'evy gory, Moscow, 119992 Russia
e-mail: kuleshov@mech.math.msu.su

1028-3358/03/4807-0385$24.00

the angular momentum around the $G\xi$ and $G\zeta$ axes take the form

$$\frac{d(p\zeta - r\xi)}{dt} - pq(\zeta\cot\theta + \xi) = \frac{R_\eta}{m},$$

$$A_1\frac{dp}{dt} + (A_3 r - A_1 p\cot\theta)q = -\zeta R_\eta, \qquad (1.2)$$

$$A_3\frac{dr}{dt} = \xi R_\eta.$$

Omitting the particular case of θ = const, taking into account that $q = -\frac{d\theta}{dt}$, and eliminating R_η from Eqs. (1.2), we obtain

$$A_1\frac{dp}{d\theta} + A_3\frac{\zeta}{\xi}\frac{dr}{d\theta} = -A_1 p\cot\theta + A_3 r,$$
$$\zeta\frac{dp}{d\theta} - \frac{(A_3 + m\xi^2)}{m\xi}\frac{dr}{d\theta} = -(\zeta\cot\theta + \xi + \zeta')p + \xi' r. \qquad (1.3)$$

Thus, two first integrals linear in p and r are determined from the set of Eqs. (1.3). Nowadays, the explicit form of these integrals is known only for an inhomogeneous dynamically symmetric moving ball. In the case of the motion of a round disk over a plane, the solution of the set of Eqs. (1.3) gives the expressions for p and r in terms of hypergeometric functions. Below, the explicit form of the first integrals linear in p and r will be determined for a body, whose shape differs from ball or disk.

2. DERIVATION OF THE FIRST INTEGRALS AND DETERMINATION OF THE BODY SHAPE

Following [1], we assume that the meridian-section shape of the moving body is such that the body can move with a constant angular velocity about the axis of symmetry:

$$r = r_0 = \text{const}.$$

To satisfy this relationship, the coordinates ξ and ζ of the point of contact have to meet the condition

$$(A_3\zeta - A_1\xi')\sin\theta = (A_3\cos\theta + n)(\xi + \zeta'), \qquad (2.1)$$

where n is an arbitrary constant.

Theorem 1. *The set of Eqs.* (1.3) *under condition* (2.1) *has the first integrals*

$$[A_1 p\sin\theta + A_3(\cos\theta + n)r]$$
$$\times\sqrt{A_1A_3 + A_1 m\zeta^2 + A_3 m\zeta^2} = c_1, \qquad (2.2)$$

$$r - mc_1\int\frac{\xi(\xi + \zeta')d\theta}{\sin\theta(A_1A_3 + A_1 m\xi^2 + A_3 m\zeta^2)^{\frac{3}{2}}} = c_2. \qquad (2.3)$$

We now determine the shape of the meridian section of the moving-body surface for which condition (2.1) is satisfied. We consider the case of $n = 0$. Substituting expressions (1.1) for ξ, ζ, and their derivatives into condition (2.1) and introducing the dimensionless parameter $k = \frac{A_3}{A_1}$, we obtain the differential equation for the function $f(\theta)$:

$$(k-1)f''\sin\theta\cos\theta - kf' + (k-1)f\sin\theta\cos\theta = 0. \qquad (2.4)$$

To solve Eq. (2.4), it is sufficient to find its arbitrary nontrivial solution. If $f_0 = f_0(\theta)$ is such a solution, the general solution of Eq. (2.4) is determined by the formula [3]

$$f(\theta) = f_0(\theta)\left(\lambda_1 + \lambda_2\int\frac{(\tan\theta)^{\frac{k}{k-1}}}{f_0^2(\theta)}\right), \qquad (2.5)$$

where λ_1 and λ_2 are arbitrary constants.

Theorem 2. *Equation* (2.4) *has the nontrivial particular solution*

$$f_0(\theta) = \frac{F\left(\frac{1}{2}, \frac{(k-2)}{2(k-1)}, 2; \frac{1}{\cos^2\theta}\right)}{\cos\theta}. \qquad (2.6)$$

The numerator of expression (2.6) involves the Gaussian hypergeometric function F, which is an infinite series depending on three parameters and variable $w = \frac{1}{\cos^2\theta}$. This series generally diverges, and expression (2.6) therefore has meaning only if the function F represents a finite sum rather than an infinite series.

Theorem 3. *The series in the numerator of expression* (2.6) *is a finite sum if either of the conditions*

$$k = \frac{2(N+1)}{2N+1} \text{ or } k = \frac{2(N+1)}{2N+3},$$

where N is the positive integer or zero, is satisfied.

Thus, it is possible to find at least two parameters k for each nonnegative integer N for which expression (2.6) has meaning. We take $\lambda_2 = 0$ in formula (2.5); i.e., function (2.6) determines the meridian section of the body of revolution moving over a perfectly rough plane. Thus, we can represent a denumerable set of surfaces, whose meridian section is determined by function (2.6). For example, for $N = 0$,

$$k = 2, \quad f(\theta) = \frac{\lambda_1}{\cos\theta}, \quad \xi = -\frac{2\lambda_1\sin\theta}{\cos\theta},$$
$$\zeta = \frac{\lambda_1\sin^2\theta}{\cos^2\theta} - \lambda_1 \qquad (2.7)$$

or

$$k = \frac{2}{3}, \quad f(\theta) = \frac{\lambda_1}{\sin\theta}, \quad \xi = \frac{\lambda_1\cos^2\theta}{\sin^2\theta} - \lambda_1, \quad \zeta = -\frac{2\lambda_1\cos\theta}{\sin\theta}. \tag{2.8}$$

The surface specified by expressions (2.7) represents the paraboloid of revolution, while the surface determined by expressions (2.8) is formed by rotating a parabola arc about an axis passing through its focus.

ACKNOWLEDGMENTS

This work was supported by the Russian Foundation for Basic Research, project no. 01-01-00141, and the "Young Candidates" Foundation, project no. MK–1393.2003.01.

REFERENCES

1. Kh. M. Mushtari, Mat. Sb. **39** (1/2), 105 (1932).
2. A. P. Markeev, *Dynamics of a Body Contiguous to a Rigid Surface* (Nauka, Moscow, 1992).
3. V. F. Zaĭtsev and A. D. Polyanin, *Handbook on Ordinary Differential Equations* (Nauka, Moscow, 1995).

Translated by V. Bukhanov